DEVELOPMENT AND EVALUATION OF THERMALLY COMPENSATED ADVANCED REUSABLE PIEZO SENSOR FOR EMI TECHNIQUE

SUSHMITA BARAL

(2017CES2512)

DEPARTMENT OF CIVIL ENGINEERING

INDIAN INSTITUTE OF TECHNOLOGY DELHI

JUNE 2019

DEVELOPMENT AND EVALUATION OF THERMALLY COMPENSATED ADVANCED REUSABLE PIEZO SENSOR FOR EMI TECHNIQUE

Submitted by

SUSHMITA BARAL

(2017CES2512)

Under the guidance of

Prof. SURESH BHALLA and Dr. PRATEEK NEGI

In fulfilment of the requirement of the degree of

Master of Technology in Structural Engineering

DEPARTMENT OF CIVIL ENGINEERING

INDIAN INSTITUTE OF TECHNOLOGY (IIT) DELHI

JUNE 2019

CERTIFICATE

This is to certify that the work which is being presented in this report entitled, "**DEVELOPMENT AND EVALUATION OF THERMALLY COMPENSATED ADVANCED REUSABLE PIEZO SENSOR FOR EMI TECHNIQUE** " which is being submitted by **SUSHMITA BARAL** (**ENTRY NO: 2017CES2512**) in the fulfilment the requirements for the award of degree of Master of Technology in "**STRUCTURAL ENGINEERING** " is a record of the student's own work carried out at **Indian Institute of Technology (IIT) Delhi, India** under my supervision and guidance.

The matter embodied in this thesis has not been submitted elsewhere for the award of any other degree or diploma.

PROF. SURESH BHALLA
Professor
Department of Civil Engineering
Indian Institute of Technology Delhi

Dr. PRATEEK NEGI
(Former) Principal Project Scientist
Department of Civil Engineering
Indian Institute of Technology Delhi

New Delhi

JUNE 2019

CERTIFICATE

I certify that the work which is being presented in this report entitled, "**DEVELOPMENT AND EVALUATION OF THERMALLY COMPENSATED ADVANCED REUSABLE PIEZO SENSOR FOR EMI TECHNIQUE**" in the fulfilment the requirements for the award of degree of Master of Technology in "**STRUCTURAL ENGINEERING**" is a record of the my own work carried out under the supervision of **Prof. Suresh Bhalla** and **Dr. Prateek Negi**, Department of Civil Engineering at **Indian Institute of Technology (IIT) Delhi, India.**

I have not submitted the record embodied in this report for the award of by other degree or diploma.

Sushmita Baral

2017CES2512

New Delhi

JUNE 2019

ACKNOWLEDGEMENTS

I feel great pleasure and privilege to express my deep sense of gratitude, indebtedness and thankfulness towards my supervisor, **Prof. Suresh Bhalla** for the valuable guidance, supervision and continuous encouragement throughout the project.

Secondly, I would also like to express my deep sense of gratitude and thankfulness towards my co-supervisor, **Dr. Prateek Negi** for his continuous support and critical reviews throughout the project.

I also acknowledge my colleague **Major Kunal Srivastava** and the research scholars **S. K. Dhawan**, **Sumit Balguvhar, Jayalakshmi Raju, Dattar Singh Aulakh,** who constantly motivated me throughout my project days. I would like to thank all staff members of Smart Structures and Dynamics Laboratory for their co-operation. I am very thankful to all the faculty of structural engineering program who helped me to explore more about structural engineering.

Lastly, I feel privileged and grateful to my husband **Sailesh Adhikari** for his continuous support and valuable comments. I am indebted to my parents for having faith in my abilities and never-ending motivation. Thanks to everyone who helped me directly or indirectly in completion of the work.

SUSHMITA BARAL

2017CES2512

ABSTRACT

The electro-mechanical impedance (EMI) technique is a signature-based structural health monitoring (SHM) technique which has gained recognition in the field of Civil Engineering in past two decades. Any deviation in the signature, if detected, points the occurrence of damage in the host structure. However bonding piezo sensors permanently on the structure increases risk of deterioration over a period. Also, it needs large number of piezo sensors. Hence, there is the need of the reusable piezo sensors which makes EMI technique cost low and efficient. The effect of temperature on the signature of piezo sensor gives false indication of damage which are ignored in regular practice. Here, this thesis focuses on the development of reusable piezo sensor using single bolt configuration acquiring the maximum repeatability using Coefficient of Correlation (CC) index. Also, it covers the effect of the temperature on the signature of the piezo sensors and proposes a simple compensation

In this study, a novel advanced reusable piezo senor using single bolt was fabricated and successfully demonstrated for damage detection on the small steel plate structure. For ensuring reusability of the sensor, the ARPS was instrumented on the host structure (a steel plate of 250×200×3mm) by applying torque of 25 Nm. Repeatability check was performed by releasing the torque to zero and again tightening on the same level of torque. Damage was induced in the plate by drilling holes, which was effectively detected by the ARPS. Further, the experiment with ARPS was extended to large scale 2D structure to localize the damage. A satisfactory repeatability was achieved as well as successful localization of damage. Simultaneously, temperature effects on piezoelectric transducers bonded on aluminum beam and free boundary condition, exposed to a controlled increase in environmental temperature was studied. The amount of horizontal and vertical shifts in the signatures was quantified by using experimental data. Both horizontal and vertical shifts are found to be frequency dependent, the amount of shift increasing with frequency. Also, other factors like modulus of elasticity, piezoelectric strain, piezoelectric permittivity etc. influence the shift in signatures were found analytically and finite element modelling. Based on experimental data a simple compensation formulation was developed.

The final outcome of this study is a simple damage localization cum thermal compensation algorithm suitable for large 2D structure.

TABLE OF CONTENTS

LIST OF FIGURES

LIST OF TABLES

LIST OF ACRONYMS

1D	One dimensional
ARPS	Advanced Reusable Piezo Sensor
EMI	Electromechanical impedance
FE	Finite Element
LCR	Inductance, Capacitance, and Resistance
MFB	Metal foil based
NBPS	Non-bonded piezo sensor
NDE	Non-destructive evaluation
PZT	Lead zicronate titanate
RBPS	Reusable Bolted Piezo Sensor
RMSD	Root mean square deviation
SBPS	Surface bonded piezo sensor
SHM	Structural health monitoring
SSD	Surface Dry Condition

LIST OF SYMBOLS

A	Area
B	Susceptance
D_3	Dielectric displacements along axis 3
d_{ij}	Piezoelectric strain coefficient of PZT patch
E	Modulus of elasticity
E_3	Electric field along axis 3 of PZT patch
G	Conductance
G_0^i	Pre - damage conductance for ith frequency point
G_i^1	Post - damage conductance for ith frequency point
h	Thickness of PZT patch
k	wave number
l	length of PZT patch
n	number of readings
S_1 (S_i)	Mechanical strain along axes 2 (1)
T	Temperature
T_1 (T_i)	Mechanical stress along axes 2 (1)
u	Displacement at the interface between the bonding layer and the beam
w	width of PZT patch
$\bar{Y}$	Complex electro mechanical admittance (G+Bj)
Y_a	Active admittance
$Y_{i,1}$	original impedance at frequency interval i
$Y_{i,2}$	interrogated impedance at frequency interval i
Y_p	Passive admittance
$\overline{Y^E}$	ComplexZYoung'sZModulusZof elasticityZ
Z	Complex mechanical impedance of
Z_a	MechanicalZimpedanceZof the PZT
Z	Complex permittivity of the PZT patch for axes i and j at constant stress
ρ	Density
ω	Angular frequency

v	Poisson ratio
δv	vertical shift
ΔH	Horizontal shift
ΔV	Vertical shift

CHAPTER 1

INTRODUCTION

1.1 BACKGROUND

In the past few decades' urbanizations is at its peak of which several civil engineering structures as a residential building, office, school and hospital are constructed. After a duration, these structures performance decreases in terms of safety. They are prone to damage due to various reasons like faulty design, environmental condition, excessive load, fatigue, etc. in their lifetime. Thus, the structures need continuous structural health monitoring (SHM) to safeguard its safety. None of the structures are 100% safe to the damage.

The SHM provides continuous measurement of a loading environment and severe responses of the structure or its components. The SHM implies the periodic check of the structure with the response of the sensors. The results extracted from the sensors then analyzed to know the current condition of structure. Sensors which gave the responsibility to monitor the structure are the smart materials. Smart materials respond to the change in the materials, which are variable in different parameters like stress, magnetic field, heat, electric field, etc. The smart sensors aid in detecting those damages which are inevitable to human eye. In this study we have used Electromechanical Impedance (EMI) technique for the actuation and sensing purpose with piezo sensor.

PZT patches once bonded on the structure cannot be retrieved. Hence reusable PZT patch is the new concept with cost effective ensuring same repeatability and reliability in measurement. Signatures acquired from the piezo sensors are sensitive to surrounding temperature fluctuation. A shift on the signatures may give a false indication of damage. Thus, before acquiring the signature, the shifts must be compensated so that the results extracted are correct.

This thesis covers the development of thermally compensated Advanced Reusable Piezo Sensors (ARPS) for monitoring steel structures.

1.2 OBJECTIVES AND SCOPE

The main objective of this project is to a develop temperature compensated advance reusable piezo sensor for SHM of the structure. Primarily the thesis focuses on comparing the performance of the advanced reusable piezo sensors over the conventional piezo sensors and evaluates its effectiveness for the damage detection. Experiment with the piezo sensor, both in bonded and free state for temperature effect on the signatures. Develop the compensation technique for the signatures of piezo sensors through analysis. Thus, the developed technique is then implemented on the reusable piezo sensor.

1.3 ORGANIZATION OF THESIS

This thesis consists of seven chapters. The content of each chapter briefs below.

Chapter 1 covers the background of the thesis, followed by the scope and organizations of the thesis.

Chapter 2 contains the introduction of SHM, smart material, literature review of EMI technique. It also discusses previous work on the non-boned piezo sensor and temperature effect on the piezo transducer. Identification of research gaps, objectives and scope are specified in detail.

Chapter 3 includes the development of a reusable piezo sensor for acquiring the signature for pristine and damaged condition on the steel plate-based structure. Different sort of ARPS has been described with progressive stage and accuracy achieved.

Chapter 4 covers the development and proof of concept experimental verification algorithm for localizing the damage on large 2D structure.

Chapter 5 discusses the effect of temperature on signatures of the piezo sensor experimentally and analytically. Development of compensation technique is also illustrated in the section.

Chapter 6 includes the algorithm for thermally compensated ARPS

Chapter 7 summarizes the study and enumerates obvious conclusions and limitations based on comprehensive study**.** Also, it covers future recommendation.

Finally, references have been provided.

CHAPTER 2

STATE OF ART IN EMI TECHNIQUE AND REUSABLE PIEZO SENSORS

2.1 INTRODUCTION

This chapter includes fundamental principle of SHM in brief. It also covers the introduction of the EMI technique and detailed literature on SHM using non-bonded piezo sensor. The effect of temperature on the signature of the piezo sensors has been discussed. Research objective and the study gap have also been discussed.

2.2 STRUCTURAL HEALTH MONITORING

SHM of a civil structure is suggested to ensure its safety and proper functioning. Dreadful incidents in engineering structures have been reduced with the increase of SHM in damage detection. Generally, any damage begins from an early stage but may finally result in catastrophic loss over a period, if not treated in time. Thus, it is necessary to determine the damage in its initial state to avoid its further propagation. Therefore, regular inspection is carried out to safeguard the well-being of a structure, which is known as 'structural health monitoring'. SHM is periodic monitoring of the structures for a safety point of view to identify, locate, and determine the severity of the damages in the structures. Also, it includes the determination of the remaining life of the monitored structure.

SHM gained esteem with the following salient features:

a. To disguise structural damages and take remedial actions.
b. To validate the design based on parameters affected by statistical variation and uncertainty.
c. Assessment of the structure after retrofitting.
d. To convey an alternative approach for conventional visual inspection, which consumes more time and cost.
e. To facilitate monitoring of external loads, stress distribution, deflection, etc. on a structure.
f. To supervise the overall behavior of the structure.

2.3 SMART MATERIALS

Monitoring of the structure is basically done by two types of sensing technologies, *i.e.*, conventional sensor and smart materials-based sensor. Electrical strain gauge, vibrating strain gauge, and accelerometer come under the traditional sensing technologies, whereas another type of sensing technology is based on the smart materials. Smart materials are the transducers whose behaviour changes in a specific manner due to a particular type of stimulus input. Some common types of smart materials are piezoelectric materials, shape memory alloys, optical fiber, electro-rheological fluids, etc.

Shape memory alloys have ability to render its original shape. Below specific temperature, it deforms its shape plastically, and above the transition temperature, it returns to its memorized shape. Electrorheological fluid under electrostatic potential can undergo an abrupt and reversible change in viscosity. Optical fibers are made up of thin fibers, *i.e.* glass and silica. They utilize fiber properties to generate optoelectronic signals which are indicative of external parameters to be measured. The piezoelectric crystals generate an electric potential across its surface on application of an external stress.

Piezoelectricity is derived from the Greek word *Piezien* which means to squeeze. Thus, the electric potential generated by pressing is piezoelectricity (Harper 1883). The piezoelectric behavior was first studied by the Curie brothers extensively in the late 19^{th} century. Until now the researchers have invented several artificial crystals showing piezoelectric behavior other than the naturally occurring crystals like quartz, rochelle salt etc. Commercially, the two most common forms are Lead Zirconate Titanate (PZT) and Polyvinylidene fluoride (PVDF) flexible composites. PZT patches have higher strength and stiffness than PVDF. PVDF is ductile and has shape conformability whereas, PZT is brittle and not acquiescent with curved surfaces.

2.4 ELECTRO-MECHANICAL IMPEDANCE (EMI) TECHNIQUE

The EMI technique was first developed by Liang et al. (1994). It is a non-destructive technique which uses piezo sensors for condition monitoring of a host structure. A PZT patch acts both as an actuator and as a sensor. When it acts as the sensor, it functions in direct mode in which it generates electric potential on the application of stress as shown in Figure 2(a). In converse effect, PZT patch produces stress when an electrical signal is applied across its surface as shown in Figure 2(b). The

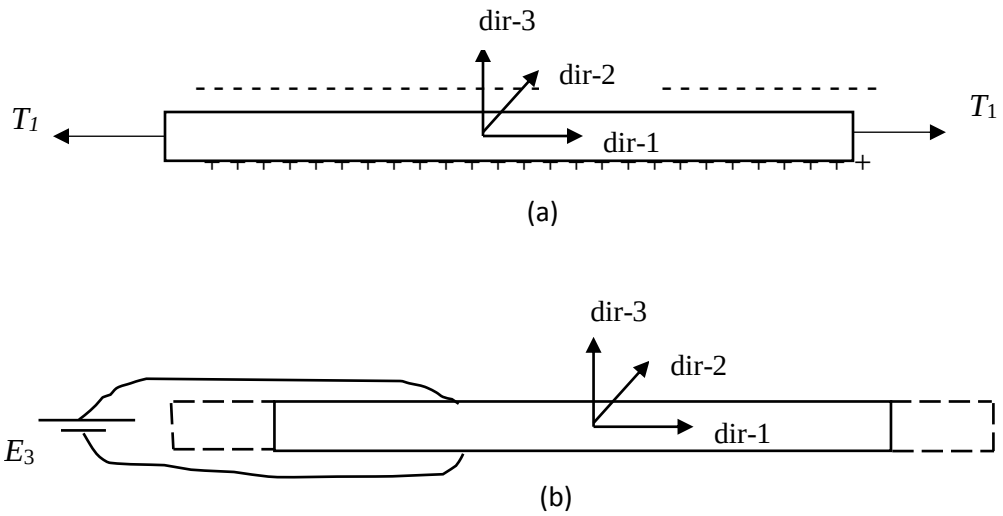

Figure 2.1: (a) Direct effect of PZT (b) Converse effect of PZT

direct and the converse effects exhibited by piezoelectric materials can be expressed by following equations respectively.

$$D_3 = \overline{\varepsilon_{33}^T} E_3 + d_{31} T_1 \tag{2.1}$$

$$S_1 = \frac{T_1}{Y_{11}^E} + d_{31} E_3 \tag{2.2}$$

where D_3 (C/m^2) is electric charge density along axis-3, S_1 is the strain along axis-1, E_3 (V/m) is the applied external electric field along axis-3 and T_1 (N/m2) is the stress along axis-1 and d_{31}(C/N) is the piezoelectric strain coefficient.

In EMI technique the PZT patches bonded on the structures are electrically excited at a higher frequency in the range of 30-400 kHz by an impedance analyzer or an LCR meter. At this frequency range, the PZT patches actuate the structure and then senses the response reflected from the structure in the form of an admittance signature. These signatures consist of a real part which is known as conductance (*G*) and an imaginary part known as susceptance (*B*). Any damage to the structure reflects a deviation in the admittance signature which is recorded in the frequency domain. Since the EMI technique uses a very high-frequency range, is capable of detecting damages in incipient stage and also immune to other low-frequency structural vibrations.

Liang (1994) proposed a 1D analytical model of Electro-Mechanical Impedance as shown in Figure 2.2.

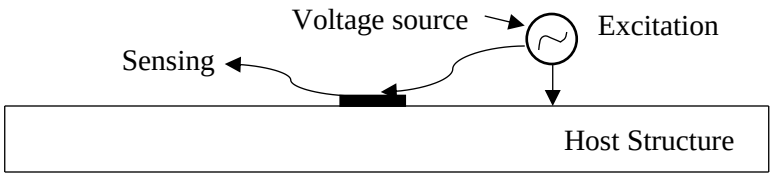

Figure 2.2: Schematic representation of Liang's Model

The governing one-dimensional wave equation for the generic system comprising one half of the patch and the structure has been solved by Liang et al. (1994) using the impedance approach.

$$\overline{Y} = 2\omega j \frac{wl}{h}\left[\overline{\varepsilon_{33}^{T}} + \left(\frac{Z_a}{Z + Z_a}\right) d_{31}^2 \overline{Y^E}\left(\frac{\tan \kappa l}{\kappa l}\right) - d_{31}^2 \overline{Y^E}\right] \tag{2.3}$$

or
$$\bar{Y} = G + Bj \tag{2.4}$$

where d_{31} is the piezoelectric strain coefficient, $\overline{Y^E}$ the complex Young's modulus of the PZT patch at the constant electric field, $\overline{\varepsilon_{33}^{T}}$ the complex electric permittivity of the PZT material at constant stress, Z the mechanical impedance of the structural system, ω the angular frequency, l, w ,h are length, width and height of the PZT patch and κ the wave number and Z_a is the actuator impedance, given by

$$Z_a = \frac{kh_p w \overline{Y^E}}{\tan kl(j\omega)} \tag{2.5}$$

The mechanical impedance Z is a function of the structural parameters, *i.e.*, the stiffness, damping, and mass. Any damage to the structure will cause these parameters to change and hence improves the drive point mechanical impedance Z. Consequently, as can be observed from the equation, the electro-mechanical admittance, $\overline{Y}$ will undergo change, and this serves as an indicator of the state of health of the structure. The measured admittance is a complex quantity consisting of real and imaginary parts, the conductance (G) and the susceptance (B) respectively. A plot of conductance over a sufficiently full band of frequency serves as a diagnostic signature of the structure and is called the conductance signature. The imaginary part susceptance, on the other hand, was regarded weak in the interaction with structure (Sun et al., 1995). Bhalla and Soh (2003) showed the relevance of the imaginary component by introducing the concept of "Active Signatures".

Electrical Admittance of Liang's Model can be further divided into two parts active admittance and passive admittance.

$$\bar{Y} = \underbrace{2\omega j \frac{wl}{h}\left[\overline{\epsilon_{33}^{T}} - d_{31}^{2}\overline{Y^{E}}\right]}_{\text{Part I}} + \underbrace{2\omega j \frac{wl}{h}\left(\frac{Z_a}{Z+Z_a}\right) d_{31}^{2}\overline{Y^{E}}\left(\frac{\tan Kl}{Kl}\right)}_{\text{Part II}} \tag{2.6}$$

where Z is Mechanical Impedance of Host Structure, and Z_a is Mechanical Impedance of the PZT. From Equation 2.6 it is seen that the part I solely depends on the properties of the PZT patch and part II on the parameters of structure and PZT patch both. Since both Z and Za appear in the expression of part II, there is electro-mechanical coupling between the structure and the PZT patch. Equation 2.6 can be written as

$$\bar{Y} = \overline{Y_P} + \bar{Y_A} \tag{2.7}$$

where $\overline{Y_P}$ denotes the PZT contribution and $\bar{Y_A}$ represents the contribution of structure and PZT interaction. $\bar{Y_A}$ is termed as the 'active' component, in which the mechanical admittance of the host structure is coupled with active admittance. Therefore, the active component of the admittance is used for the damage diagnosis. Whereas, $\overline{Y_P}$ is regarded as the 'passive' component, which is not affected by any damage near the patch. Hence it can be decomposed in real and the imaginary part by expanding $\overline{\epsilon_{33}^{T}} = \epsilon_{33}^{T}(1-\delta j)$ and $\overline{Y^{E}} = Y^{E}(1+\eta j)$ and substituting in equation 2.6 we get,

$$\overline{Y_P} = \left[2\omega \frac{wl}{h}\{\delta\epsilon_{33}^{T} + d_{31}^{2}Y^{E}\eta\}\right] + j\left[2\omega \frac{wl}{h}\{\epsilon_{33}^{T} - d_{31}^{2}Y^{E}\}\right] \tag{2.8}$$

or,
$$\overline{Y_P} = G_P + jB_P \tag{2.9}$$

Where G_P is the real and B_P is the imaginary component. In comparison to B_P, G_P has a small magnitude due to the presence of δ and η. B_p covers the active component for the SHM of structure raw-susceptance signature is not ideally considered. The contribution of a PZT patch in the acquired signature can be filtered off, so that the remaining signature will reflect only the behaviour of the structure. Remaining active part conductance and susceptance given as

$$G_A = G\text{-}G_P \tag{2.10}$$

$$B_A = B\text{-}B_P \tag{2.11}$$

After ignoring the passive part from the raw admittance signature, active part reflected the structure characteristics prominently. Active part is more contributing in EMI technique of the structure (Bhalla and Soh, 2003).

2.5 NON- BONDED PIEZO SENSORS

Yang et al. (2010) proposed use of reusable PZT patch for the monitoring cement hydration and structural health. They bonded a PZT patch (20×20×0.5mm) on the plastic enclosure and aluminum sheet with two bolts tightened inside the holes drilled in the enclosure as shown in Figure 2.3 (a). Once the readings were obtained from the sensor, attached on cube during casting then bolts were unscrewed. The presence of water hinders the functioning of a PZT patch hence, they cover it with plastic DIP as shown in Figure 2.3 (b). However, the encasing reduced its sensitivity. Figure 2.3 (c) shows a schematic of the sensor setup.

The repeatability of a piezo sensor is affected by quality of PZT transducer, human errors and modulus of elasticity (Yang et al. 2010). They performed the repeatability in the frequency range of 70-120 kHz for the four times. They experimented with thicker (20×20×2mm) and thinner piezo sensors (20×20×0.5mm) in which the magnitude of thicker PZT patch is four times of thinner PZT patch. The sensitivity of a thicker patch is higher than the thinner PZT patch. Also, for similar bonding condition, the repeatability of thicker PZT patch was found to be better.

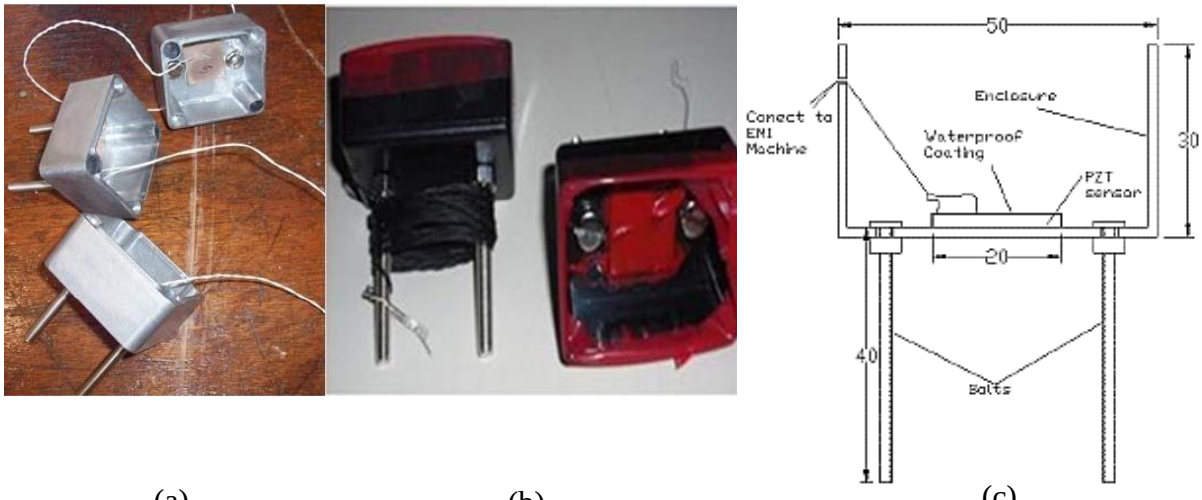

(a) (b) (c)

Figure 2.3: Bolt with enclosure reusable PZT setups (Yang et al., 2010) (a) reusable set and (b) waterproofed reusable setup (c) schematic of the sensor setup.

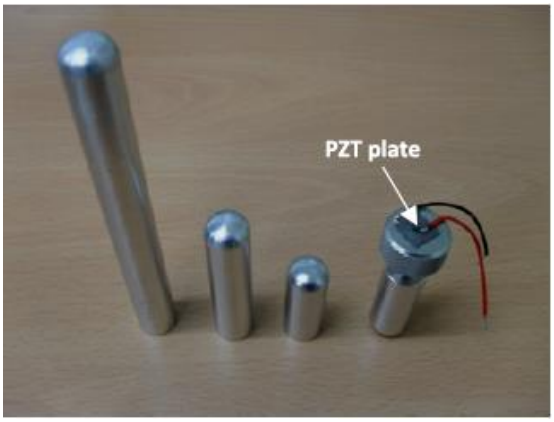

(a)

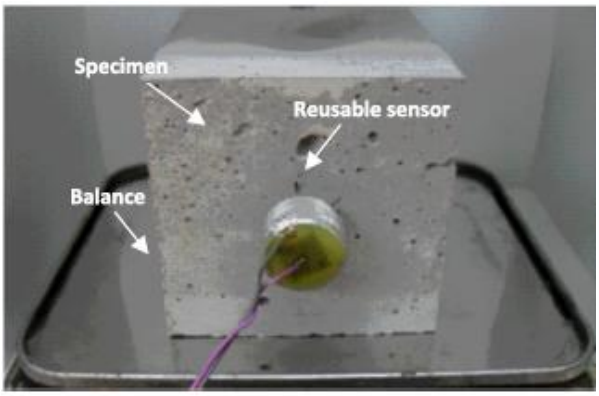

(b)

Figure 2.4: Bolt with reusable rod setup (Tawie and Lee, 2011) (a) different length of rods (b) shows the sensor on the concrete cube.

A piezo sensor is not bonded directly on a concrete specimen for monitoring hydration without any protection. Even the Yang's enclosure setup is also not feasible as the bolts get unscrewed after hardening and give spurious results. To overcome such problem **Tawie and Lee (2011)** proposed a setup in which sensor was attached on the bolt and fixed with the different lengths of the rod. Here the developed setup was more effective and efficient for monitoring setting time of cement mortar in the field using impedance analyzer. The configuration of the sensor can be easily removed and reused for other repetitive tests. Here they replaced the Vicat's needle apparatus which measures the setting time and moisture loss. The reusable setup effectively estimated the damage in hardened mortar. The setup is less sensitive to fine localized cracks compared to a surface bonded PZT. This setup is favorable for evaluating the prestress loss of tension cables in prestressed concrete structures. Figure 2.4(a) shows the reusable setup with different length of rods and Figure 2.4(b) shows the reusable sensor over the concrete cube.

Na et. al., (2012) proposed a new setup based on a magnet that was easy to install and remove in the composite or metallic structures. They used EMI technique for evaluating the setup with the sensor. Here to avoid the temperature errors measurements taken at room temperature, *i.e.* 24±0.3 ºC. The reusable setup consists of commercial neodymium magnet made of $Nd_2Fe_{14}B$ tetragonal crystalline structure. They prepared the reusable setup with varying thickness of magnet, *i.e.* 3, 5 and 10mm. Repeatability test was performed by detaching the specimen and again attaching it for three times. To acquire better repeatability the position must be fixed, no displacement of PZT

Figure 2.5: Reusable Magnet setup (Na et. al., 2012)

transducer. Small movement can result in significant change in impedance signature which gives false results. Figure 2.5 shows the reusable setup.

Being brittle in nature, bonding of PZT patches in complex geometric structure is complicated. To overcome such problem **Na and Lee (2013)** developed a coupling setup with steel wire and PZT patches. They performed the proposed setup with various length and diameter of steel wire and with the different size of the PZT sensor. Thicker steel wire gave a higher amplitude in the resonance frequency range. Different size sensor 3×1 cm suitable for sensing larger area and 2×1 cm suitable for monitoring cracks with higher frequencies. This setup was able to monitor the progressive damage, debonding and deterioration of adhesive bonding of the composite layers. Figure 2.6 shows the proposed steel wire setup for monitoring a complex structure.

Bonding of PZT patches directly on the structure in remote place is very difficult or impossible due to its fragile nature. **Naskar and Bhalla (2016)** proposed metal foil based EMI technique for such type of structures. They replaced the steel wire with the metal foil which improved the sensitivity of damage detection. They developed an algorithm, directly applied in the field utilizing the metal foil based (MFB) variant which reduced the number of the piezo sensor for damage

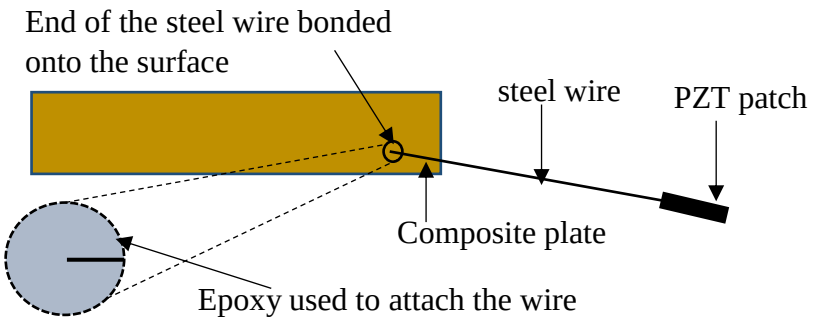

Figure 2.6: Steel wire setup by Na and Lee (2013)

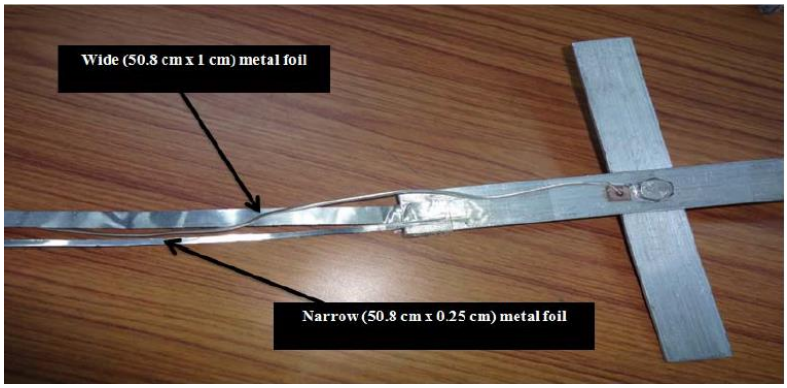

Figure 2.7: Specimen with wide and narrow metal foil (Naskar and Bhalla 2016)

detection. This MFB variant first simulated through finite element method then coupled with basic impedance model. A mild steel plate of 1200mm×3970mm×38mm was numerically modeled to test the algorithm then implemented on the actual plate covering various damage locations. Figure 2.7 shows the developed MFB variant for damage detection.

Srivastava et al., (2017) proposed a jubilee clamp piezo sensor (non-bonded) for the biomedical purpose. Here they first bonded the piezo sensor on a thin aluminum strip, which was clamped on the biomedical subject as shown in Figure 2.8. They observed the signatures for both the damaged and undamaged condition had a good correlation with the bonded and clamped piezo sensor. Repeatability of signatures was found to be RMSD of 2.1% which was satisfactory. This non bonded configuration was then extended to monitor the condition of bones covered with skin and tissue of living human subject with the aid of silicone-based coating. The study showed good prospects of using non-bonded for biomedical disciplines.

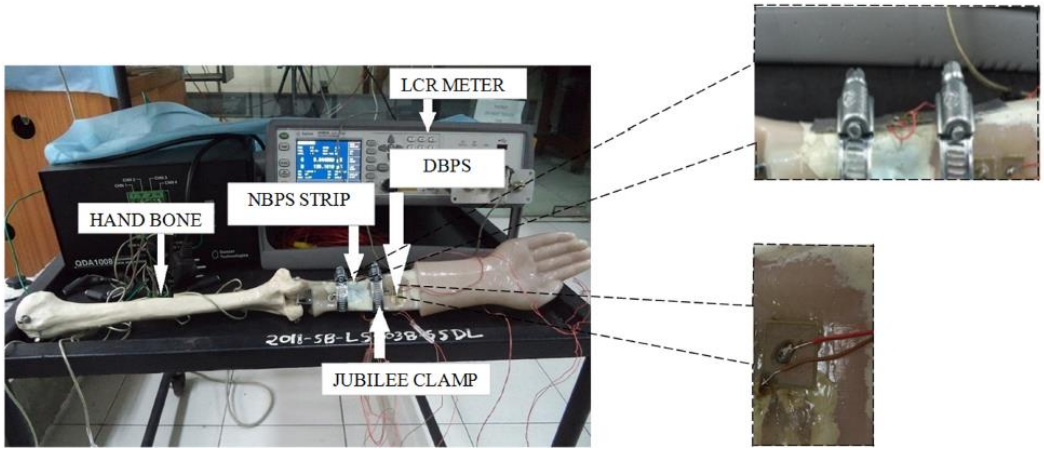

Figure 2.8: Jubilee clamp non bonded configuration (Srivastava et al., 2017)

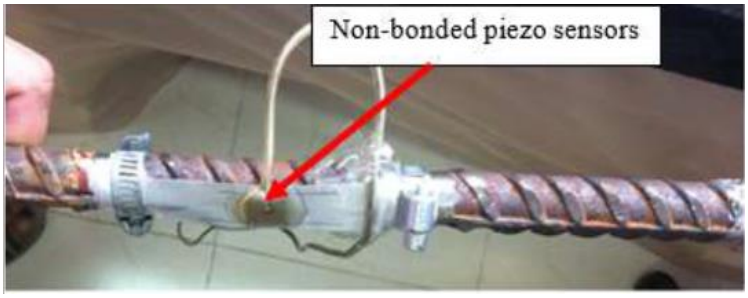

Figure 2.9: Jubilee clamps non-bonded piezo sensor (Thakuri, 2017)

Thakuri (2017) experimentally validated and evaluated corrosion on rebar with the reusable configuration of PZT patches such as metal foil piezo sensor (MFPS) and non-bonded piezo sensor (NBPS) as shown in Figure 2.9. Corrosion was detected with directly bonded and embedded piezo sensor. Both the reusable piezo sensor, *i.e.* MFPS and NBPS showed considerable variation on the conductance signature. The results demonstrated by the RMSD variation was not reliable. RMSD may work as a good indicator of damage but for quantification of damage structural parameters computation is more reliable as it correlates with actual variation of mass through gravimetric mass loss. Overall, the study established the feasibilty of reusable type piezo sensors.

Supriya (2018) proposed the reusable bolted piezo sensor (RBPS) for the damage detection on the metal structure. They bonded the piezo sensor on the center of the aluminum strip of 70×25 mm then on the two end bolt was fixed. The complete reusable setup developed is shown in Figure 2.10. At first, the structure was demonstrated on the aluminum plate which showed the repeatability of RMSD of 0.21%. In pristine and damaged condition the conductance signatures showed suitability and reliability of RBPS and correlated with the conventional bonded piezo sensor. The setup was then extended to a 2D steel plate for damage localization.

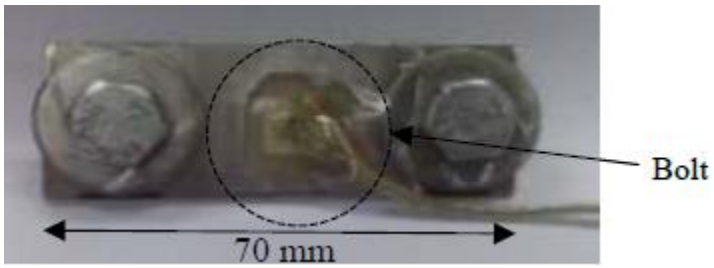

Figure 2.10: Reusable bolted piezo sensor (Supriya, 2018)

Table 2.1 gives the review of the non-bonded piezo sensor discussed above.

Table 2.1: Review on the nonbonded piezo sensor

Investigators (Year)	**Area of research**	**Procedure of repeatability**	**RMSD**	**Frequency range**
Yaowen Yang, Bahador Sabet Divsholi and Chee Kiong Soh (2010)	An enclosure with bolts for initial monitoring hydration and structural health of concrete	Unscrewing and tightening the bolt	Not specified	80-120 kHz
Rudy Tawie and Haeng-Ki Lee (2011)	A bolt with PZT patch over it connected to the rod	Unscrewing and screwing the bolt	Not specified	113-133kHz
Sam Na, Rudy Tawie and Haeng-Ki Lee (2012)	PZT placed on the magnet for corrosion assessment	Attaching and detaching the sensors	1%	50-60 kHz
Susmita Naskar and Suresh Bhalla (2016)	Metal-wire-based twin one-dimensional orthogonal array configuration of PZT patches for damage assessment of two-dimensional structures	Readings were taken after one month without damage	0.01%	100-150kHz
Shashank Srivastava, Suresh Bhalla, and Alok Madan (2017)	The PZT patch first bonded to a very thin metal plate, which in turn clamped onto the live subject	Clamped and screwed	2.1%	40-180 kHz
Supriya Thakur, Prateek Negi, Suresh Bhalla (2018)	Reusable Bolted Piezo Sensor (RBPS) for damage assessment	Unscrewing and screwing of the bolt	0.5%	100-150kHz

2.6 TEMPERATURE EFFECT ON PIEZO SENSORS

Krishnamurthy et al., (1996) found a decrease in the magnitude of the impedance peaks of a free PZT patch due to the increase in temperature. They choose a range of 25 to 75 °C in which the dielectric and piezoelectric properties of piezoceramic PSI-5A shows a linear trend. Though it is nonlinear at a border temperature range. Normalization of the variation of impedance with temperature eradicates the effect of a change in the magnitude of impedance which makes the variation independent of frequency. Changes in temperature, boundary condition, loading effects, etc. lead to a variation on the susceptance signature whereas little change in the conductance signature. Insignificant change in the resistive portion of electrical impedance suggests the utilization of real part of electrical admittance for the damage response which minimizes the effect of temperature

Park et al., 1999 found a significant horizontal and vertical shift in signatures due to a temperature in contrast to damage where the shifts are irregular. Empirical temperature compensation technique was developed which can be applied in a complex structure. For the horizontal shift he performed the iteration on the shift and for the vertical he gave the formula as given below.

$$\delta_v = \frac{\sum_{i=1}^{n} Re(Y_{i,2})}{n} - \frac{\sum_{i=1}^{n} Re(Y_{i,1})}{n} \tag{2.12}$$

Where, δ_v is the vertical shift, $Y_{i,1}$ is the original impedance at frequency interval I (baseline measurement), $Y_{i,2}$ interrogated impedance at frequency interval i (subsequent measurement) and n is the number of data points measured. Compensation technique was validated on a bolted pipe joint, a gear, and a composite reinforced aluminum plate along with the experiments.

The experiments conducted in a lab-controlled environment gives stable results, but in actual field condition, it is not possible due to the fluctuation of temperature (**Bhalla 2001**). He performed the simulation study of each parameter controlling another parameter in which he found the horizontal shift in the signature is due to change in Young's modulus of the structure, and the vertical shift is due to the change in ε_{33} and d_{31}.

Structural peaks are more affected rather than the PZT peaks on various temperatures (**Yang et al., 2008**). The shift of PZT resonance towards left is mainly due to the softening if the bonding layer, structural properties and piezoelectric properties PZT patch. Through simulation on FE

software ANSYS, they validated the shift of the signatures is caused by a reduction of stiffness of the bonding layer against increasing temperature.

The variations in the amplitude of the impedance signatures were related to the temperature-dependence of the capacitance of the piezoelectric sensor (**Baptista et al., 2014**). As a result of temperature variation, the shift in the resonance peak is not constant but increases with the increase in the frequency. The frequency band used to calculate the damage indices played an essential role in compensating for temperature effects by maximizing the correlation coefficient.

2.7 IDENTIFICATION OF RESEARCH GAPS

Bonding of piezo sensor directly on the structure makes EMI technique costly owing to requirement of large number of sensors. Hence, reusable piezo sensors make a strong case. Permanently bonding of sensor may hinder the working of moving parts in the host structure. Leaving piezo sensors forever on the host structure increases the risk of deterioration in their internal packing over some time. All the previous specimens for reusable piezo sensors are big which is challenging to handle. So far, two bolt system has been shown feasible for reusable sensor (Supriya, 2018) in the steel structure. This also limits their applicability. There is no single bolt type reusable sensor till date.

The effectiveness of the EMI technique highly depends upon the surrounding conditions of the host structure. Still, compensation for temperature changes is skipped in regular practice. Temperature effect cannot be ignored in the practical field conditions. The signature of the piezo sensors is very sensitive to the temperature fluctuation which triggers a false alarm.

2.8 AIMS AND SCOPE OF THE PROJECT

This project aimed to develop thermally compensated advanced reusable piezo sensor based on a single bolt to detect damage on a metal structure.

The specific aims and scope of the project are:

1. To develop an advanced reusable non-bonded piezo (ARPS) prototype for SHM of thin metallic structures based on single bolt configuration.
2. To compare the results over the conventional surface bonded PZT patches technique.
3. Development of an algorithm for damage and localization in prototype 2D structure.

4. To study the graduating effect of temperature on the EMI signatures of thin PZT patch in free and bonded conditions.
5. To develop the compensation technique for the admittance signatures.
6. To perform a numerical and analytical study on the effect of temperature on free and bonded PZT.
7. To validate the calculated temperature compensations in a real-life steel plate.

CHAPTER 3

DEVELOPMENT AND EXPERIMENTAL EVALUATION OF ADVANCED REUSABLE PIEZO SENSOR (ARPS)

3.1 ARPS DESIGN

In current practices, EMI technique includes permanent bonding of sensors with the host structure. This may hinder the functionality of the structure due to wired connecting system. Their connection may get deteriorated due to various environmental factors. Hence, requirement of a non bonded piezo sensor is necessary to overcome such problems. Here in this project, reusable piezo sensors were developed to monitor multiple region for damage. In the proposed configuration, three prototypes were developed. First two prototypes were made of bolt only, and the third prototype bolt with washer. In the prototype I and II at first bolt head surface were made plain. Then PZT patch is attached on the surface of the bolt head with the adhesive layer (epoxy). Figure 3.1 shows all the configuration of the reusable piezo sensor.

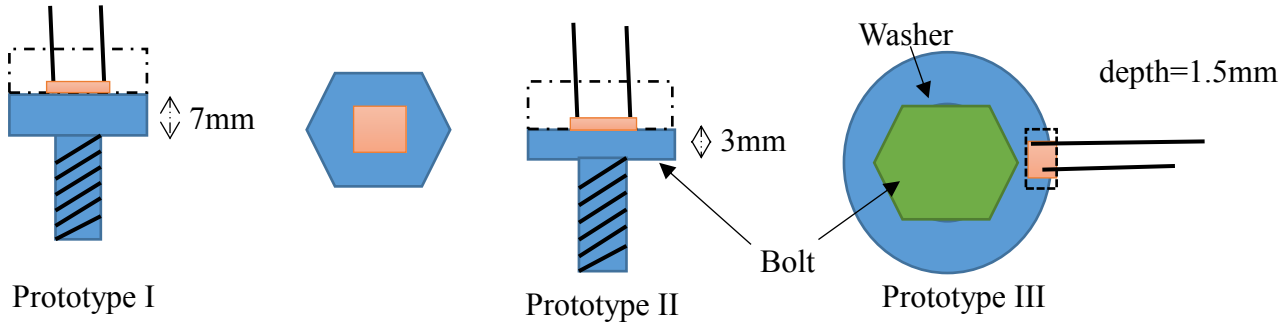

Figure 3.1: Advanced reusable piezo sensor

3.2 EXPERIMENTAL DETAILS

In this investigation, a steel plate of 25×15×3 mm (Figure 3.2a) with a hole of 9.5mm diameter at the center was designated as a test specimen for testing all the Non-bonded prototypes. A bolt of 9.3mm diameter was chosen for all prototypes. The prototype-I consist of a bolt of 9.3mm with

head thickness of 7 mm whereas prototype-II was 3mm thick. A PZT patch of 10×10×0.3 mm was bonded on the bolt head using adhesive layer (epoxy).

Prototype-III consist of 44 mm external diameter washer and a bolt of 9.3mm diameter fixed with epoxy. Three piezo sensors, Central Electronic Limited (CEL) of 10×10×0.3 mm, Piezo Ceramic 151A (PI) of 10×10×0.3 mm and Piezo Ceramic 151A (PI) of 5×5×0.3 mm were bonded in the washer at an angle of 120 as shown in Figure 3.5. All the prototypes were bolted to the steel plate and were tightened at a torque of 25 Nm. Figure 3.2 (b) shows the close view of the torque wrench. Through LCR meter signatures were acquired in the range of 100-300 kHz using VEE PRO 9.2 platform. Figure 3.3 shows the complete setup of the experiment.

(a) (b)

Figure 3.2: (a) Steel plate as a test specimen and (b)Torque wrench

3.3 ROOT MEAN SQUARE DEVIATION (RMSD)

In EMI technique, change in the admittance signatures reflects the damage in the structure. The horizontal or vertical shift in the signature or the appearance of new peaks or reduction of old peaks are the key indicators of the damage. To calculate the deviation in the admittance signature, RMSD is used which is common in SHM. Giurgiutiu and Rogers in 1999 defined the RMSD index as

$$RMSD(\%) = \sqrt{\frac{\sum_{j=1}^{N}\left(G_j^1 - G_j^0\right)^2}{\sum_{j=1}^{N}\left(G_j^0\right)^2}} \times 100\ \% \qquad (3.1)$$

where G_j^1 is the conductance after the damage at a j^{th} frequency and G_j^0 is the conductance at pristine state at the same j^{th} frequency respectively.

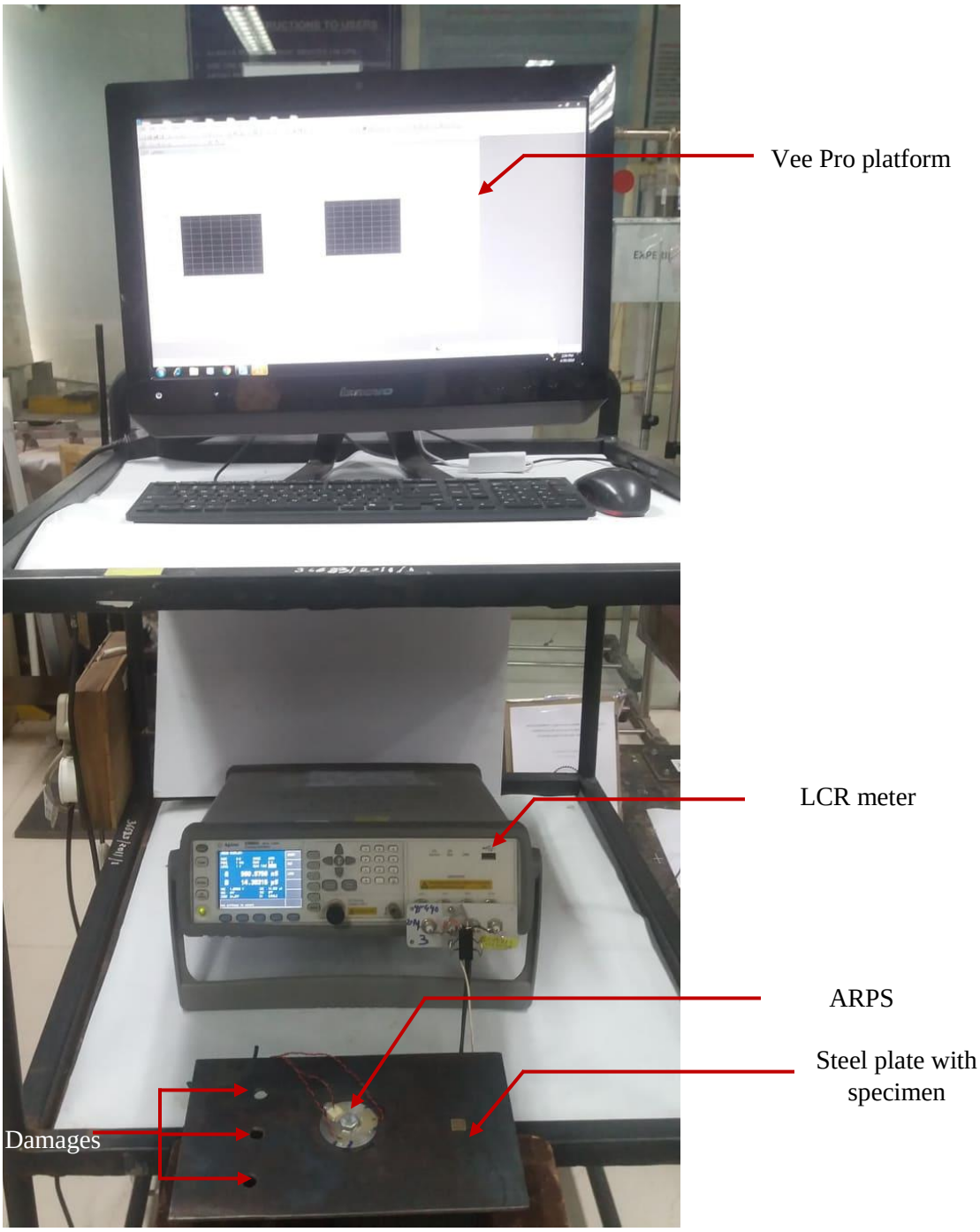

Figure 3.3: Experimental details of the specimen

3.4 COEFFICIENT OF CORRELATION (CC)

CC index was used for the repeatability of the admittance signatures in this thesis which is given as

$$CC = \frac{\sum_{i=1}^{N}(x_i-\bar{x})(y_i-\bar{y})}{(N-1)\sigma_x\sigma_y} \quad (3.2)$$

where x_i is the conductance of the signature-I and y_i is the conductance reading of the signature-II at the same frequency respectively. σ_x and $\bar{x}$ are the standard deviation and mean of signature-I respectively and σ_y and $\bar{y}$ are the standard deviation and mean of signature-II.

3.5 REPEATABILITY OF CONDUCTANCE SIGNATURE

In this study, a torque of 25 Nm was used to acquire the signature of all ARPS prototype to check the repeatability of the signatures. An accepted repeatability in signatures ensures better efficiency of the ARPS which is very important. At constant torque signature are acquired at full tightening of bolt and loosening it to full and again tightening it. For good repeatability CC value should be greater the 99.5%. Higher the value of CC better is the repeatability. During the study three prototypes were made (prototype-I, prototype-II, prototype-III) which is shown in Figure 3.4 and described in Table 3.1.

Table 3.1: Details of the prototypes

Parameters	**Prototype -I**	**Prototype -II**	**Prototype -III**
Material	Steel	Steel	Steel
Specimen	Bolt and nut	Bolt and nut	Bolt, nut and washer
Dimensions	Bolt head thickness - 7mm Diameter- 9.3mm	Bolt head thickness - 3mm Diameter- 9.3mm	Bolt head thickness -7mm Diameter- 9.3mm Washer outer diameter 45mm Inner diameter 9.5mm

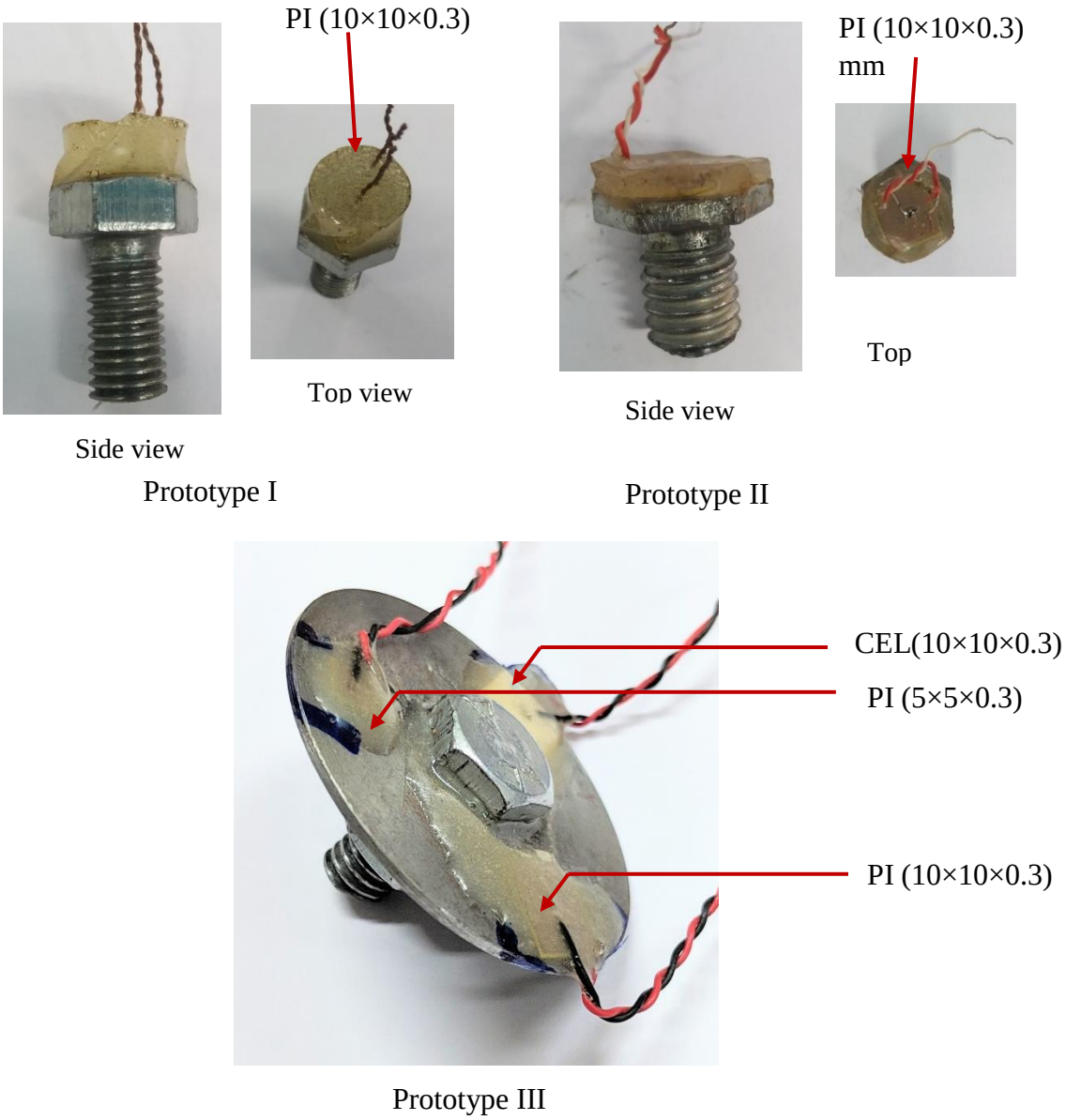

Figure 3.4: Prototypes of Advanced Reusable Piezo Sensor

Here in this study prototype III consist of three different piezo (CEL-(10×10×0.3) mm, PI-(10×10×0.3) mm, PI-(5×5×0.3) mm) attached on same washer. For prototype III, CC index was calculated as the specimen kept as it is and connection opened and closed again along with the torque applied. Following procedure were adopted to check the repeatability

i. The ARPS was tightened to a torque of 15N-m.
ii. At the frequency range of 100-300 kHz signature-I.

iii. Torque was reduced to zero.

iv. Signature-II was acquired in 100-300 kHz.

v. Signature-I and signature-II were plotted and CC and RMSD were computed.

Below Figure 3.5, 3.6, 3.7 showed the repeatability of the conductance signature of prototype-I, prototype-II and prototype-III respectively. Table 3.2 showed the CC index of prototype-III different piezo with as it is, connection open and closed and torque applied. Hence best repeatability was found in prototype-III which will be used in future part in this thesis.

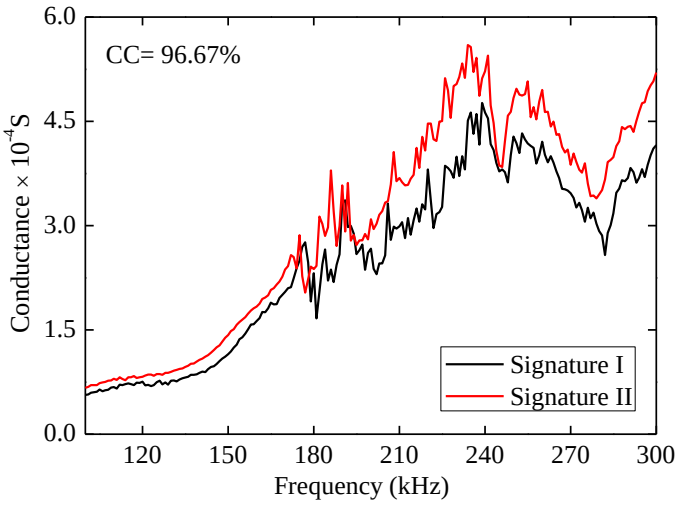

Figure 3.5: Repeatability of conductance signature of prototype-I

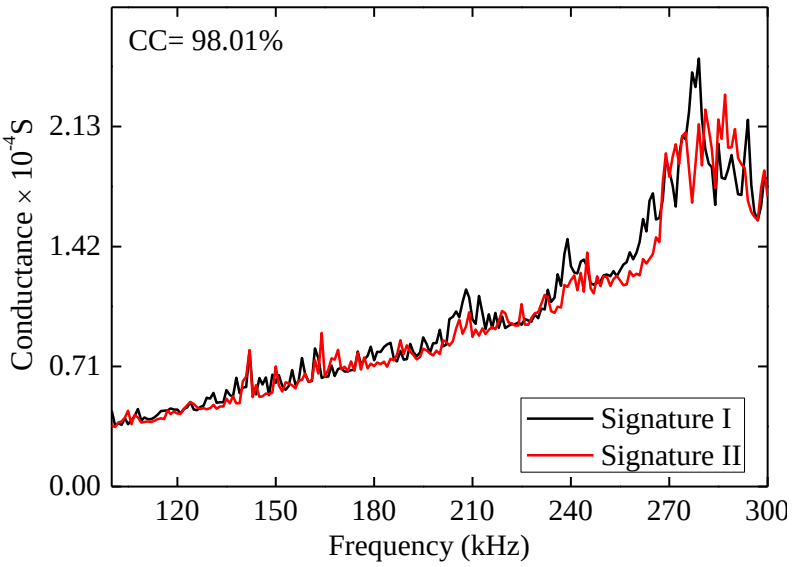

Figure 3.6: Repeatability of conductance signature of prototype-II

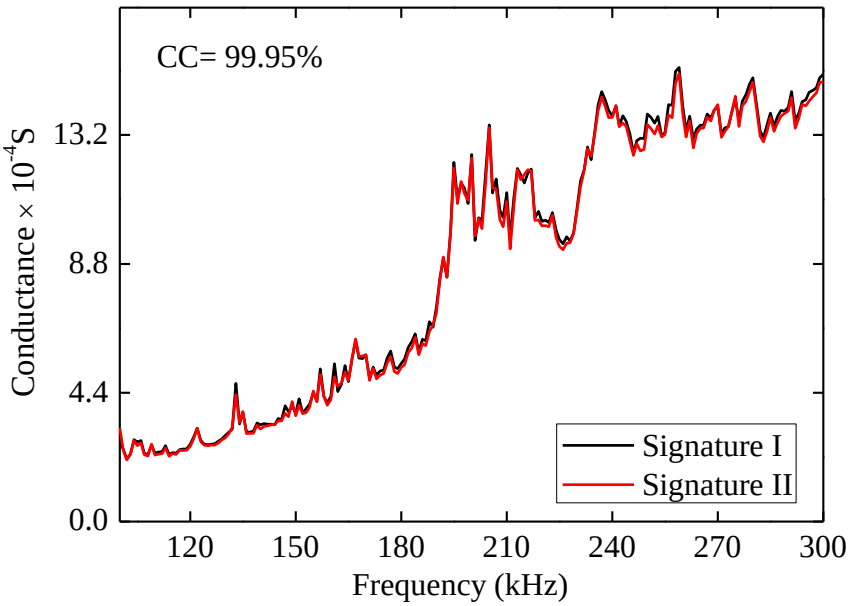

Figure 3.7: Repeatability of conductance signature of prototype-III- CEL piezo

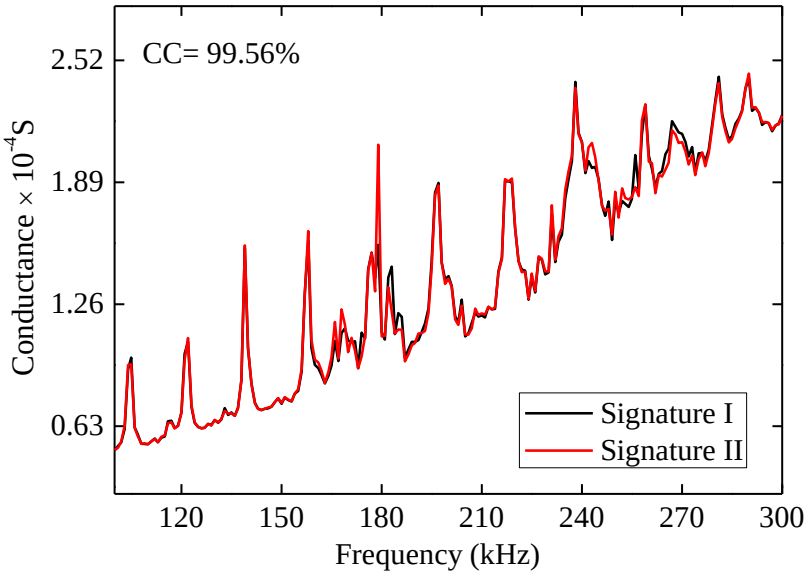

Figure 3.8: Repeatability of conductance signature of prototype-III- PI-5mm piezo

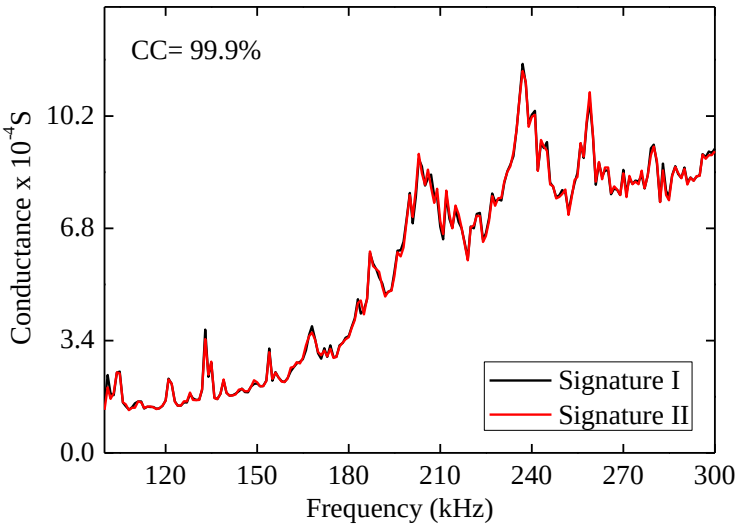

Figure 3.9: Repeatability of conductance signature of prototype-III- PI-10mm piezo

Table 3.2: Prototype III in different condition

Condition	**CEL**	**PI-10mm**	**PI-5mm**
	CC	CC	CC
As it is	99.99%	99.99%	99.99%
Connection open and close	99.99%	99.99%	99.99%
Torque applied	99.95%	99.92%	99.56%

3.6 EFFECT OF DAMAGE

On the host structure (main plate) a hole of 10mm diameter was introduced at a distance of 7.5mm from center towards length of 25mm as damage-1, in Figure 3.10. After the damage in the plate, the signatures correlate to damage state. Consequently, two other damages were induced and EMI signatures were acquired at 25Nm torque. Both the pristine and damaged data acquired were evaluated to calculate the RMSD index. Table 3.3 shows the RMSD for different damage condition. Figure 3.11-3.14 shows the plots of signatures of pristine and damage with CEL, PI-10 and PI-5 piezo sensor respectively.

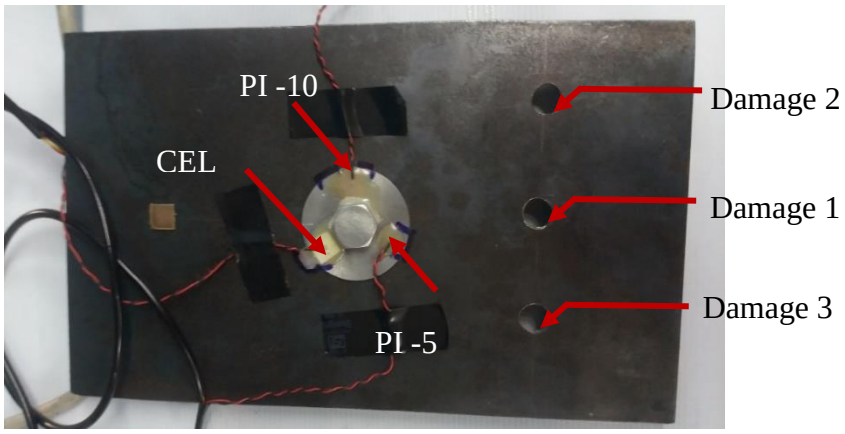

Figure 3.10: Damages on the steel plate

Table 3.3: RMSD index for different damage condition

Location	CEL	PI-10mm	PI-5mm
	RMSD	RMSD	RMSD
Damage 1	6.76 %	8.9 %	5.69 %
Damage 2	5.94 %	7.59 %	5.32 %
Damage 3	5.86 %	7.96 %	6.22 %

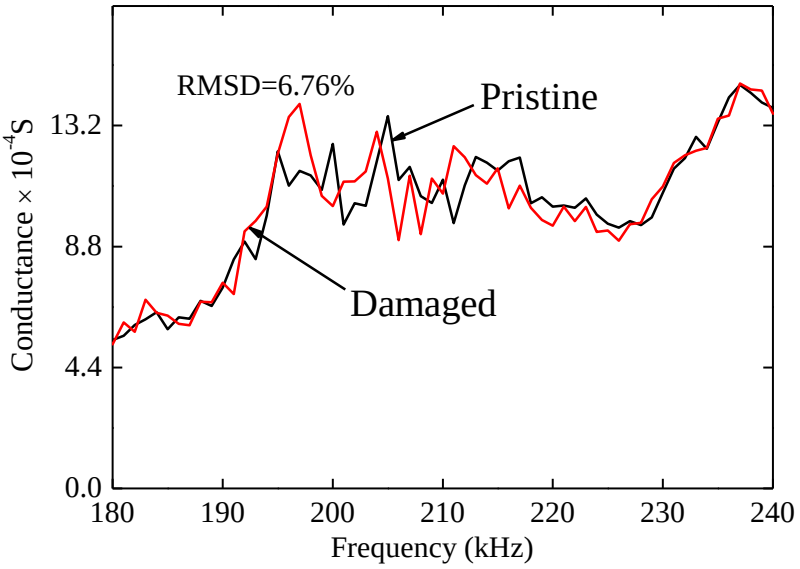

Figure 3.11: Conductance signature of ARPS at the pristine and damaged condition with CEL piezo sensor

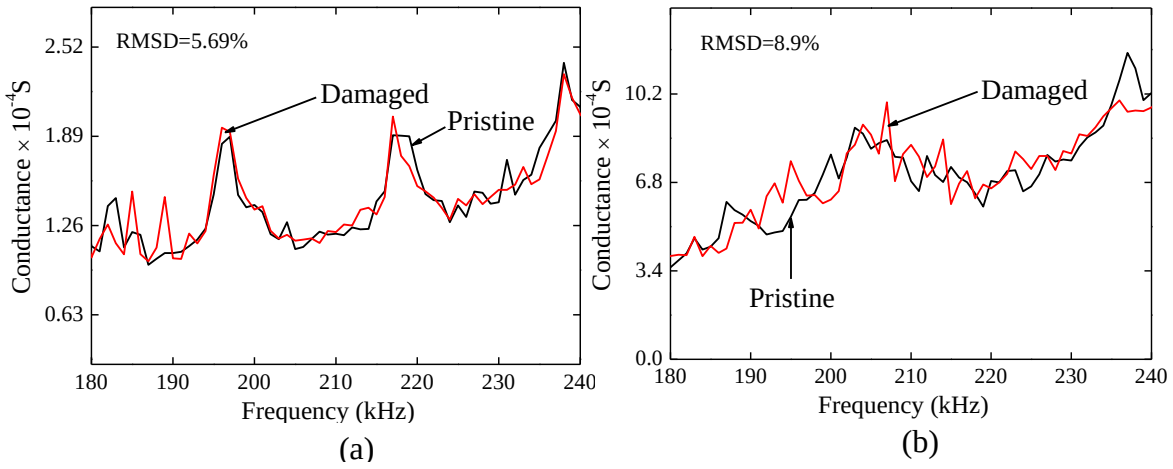

Figure 3.12: Conductance signature of ARPS at the pristine and damaged condition with (a) PI-5mm piezo sensor (b) PI-10mm piezo sensor

3.7 CONCLUDING REMARKS

In this study development and evaluation of ARPS was successfully tested. Out of three prototypes, prototype-III gave the best repeatability which was within the limit, *i.e.* CC index all greater than 99.5%. Here three different piezo sensors were analyzed. From the analysis best repeatability was acquired by both CEL and PI-10 mm piezo sensor. In case of damage, PI-10mm showed the satisfactory sensitivity of the damage. Thus, ARPS is more economical than the bonded piezo sensor. The proposed ARPS is simple and easy to handle since it is a simply a bolt with washer. For the fabrication on 2D structure prototype III will be discussed which is in the next Chapter.

CHAPTER 4

DEVELOPMENT AND EXPERIMENTAL VALIDATION OF DAMAGE DETECTION AND LOCALIZATION ALGORITHM USING ARPS ON 2D STRUCTURE

4.1 INTRODUCTION

For several past centuries steel has become one of the essential constructing materials and its application is overgrowing. In the previous chapter, ARPS was successfully developed. In the present study, a real-life structure, i.e., the 2D steel plate is considered for the validation of ARPS. At first assessment of structure was done by acquiring signatures. Later sensitivity of the damage was performed by EMI technique.

4.2 PROPOSED DAMAGE DETECTION ALGORITHM

The proposed algorithm is the extension of the algorithm on MWEMI by Naskar and Bhalla (2014). In this algorithm, ARPS is connected along X and Y axis of the steel plate.

The steps given below are followed in damage detection and localization.

i. Along both the axes acquire baseline signature of the 2D plate structure on each location, i.e., A to D and 1 to 4.
ii. For the assessment of the structure at any stage of the life again acquire the signature on each location.
iii. Compute the CC index in each location. CC less than 99.5% there is the chance of damage in the structure, then compute the RMSD index for the damage identification and localization. Here the ARPS gives the damage index along the gridline of the PZT patch.
iv. The average of the RMSD index is then calculated along the edge of the i and (i+1) sensor.
v. Plot the average RMSD index along both the axes. Maximum value of RMSD index along the axes defines the damage location.
vi. The exact location of the damage is identified by plotting the maxima histogram from the both axes.

4.3 FABRICATION DETAILS OF EXPERIMENTAL PROTOTYPE STRUCTURE

The experimental specimen used earlier by Shanker (2010), Naskar (2014) and Supriya (2018) was used in this study. The steel plate of size 1200 × 970 mm^2, supported on box type pipe of cross section 38×38 mm^2 and 3mm thickness was used. The pipeline was welded along the steel plate and supported by wheel on four corners. The steel plate composes of carbon (0.23 %), manganese (1.5 %), sulphur (0.045%), phosphorus (0.045%) and silicon (0.40%) as per IS-2062, 2006.

In the test specimen ARPS is attached as shown in Figure 4.1 (a), using the torque 25 Nm in (m + n) fashion. Two damage location were chosen as shown in Figure 4.1 (b) and (c). In the pristine condition these holes were covered by plates of 150×150 mm in size. This plate was attached in the main plate by the four bolts of 10mm diameter with 35Nm torque. Damage was created on the plate by loosening the bolt. The ARPS is attached on both the direction, i.e. x-direction and y-direction as shown in Figure 4.1 (d).

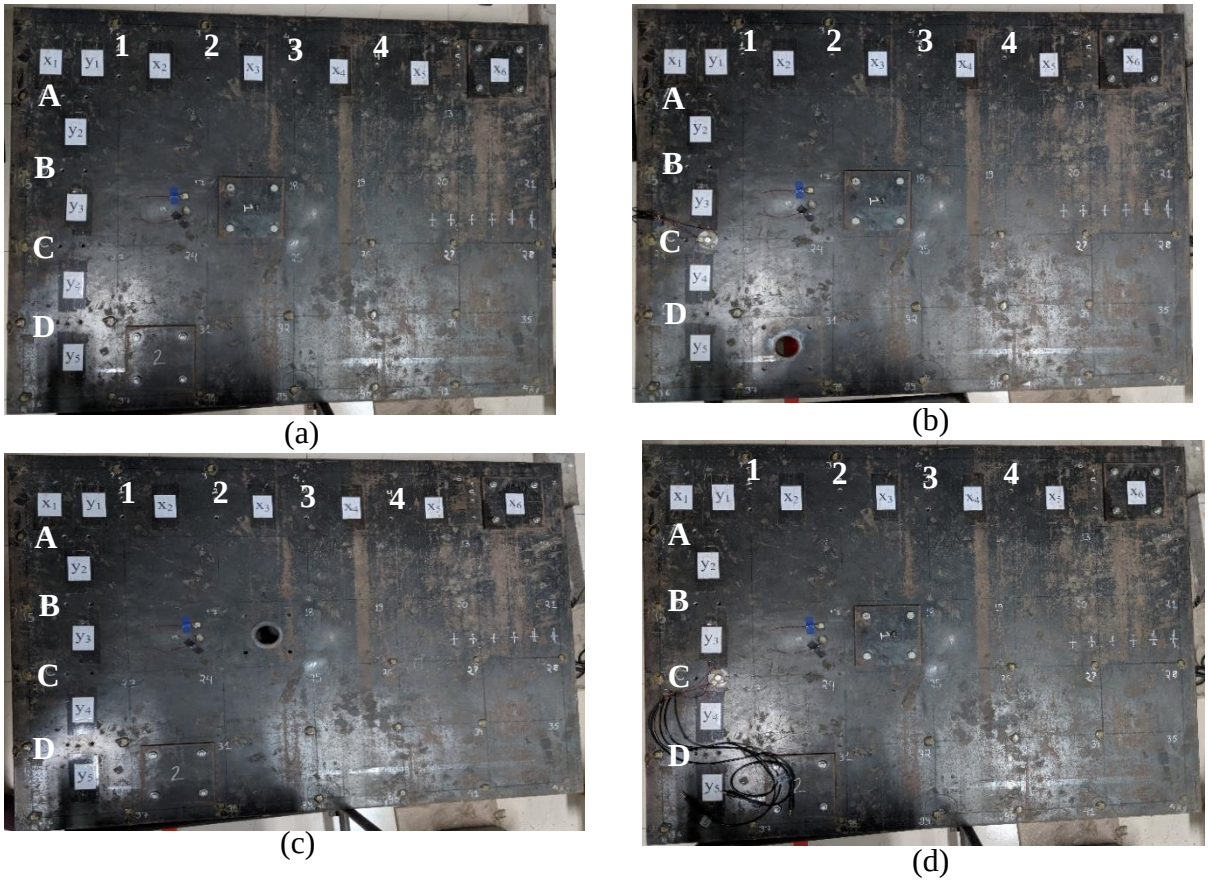

(a) (b) (c) (d)

Figure 4.1: Experimental prototype structure (a) 2D steel plate (b) plate with damage-1 (c) plate with damage-2 (d) plate with ARPS

4.4 EXPERIMENTAL DETAILS

The ARPS attached to the monitored structure was electrically excited at frequency of 100-300kHz through impedance analyser (Agilent E4980A) to acquire the admittance signature. These admittance signature can be decomposed and analysed to extract the impedance parameters of the structure. Thus, obtained impedance parameters are used to identify the exact damage in the structure. Here in this study RMSD index is used to quantify and localize the damage. Figure 4.2 shows the overall view of the experimental detail.

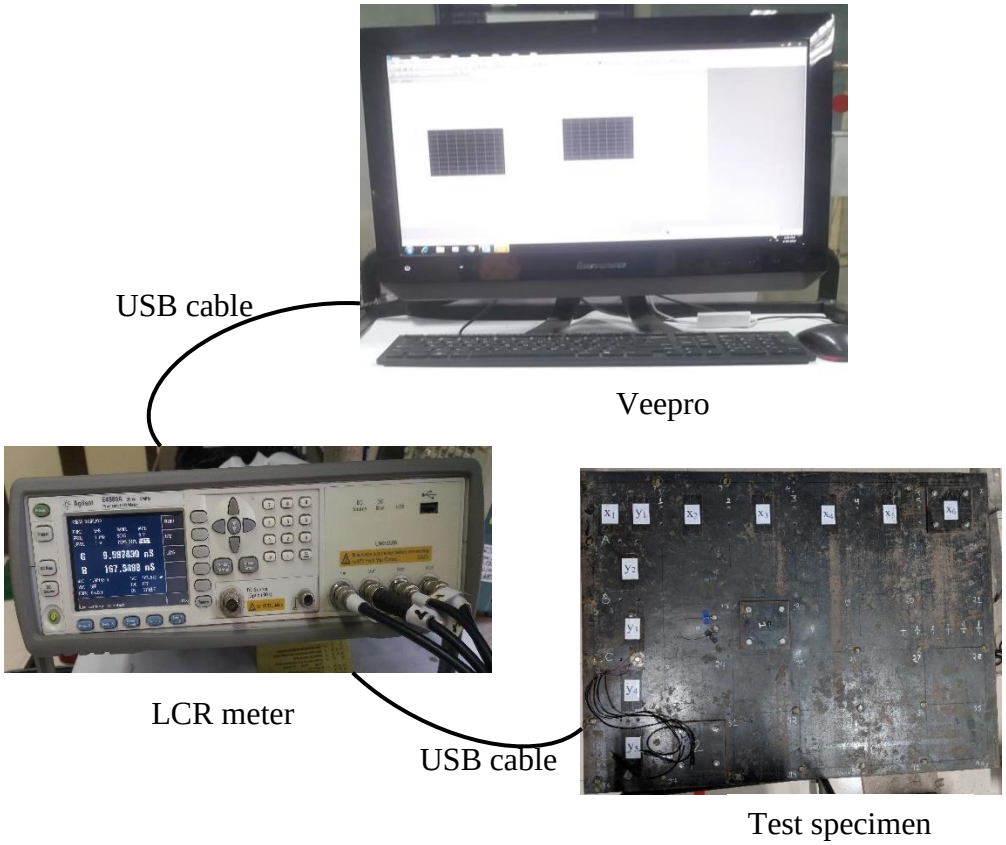

Figure 4.2 Overall view of experimental detail

4.5 REPEATABILITY OF SIGNATURES

Repeatability of the signature is important to maintain consistency of signatures obtained. In this test, repeatability of the signatures was checked on the same ARPS at 8V and temperature 25ºC by tightening at torque of 25Nm, loosening it to full and again tightening at same torque. Here

repeatability of the signature in CC index was found to 99.92%. Figure 4.3 shows the conductance signature of ARPS for repeatability.

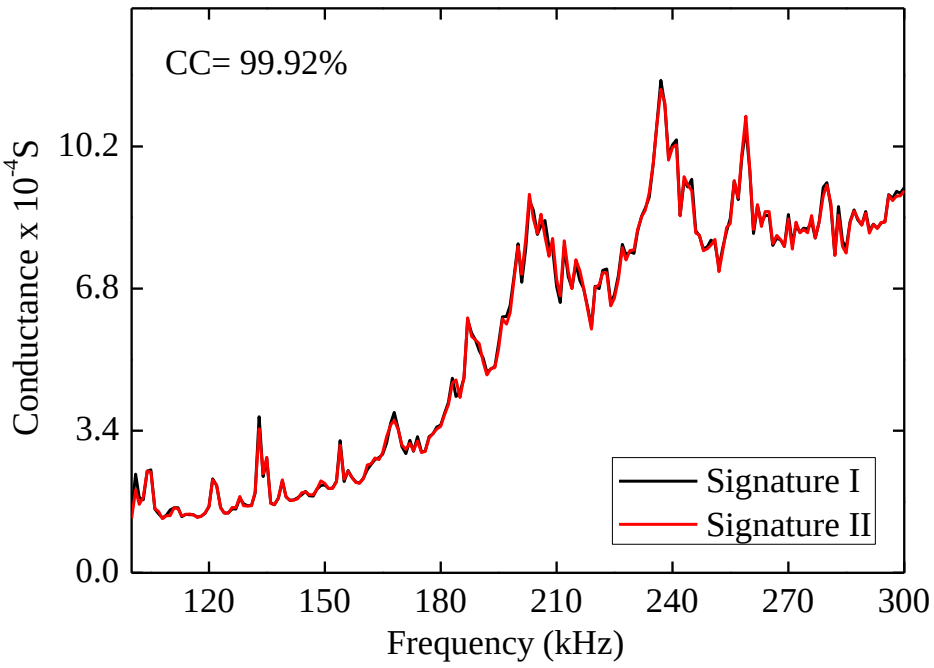

Figure 4.3: Repeatability of signature

4.6 EXPERIMENTATION FOR DAMAGE LOCATION IDENTIFICATION

The main aim of this experiment is to validate the ARPS damage location algorithm. Also, detection and localization of damage. Here, in this study two damages damage-1 and damage-2 in the 5cm size hole diameter as shown in Figure 4.4 (a) and (b) respectively. Retrofitting measure was applied as placing the plate of size 15×15cm with four 10mm bolts tightened with 35Nm torque. The cover plate was placed to achieve a repaired condition. Total eight holes were drilled four along X-axis and four along Y-axis, on each location ARPS was tightened with torque range and signatures were obtained. In case of damaged condition, four bolts with the cover plate were removed and signatures were acquired closing the other hole.

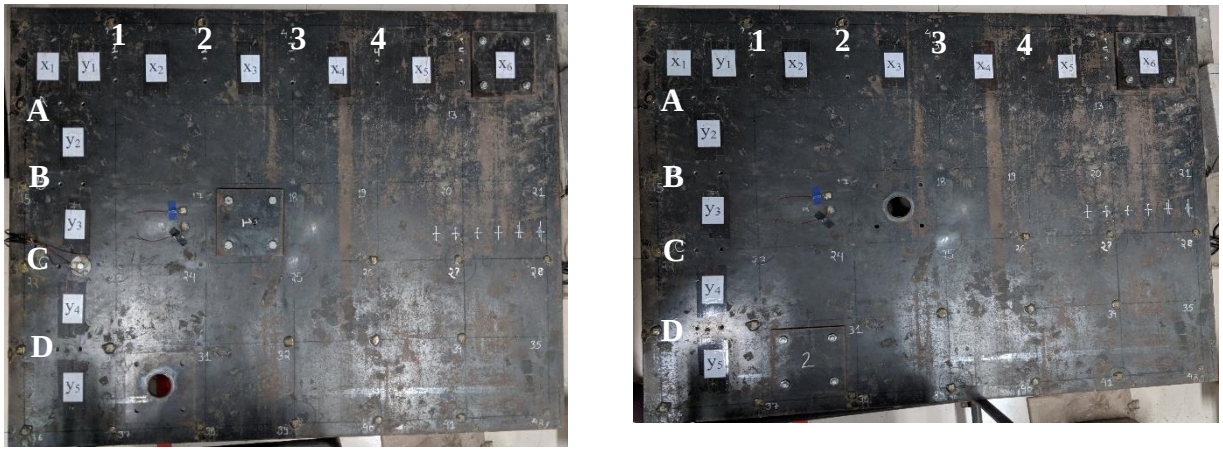

(a) (b)

Figure 4.4 Damage Location on the steel plate (a) damage location-1 (b) damage location-2

4.7 EXPERIMENT RESULTS

4.7.1 Damage localization for location 1

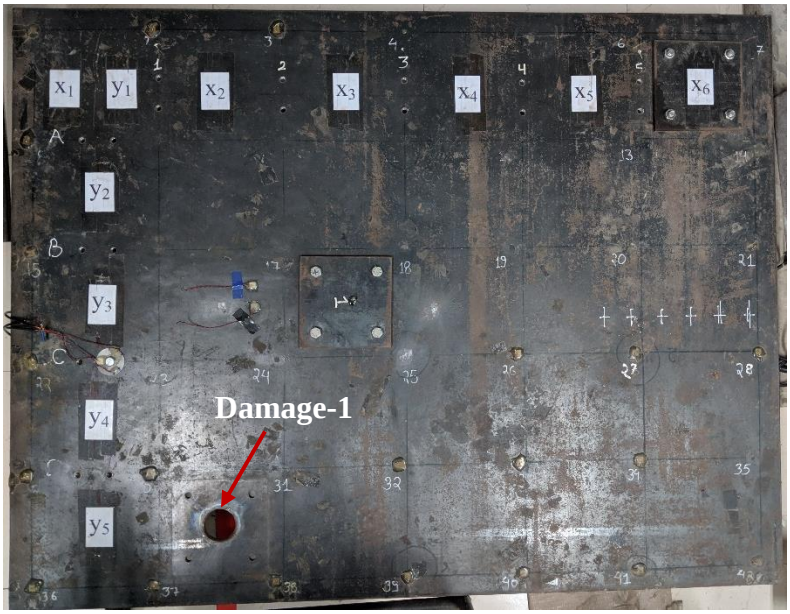

Figure 4.5: Steel plate with damage location 1

For the damage location 1, the pristine and damaged condition reading were compared and shown in Appendix A. The RMSD of all the three sensors were determined and plotted for the damage location as shown in Figure 4.6-4.9.

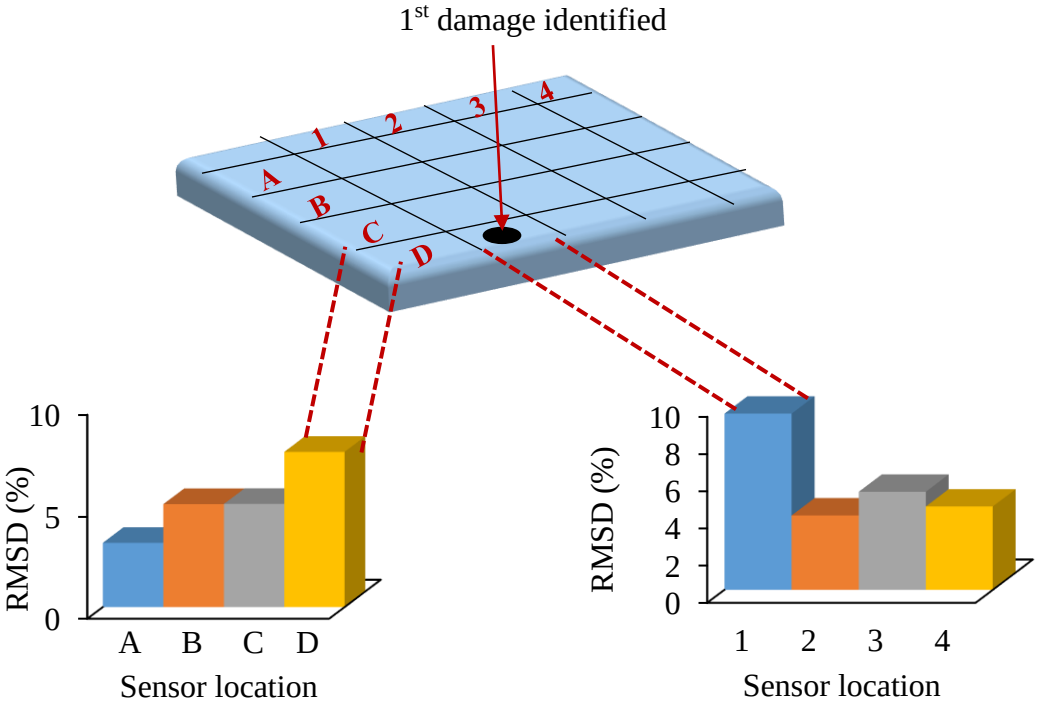

Figure 4.6: Damage location by CEL piezo sensor

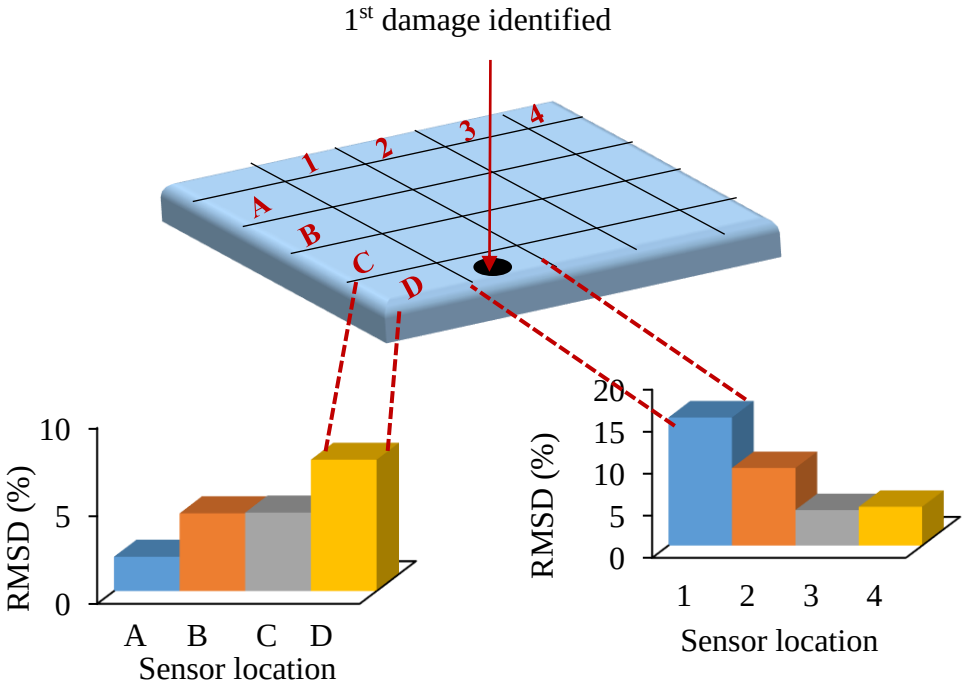

Figure 4.7: Damage location by PI-5mm piezo sensor

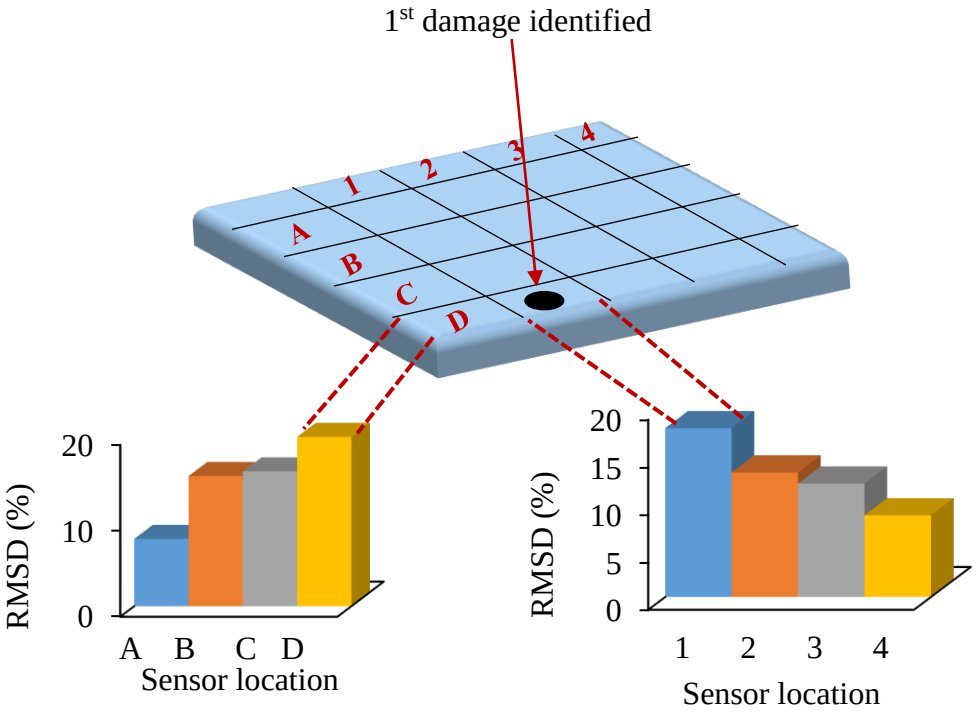

Figure 4.8: Damage location by PI-10mm piezo sensor

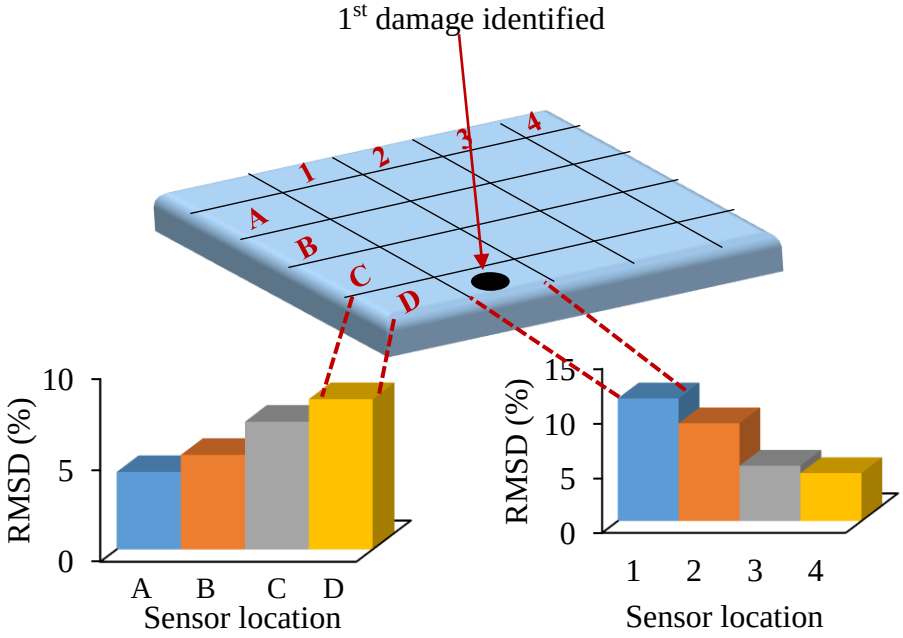

Figure 4.9: Damage location-1 by RBPS

4.7.2 Damage localization for location 2

For the damage location 2, the pristine and damaged condition reading were compared and shown in Appendix B. The RMSD of all the three sensors along with RBPS were determined and plotted for the damage location as shown in Figure 4.11-4.14.

Figure 4.10: Damage-2 on the steel plate

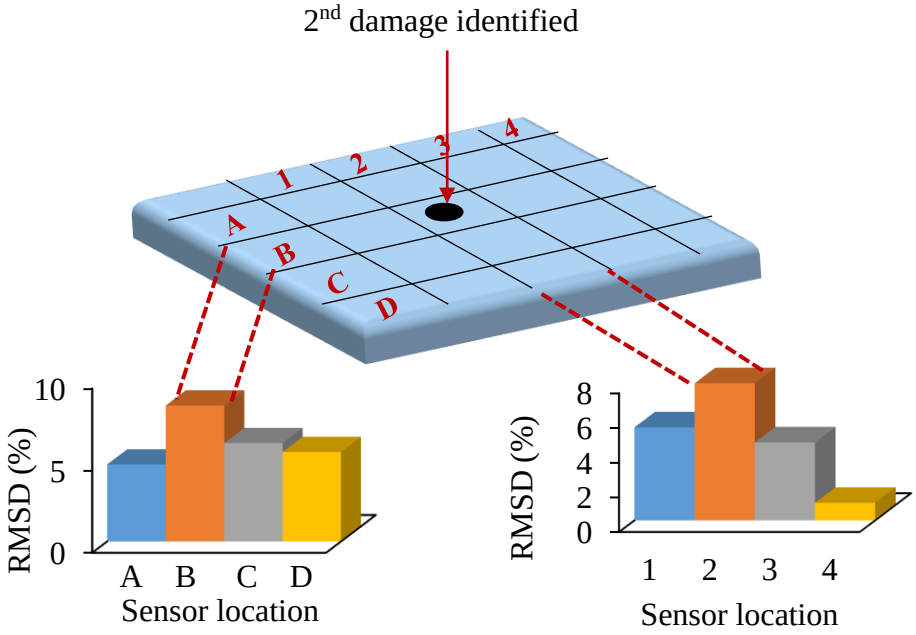

Figure 4.11: Damage location-2 by CEL piezo sensor

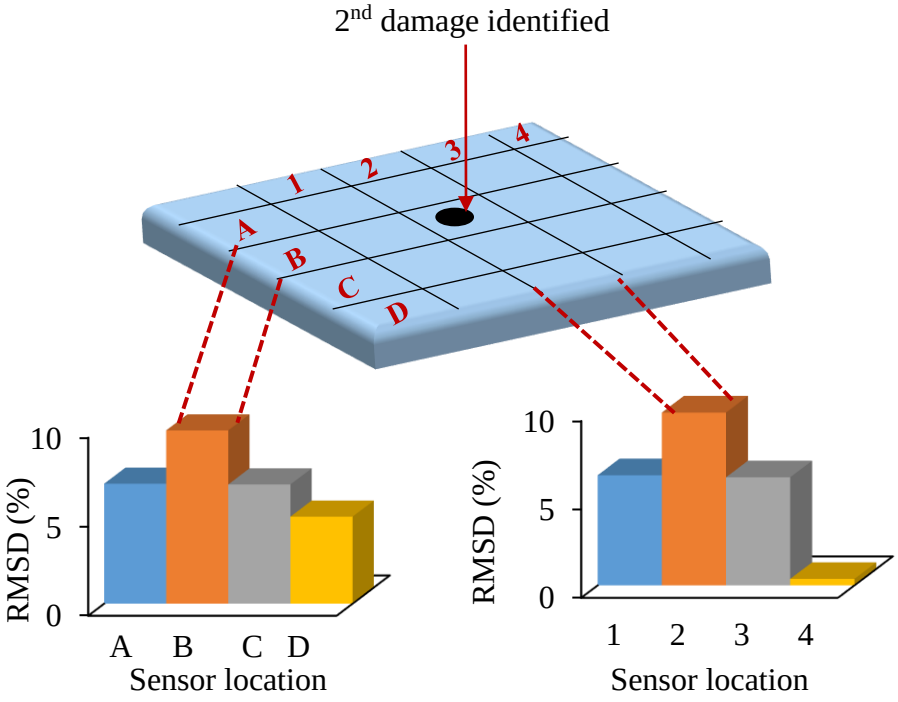

Figure 4.12: Damage location-2 by PI-5mm piezo sensor

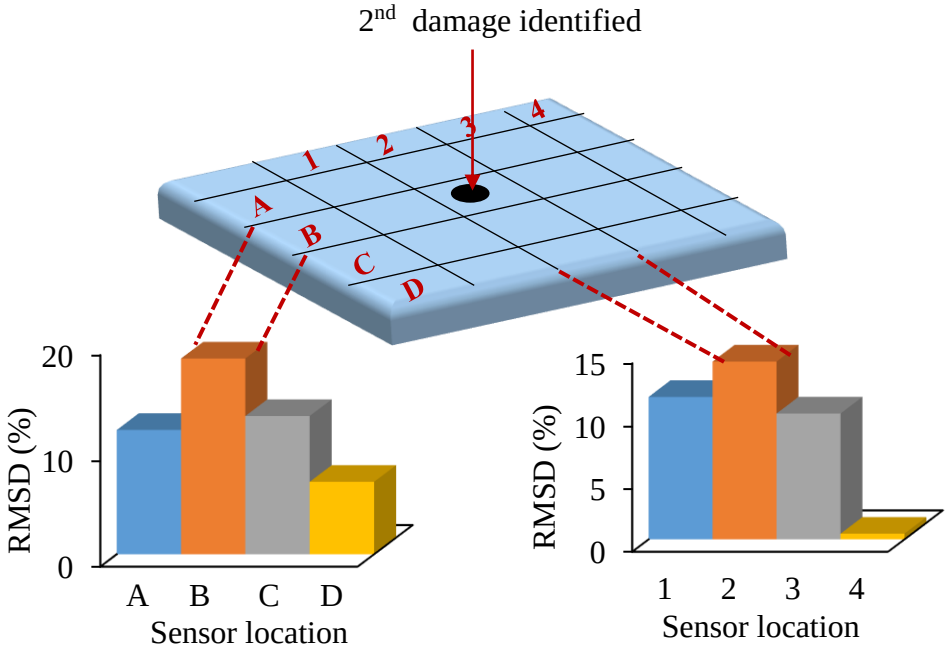

Figure 4.13: Damage location-2 by PI-10mm piezo sensor

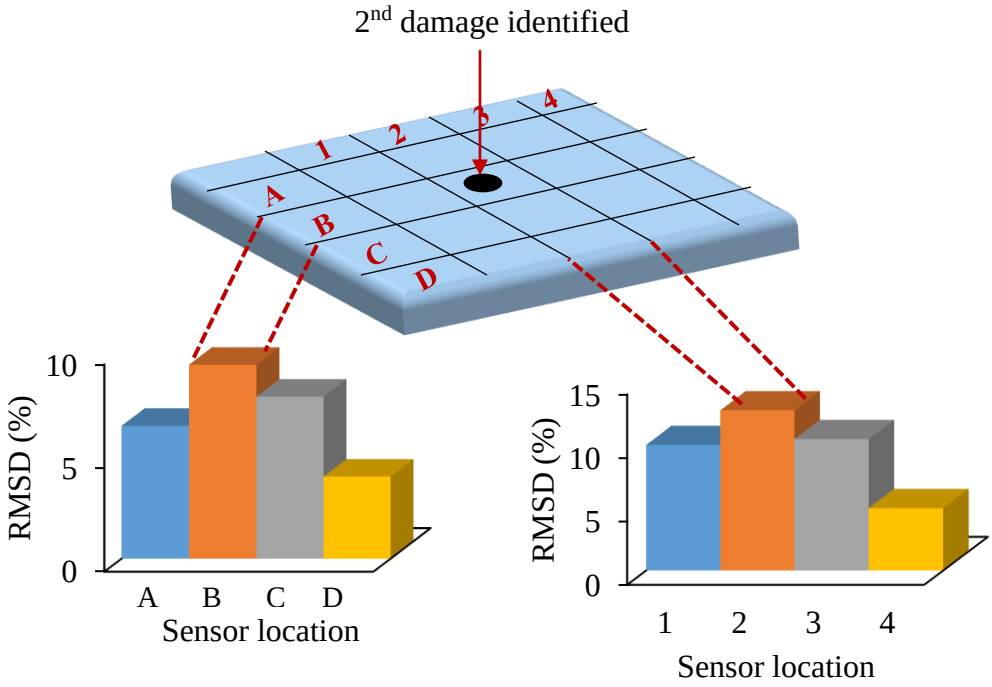

Figure 4.13: Damage location-2 by RPBS

4.8 SUMMARY CONCLUDING REMARKS

Experimental results shown in this chapter shows the effectiveness of ARPS. The damages were correctly identified. Since conventional reusable piezo sensor identified the damage but handling it was difficult with time consuming. ARPS minimized the time and handling was easy. This shows ARPS can be used for the large host structure.

CHAPTER 5

TEMPERATURE EFFECT ON PIEZO SENSOR SIGNATURE

5.1 INTRODUCTION

It is a well-known fact that the signature of the piezo sensors is very sensitive to the temperature changes. This may, however, trigger a false alarm. Experimental investigations conducted in controlled environment do not require temperature compensation to be carried out. However, in real life situations, temperature effects cannot be ignored. This chapter investigates the effect of temperature on EMI signature of the piezo sensors and its compensation.

5.2 IMPEDANCE RELATION FOR A FREE PZT PATCH

Liang et al. (1994) derived admittance value as given in equation 5.1 by impedance approach.

$$\bar{Y} = 2\omega j \frac{wl}{h}\left[\overline{\varepsilon_{33}^{T}} + \left(\frac{Z_a}{Z+Z_a}\right) d_{31}^2 \overline{Y^E}\left(\frac{\tan \kappa l}{\kappa l}\right) - d_{31}^2 \overline{Y^E}\right] \tag{5.1}$$

For free-free condition impedance of the structure (Z) is zero. For quasi static condition, $f=1/5f_N$, $\frac{\tan kl}{kl}$ =1 substituting both the values in equation 5.1 we get,

$$\bar{Y} = 4\omega j \frac{wl^2}{h}\left[\varepsilon_{33}^{T}(1-\delta j)\right] \tag{5.2}$$

where, conductance is $G = \frac{4\omega l^2}{h}\delta\varepsilon_{33}^{T}$ and susceptance is $B = \frac{4\omega l^2}{h}\varepsilon_{33}^{T}$

Bhalla (2001) derived ε_{33} from below relation,

$$d_{31} = k_{31}\sqrt{\varepsilon_{33}^{T} S_{11}^{E}} \tag{5.3}$$

where, S_{11}^{E} is the inverse of the Young's modulus of the PZT patch.

5.3 EXPERIMENTAL DETAILS

For this present study, a piezo sensor of 10 × 10 × 0.3 mm was surface bonded on an aluminum plate of 200 × 25 × 2 mm (Figure 5.1a) using a two-part epoxy adhesive. Besides this for testing the free piezo behaviour, a single PZT patch was held between two pointed terminals as shown in Figure 5.1b. Signatures were acquired through Agilent E4980A LCR meter using VEEPRO platform in a temperature range of 40-70 °C. The structure with the bonded piezo sensor and the free piezo sensor was placed in the oven and admittance signature were acquired in the range of 1-200kHz. Figure 5.2 shows the complete setup of the experiment.

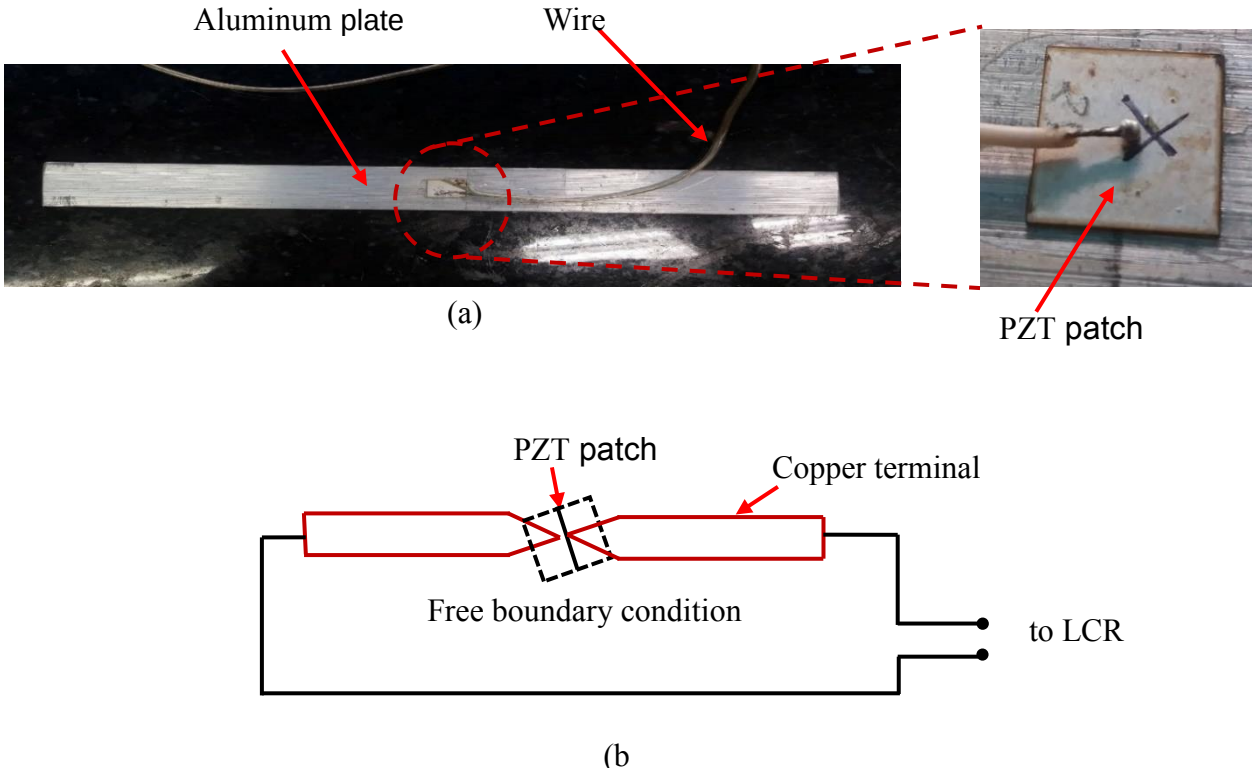

Figure 5.1: (a) Surface bonded PZT patch on aluminum plate (b) free PZT patch setup

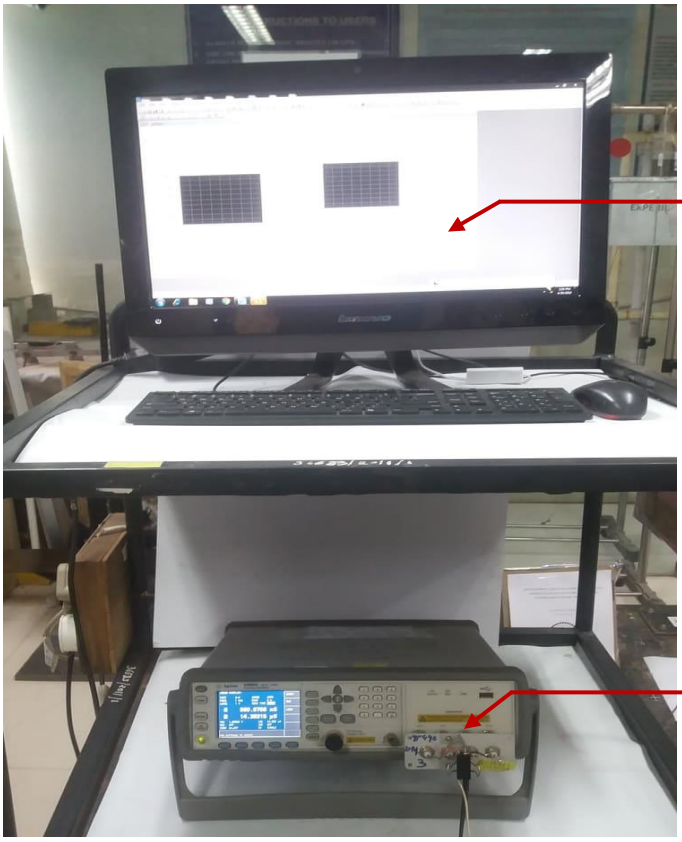

(a)

(b)

(c)

Figure 5.2: Complete set up of the experiment (a) LCR meter and Vee Pro platform (b) Specimen inside oven (c) Oven

5.4 EXPERIMENTAL OBSERVATIONS

a. Surface bonded piezo sensor

Figure 4.3 shows a plot of the conductance and susceptance signatures in 1-200 kHz range.

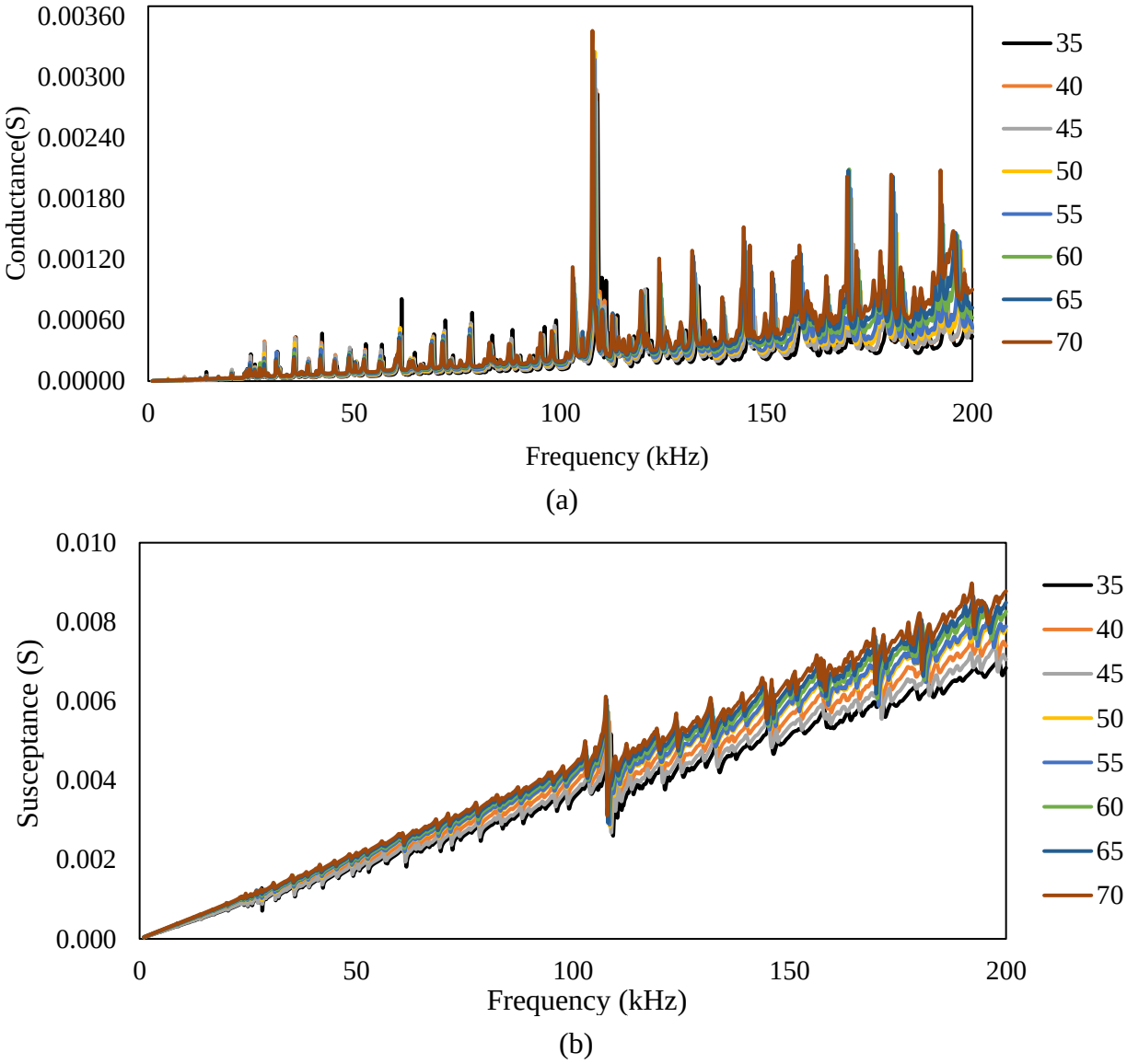

Figure 5.3: (a) conductance and (b) susceptance signature for bonded PZT patch at various temperature

It is observed that both the conductance and susceptance signatures shift towards the left with the increase on temperature. Figure 5.4 shows the RMSD index for different temperature. The horizontal shift was computed using iterations for different frequencies and vertical shift was

calculated by taking the average of the difference between two signatures. Figure 5.5 and 5.6 below shows the nature of shift horizontally and vertically.

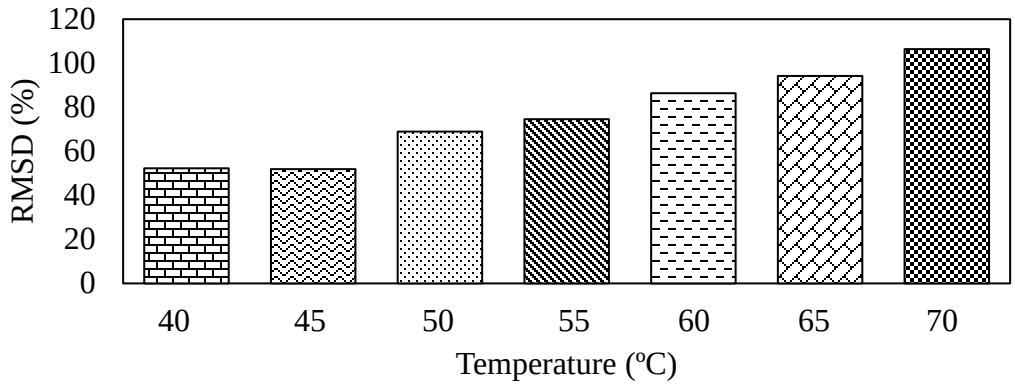

Figure 5.4: RMSD index at different temperature

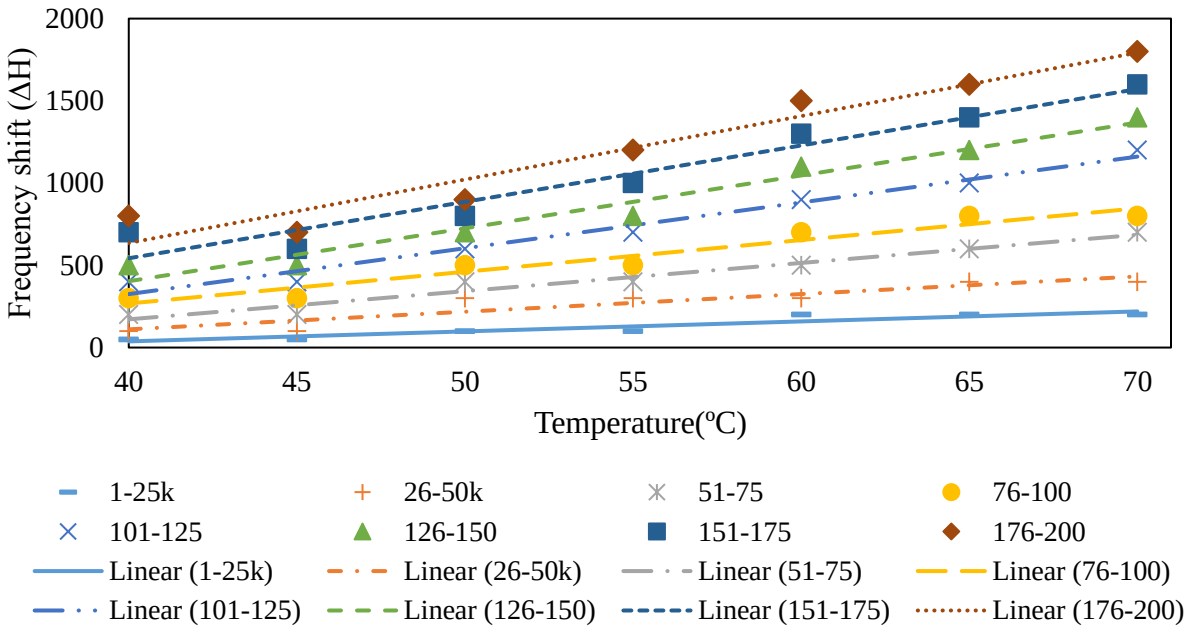

Figure 5.5: Horizontal shift as a function of temperature

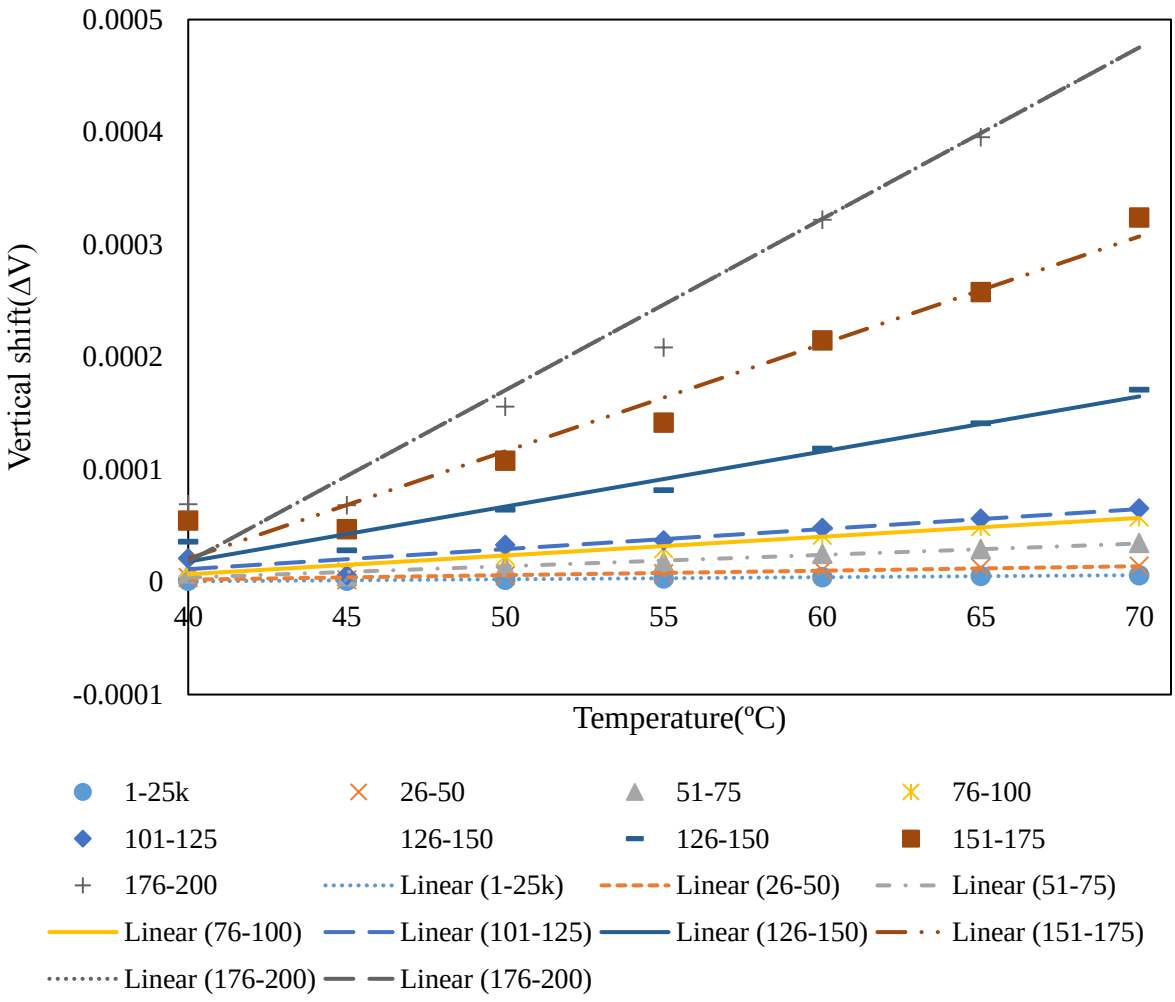

Figure 5.6: Vertical shift as a function of temperature

From Figure 5.5 and 5.6, it was clearly observed that both horizontal and vertical shifts are temperature dependent, the amount increasing with temperature. The shift shows a linear variation with increase in the temperature for all the frequency changes. The slope of the curve increases in both shifts which indicates shifts are also frequency dependent. This fact was incorporated into the raw compensation technique of the signatures.

b. Free piezo sensor

Figure 5.7 shows a plot of the conductance and susceptance signatures in 1-200 kHz range

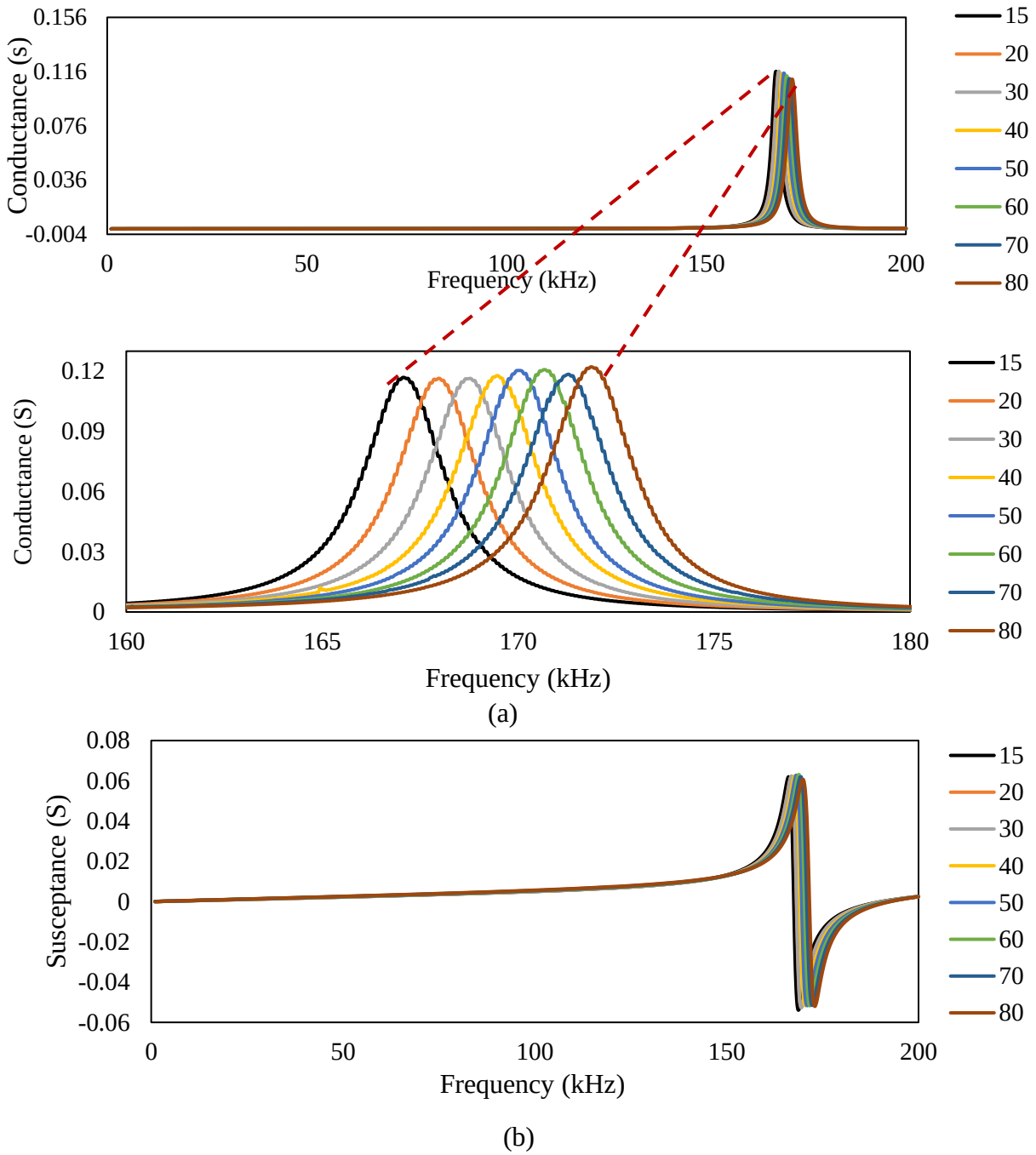

Figure 5.7: Signature plot of free piezo for various frequency range (a) Conductance (b) Susceptance

Unlike bonded piezo, it was observed that in case of free PZT patch both the conductance and susceptance signatures shifted towards the right with the increasing temperature.

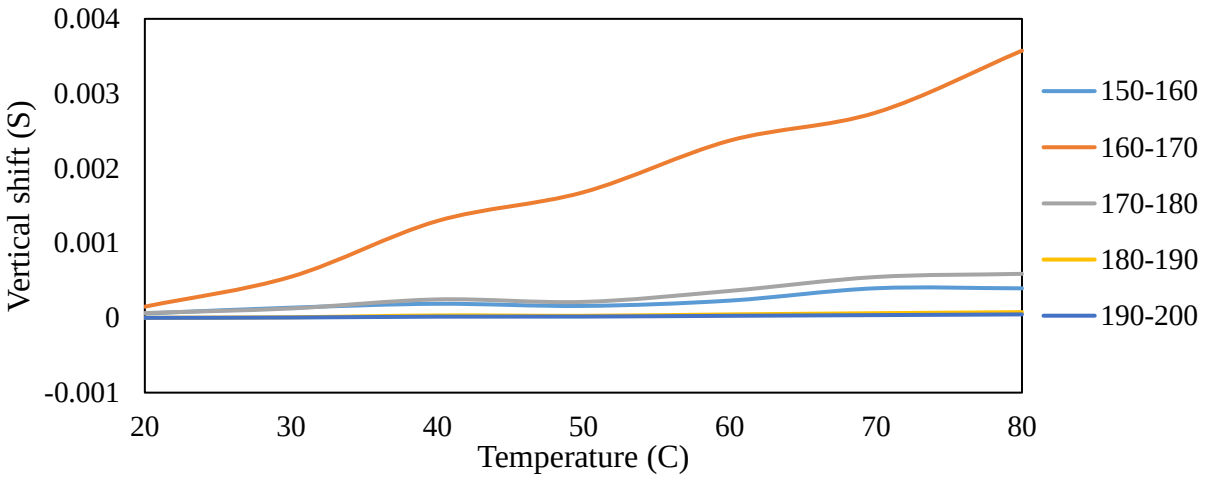

Figure 5.8: Vertical shift as a function of temperature

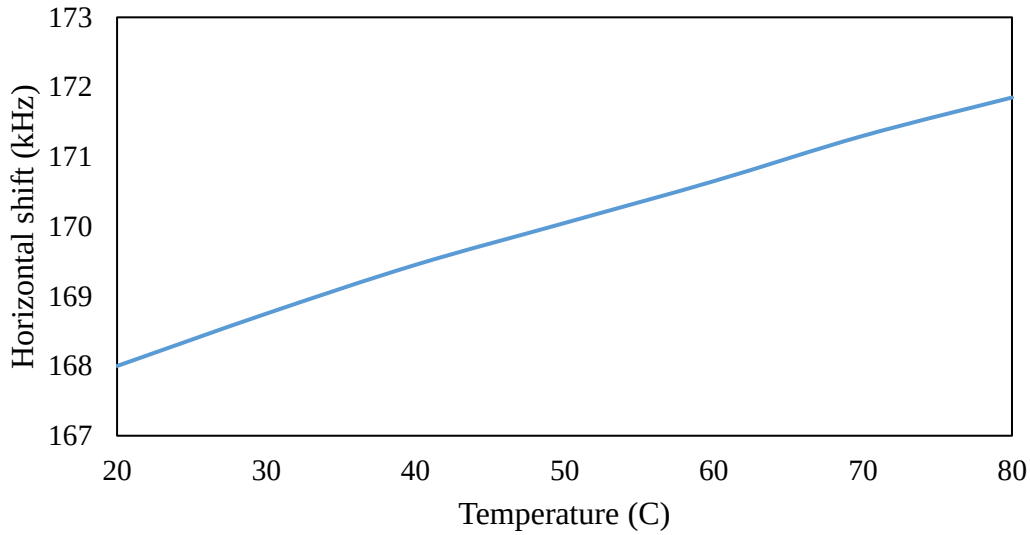

Figure 5.9 Horizontal shift as a function of temperature

Here, the shift in the signature (Figure 5.8 and 5.9) is shift in first natural frequency with respect to temperature. Both horizontal and vertical shift with temperature have linear variation.

5.5 ANALYTICAL OBSERVATION

Free piezo signatures were acquired analytically for different temperatures using MATLAB program (Appendix-D). Here, for different temperature, value of d_{31} and ε_{33} are different as shown in Figure 5.10. These values were considered along with the compensation of thermal expansion for length of PZT patch to obtain the signatures of the free piezo sensor.

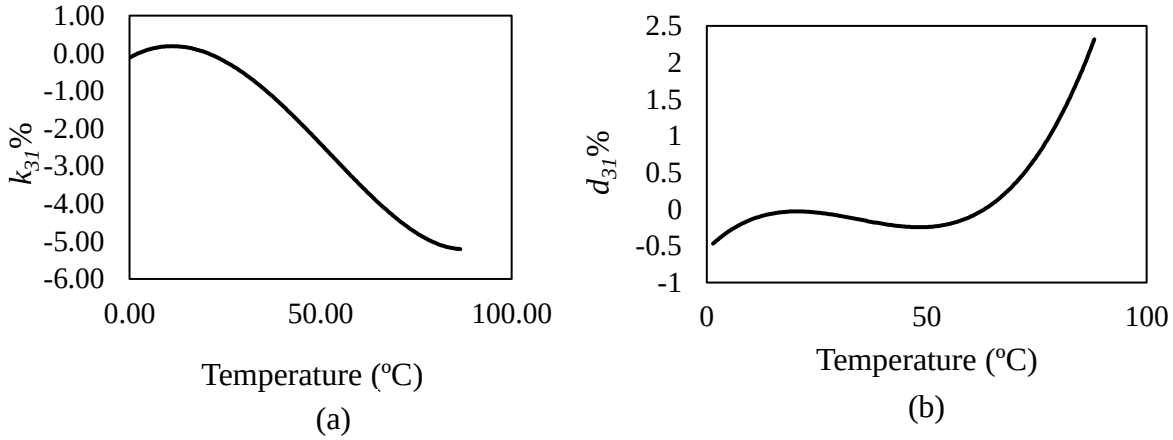

Figure 5.10: (a) Temperature dependence of k_{31} (b) temperature dependence of d_{31}

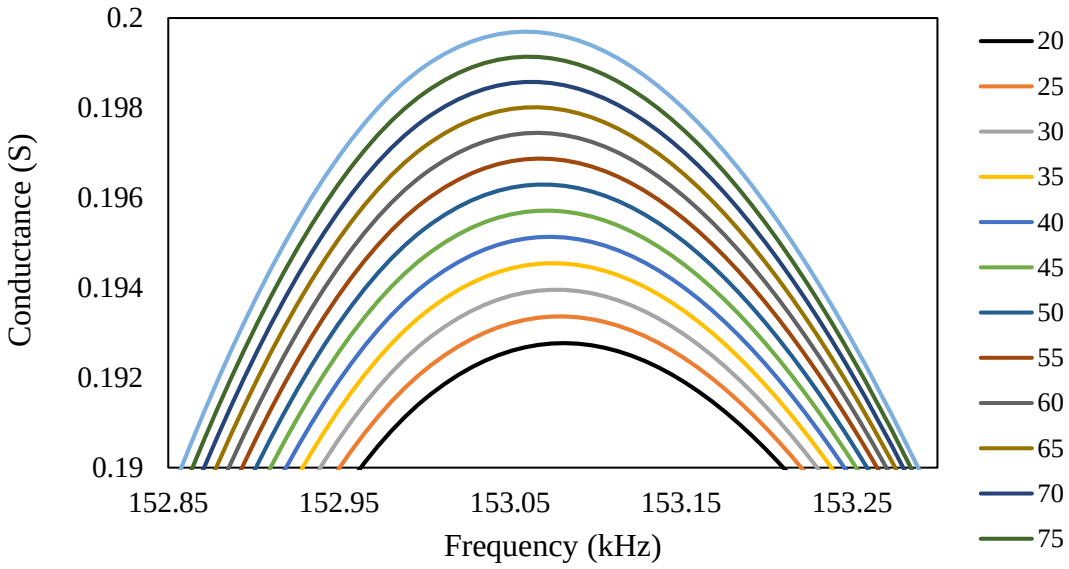

Figure 5.11: Signatures on different temperature due to change in length

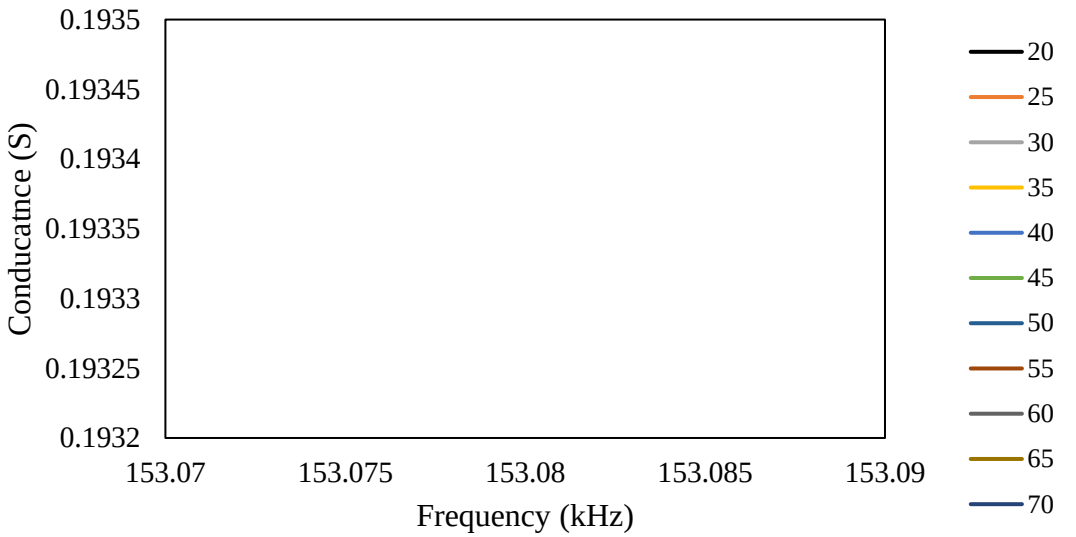

Figure 5.12: Signatures on different temperature due to change in ε_{33}

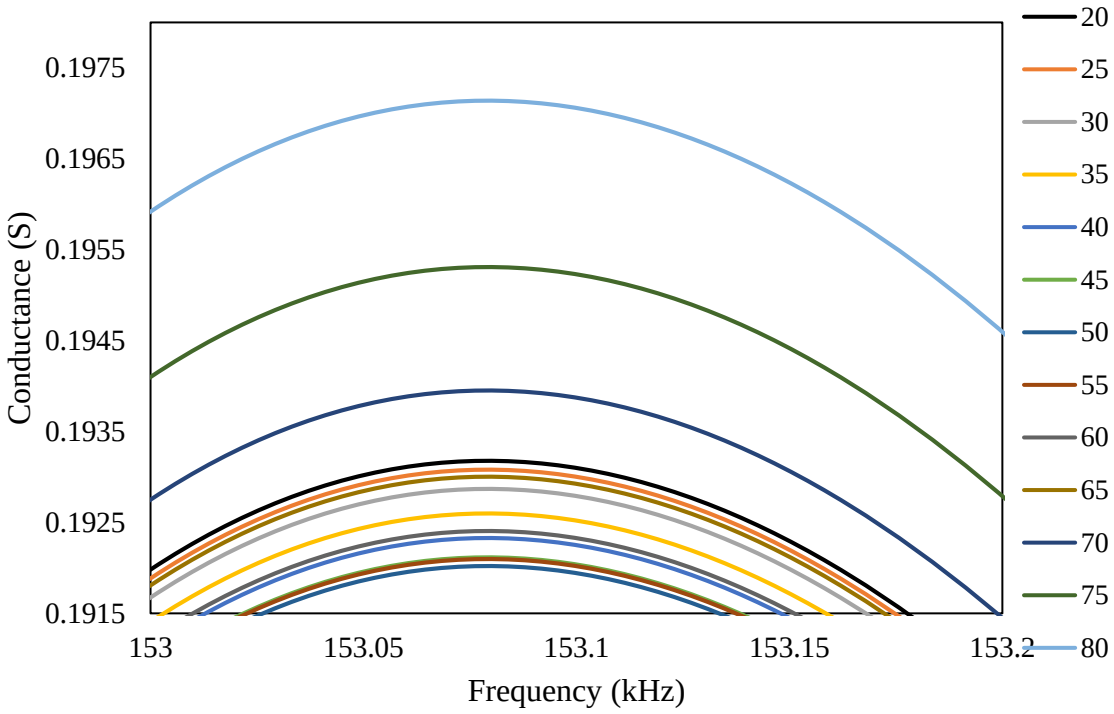

Figure 5.13: Signatures on different temperature due to change in d_{31}

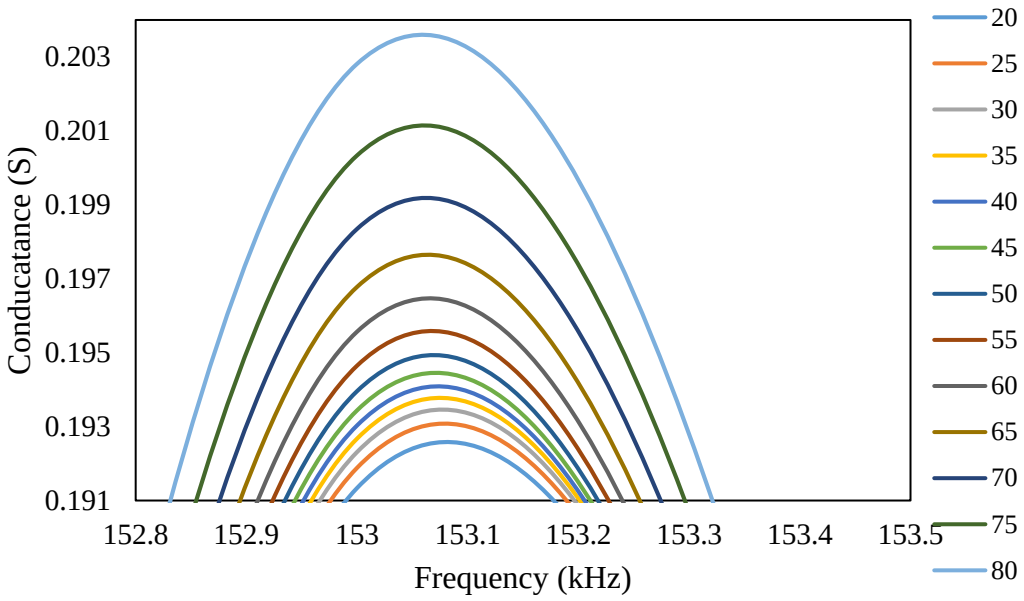

Figure 5.14: Signatures on different temperature due to change in all parameters

It was clearly seen that due to thermal expansion of the length there is vertical shift in the signature as shown in Figure 5.11. Effect of ε_{33} is minimum in the signatures as shown in Figure 5.12 whereas d_{31} showed the minimum effect at lower temperature and shift increased with the increasing temperature in Figure 5.13. Combining all the parameters *i.e.* length, d_{31} and ε_{33} the shift increases with the increase in temperature as shown in Figure 5.14.

5.6 FE MODELLING BY COUPLED FIELD ANALYSIS

Coupled field analysis was performed which encounter both electric and structural degree of freedom. To study the interaction of piezoelectric sensor with the host structure coupled field analysis was done which reflects the electro-mechanical coupling character of the piezoelectric material. The present coupled field analysis used the host structure as aluminum beam of dimension 200×25×2 mm on which a PZT patch of 10×10×0.3 mm was modelled. Only 1/4th of the specimen was modelled due to its symmetry on both the axes. This reduced the significant computational time on the modelling (Adhikari and Bhalla, 2018). Figure 5.15 (a) shows the 1/4th modelling of the aluminum block with PZT patch on it.

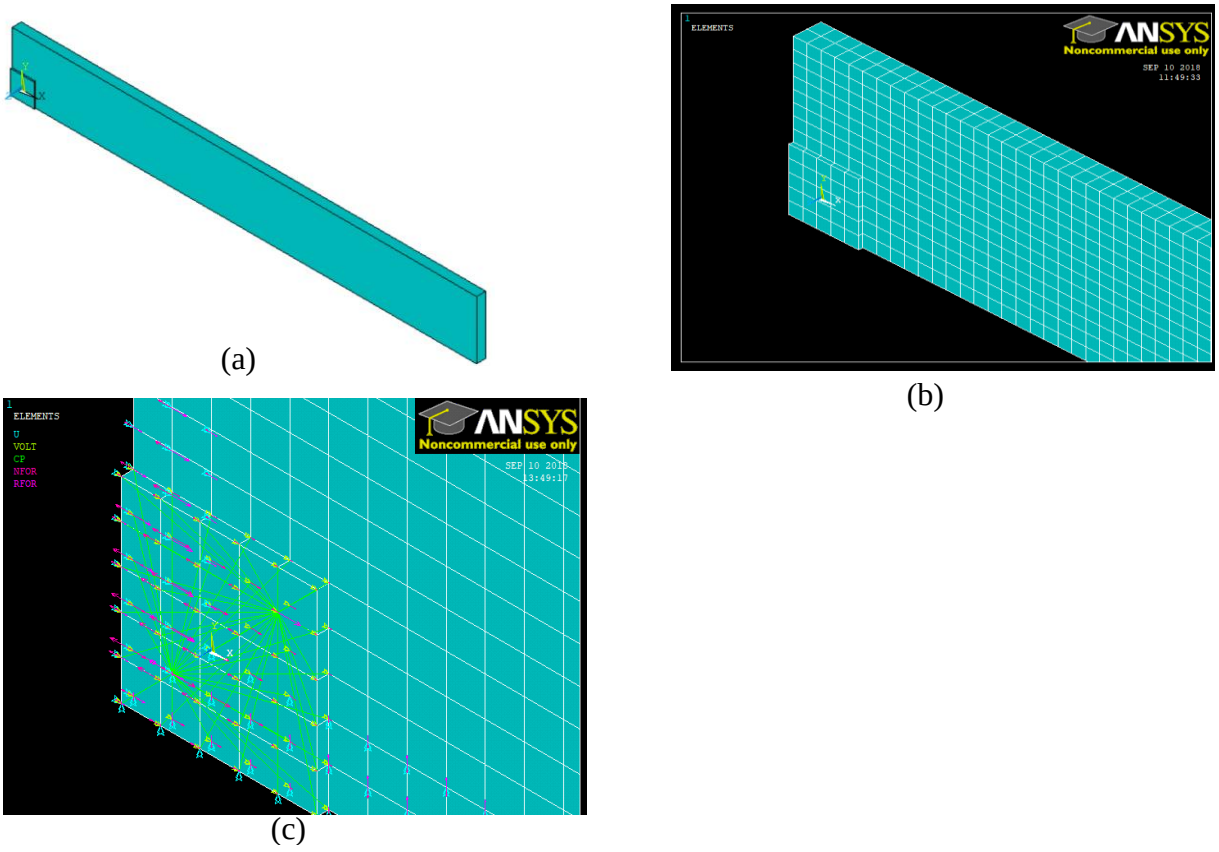

Figure 5.15: (a)1/4th modelling of the aluminum block with PZT patch (b) meshing of the model (c) coupling effect

Table5.1: Properties of test specimen (Aluminum Beam at ambient temperature)

Modulus of Elasticity (E)	68.95 GPa
Poisson Ratio (υ)	0.33
Density (ρ)	2715 kg/m^3
Mass damping factor (α)	0
Stiffness Damping factor (β)	3×10^{-9}

The key properties of the aluminum block were listed on Table 5.1. Young's modulus, Poisson's ratio, density, Rayleigh damping coefficient were considered on the FE modelling of aluminum beam as given in Table 5.1. For the aluminum beam solid 45 element and for PZT solid 5 was taken and a volume was created. The piezo properties were assigned according to the data given in Table 5.2.

Table 5.2: Properties of piezoelectric of PIC 151.

Parameters	Symbols	Values	Unit
Density	ρ	7800	kg/m^3
Dielectric loss factor	$tan\delta$	0.02	-
Compliance	S_{11}	15	$\times 10^{-12}$ m^2/N
	$S_{22} = S_{33}$	19	
	$S_{12} = S_{21}$	-4.5	
	$S_{13} = S_{31}$	-5.7	
	$S_{23} = S_{32}$	-5.7	
	$S_{44} = S_{55}$	39	
	S_{66}	49.4	
Electricity Permittivity	ε_{11}^{T}	1.75	$\times 10^{-8}$ F/m
	ε_{22}^{T}	1.75	
	ε_{33}^{T}	2.12	
Piezoelectric Strain Coefficients	d_{31}	-2.10	$\times 10^{-10}$ m/V
	d_{32}	-2.10	
	d_{33}	5.0	
	d_{24}	5.8	
	d_{15}	5.8	

Boundary condition was given appropriately to the model. In x-z plane displacements in y-direction was given zero and in y-z plane displacements in x direction was given zero. At the middle of the bottom of the specimen displacement in all directions i.e. in x, y and z axes was zero. The free edges did not have any loading conditions. The model was mesh with the global mesh size of 1 mm. As PZT was kept in the middle of the specimen it was also modelled $1/4^{th}$ of its size. The nodes were then at the spacing of 1mm, then the load against the corresponding PZT dimensions were applied. The specimen was then excited to the frequency of 1-200 kHz. From Figure 5.15 (a) modulus of elasticity of aluminum beam at different temperature was taken. Density of aluminium beam (alloy 7041) at different temperature as shown in Figure 5.15 (b).

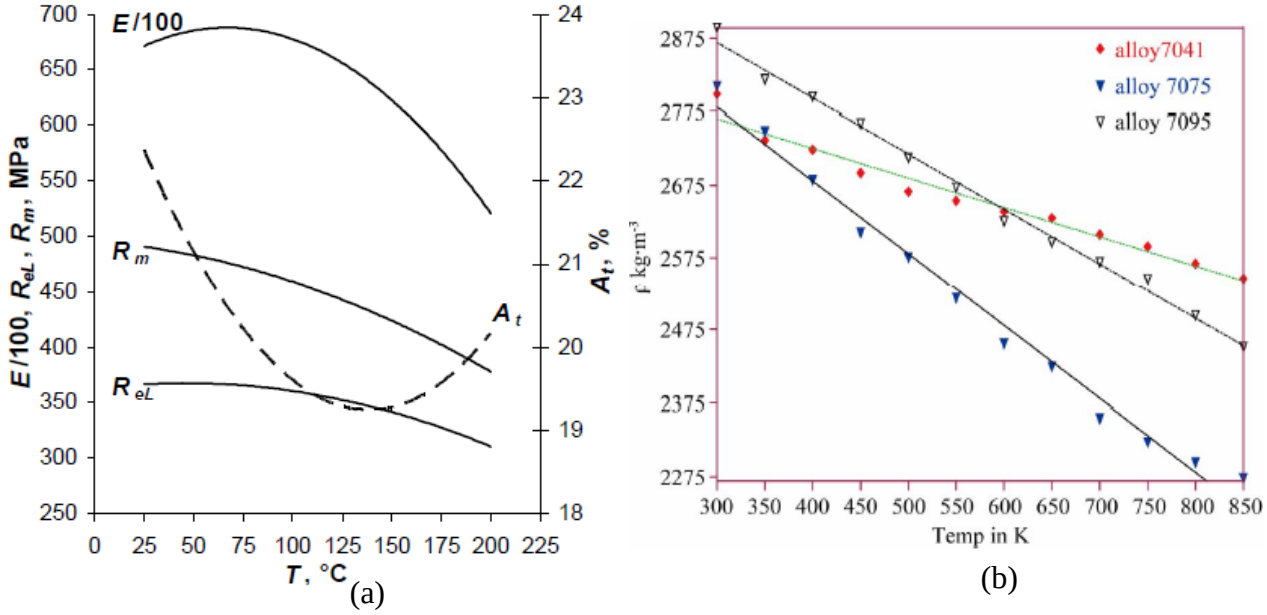

Figure 5.16: (a) Modulus of elasticity (Lipski and Mrozinski, 2012) and (b) density (Narender et. al., 2013) of aluminium beam at different temperature

For different temperature, modulus of elasticity and density of aluminim was varied to obtain admittance signature in the range of 1-200 kHz as shown in the Figure 5.17 and 5.18.

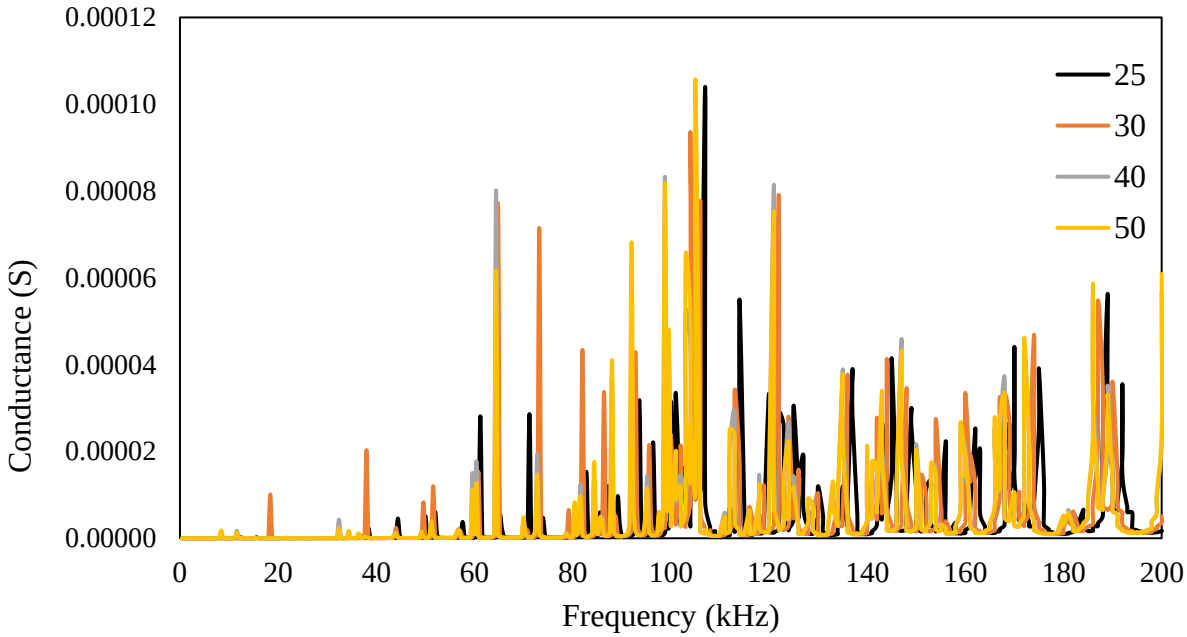

Figure 5.17: Conductance signature plot varying modulus of elasticity of the structure at different temperature.

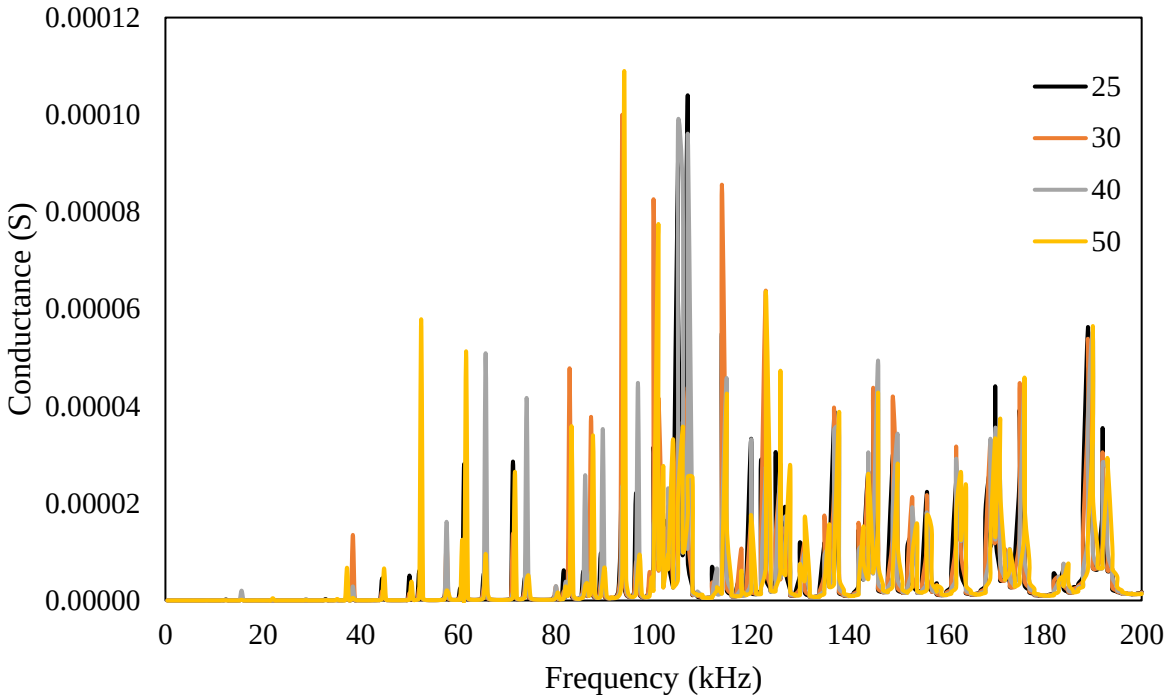

Figure 5.18: Conductance signature plot varying density of the structure at different temperature.

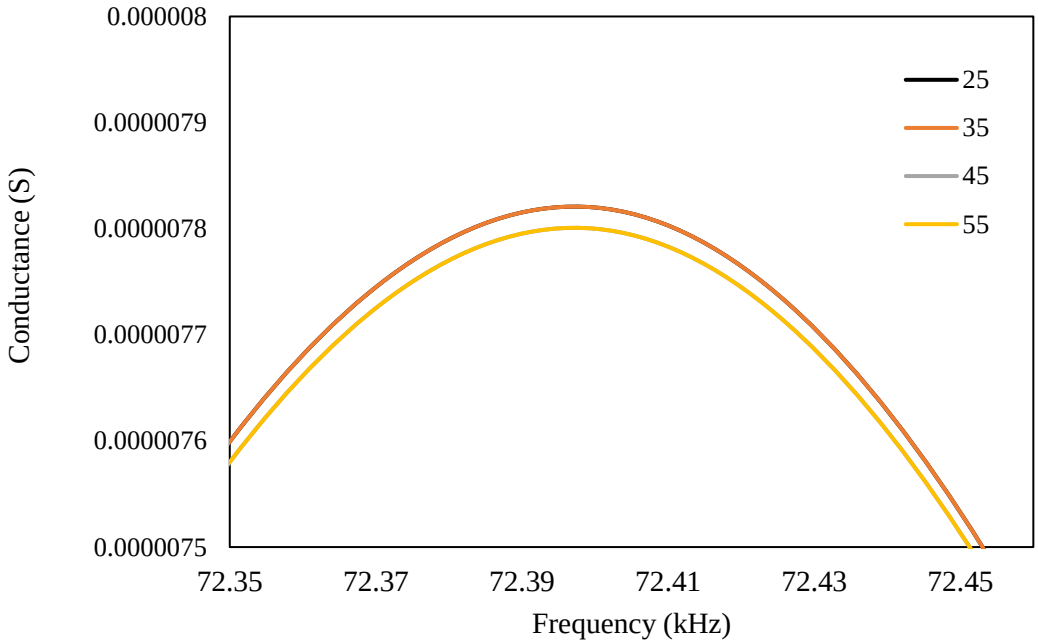

Figure 5.19: Conductance signature plot varying of ε_{33} PZT patch at different temperature.

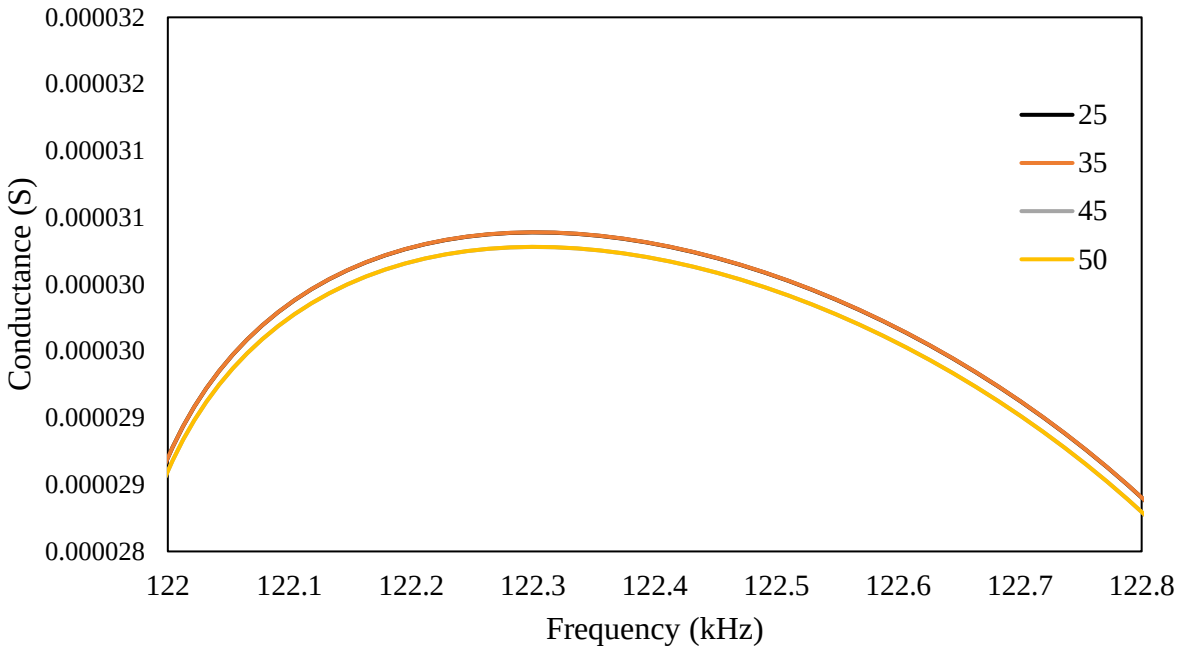

Figure 5.20: Conductance signature plot varying of d_{31} PZT patch at different temperature.

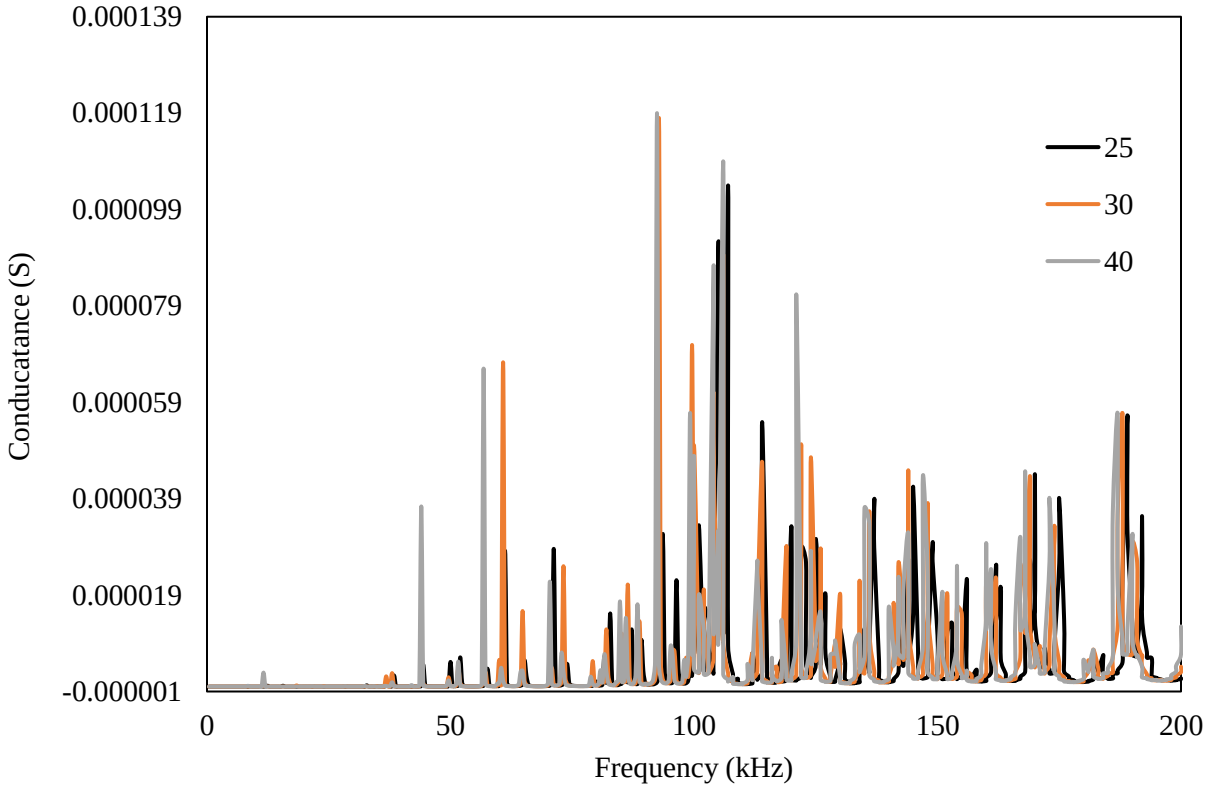

Figure 5.21: Conductance signature plot varying all the properties at different temperature.

It was observed from the ANSYS modelling results that modulus of elasticity and density of structure cause both horizontal and vertical shift in the admittance signature where as ε_{33} and d_{31} causes vertical shift.

5.7 COMPENSATION OF THE SHIFT

From the observation it can be deduced that the shift in the signature is a function of frequency range. Hence, different compensations were calculated for different frequency range. These factors were utilized to develop the compensation formulation which are as follows:

Horizontal shift (ΔH)

$\Delta H=6.0714 \times T-205.36$	(1-25 kHz)
$\Delta H=10.714 \times T-317.86$	(26-50 kHz)
$\Delta H=17.143 \times T-514.29$	(51-75 kHz)
$\Delta H=19.286 \times T-503.57$	(76-100 kHz)
$\Delta H=27.857 \times T-789.29$	(101-125 kHz)
$\Delta H=32.143 \times T-882.14$	(126-150 kHz)
$\Delta H=34.286 \times T-828.57$	(151-125 kHz)
$\Delta H=38.571 \times T-907.14$	(176-200 kHz)

Vertical shift (ΔV)

$\Delta V=2\times10^{-07}\times T-7\times10^{-06}$	(1-25kHz)
$\Delta V=4\times10^{-07}\times T-1\times10^{-05}$	(26-50kHz)
$\Delta V=1\times10^{-06}\times T-4\times10^{-05}$	(51-75kHz)
$\Delta V=2\times10^{-06}\times T-6\times10^{-05}$	(76-100kHz)
$\Delta V=2\times10^{-06}\times T-6\times10^{-05}$	(101-125kHz)
$\Delta V=5\times10^{-06}\times T-0.0002$	(126-150kHz)
$\Delta V=5\times10^{-06}\times T-0.0002$	(151-175kHz)
$\Delta V=5\times10^{-06}\times T-0.0002$	(176-200kHz)

The above compensation was used for different temperature plotted in Figure 5.3a. The results after temperature compensation are plotted below in Figure 5.22.

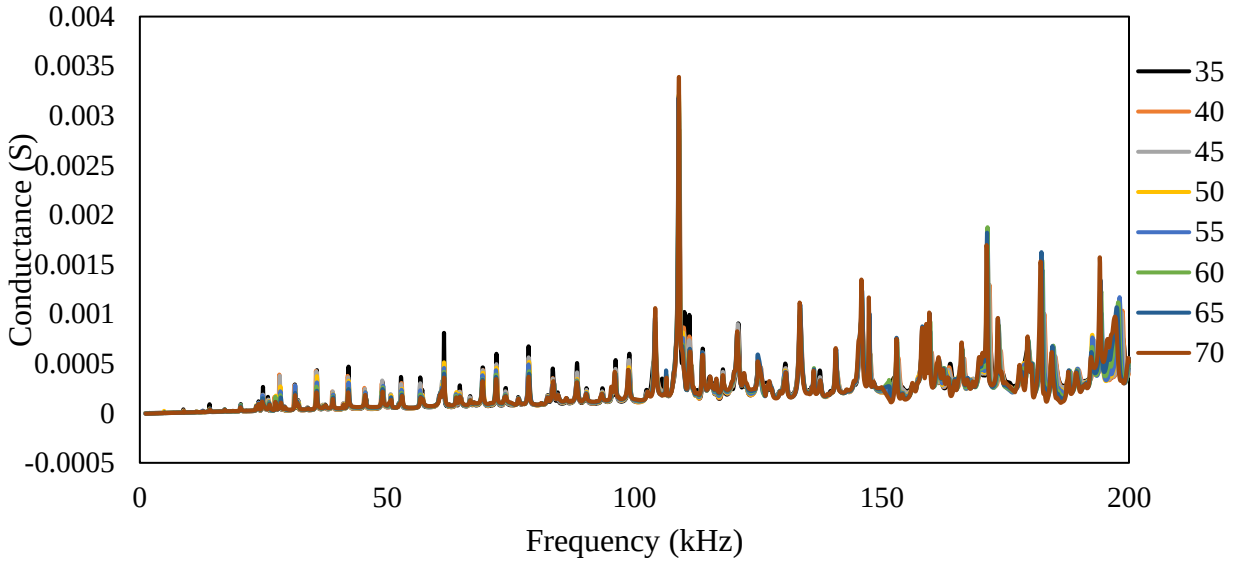

Figure 5.22: Compensated conductance signature for different temperature

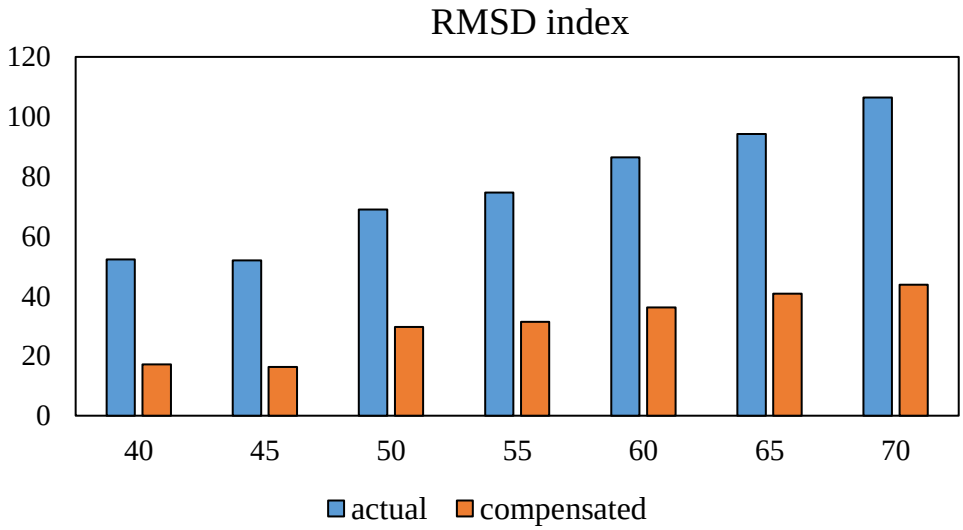

Figure 5.23: RMSD index plot of uncompensated and compensated signatures

5.4 SUMMARY AND CONCLUDING REMARKS

This chapter has presented experiments conducted to study the effect of temperature on conductance signatures. The study indicates strong dependence of shifts on temperature and frequency for both the bonded and free piezo sensor. Based on these observations, a new compensation technique was formulated. The compensation technique showed the good matching result. Both the analytical and modelling observations showed ε_{33} and d_{31} causes vertical shift in the admittance signature.

CHAPTER 6

DEVELOPMENT AND EXPERIMENTAL VALIDATION OF TEMPERATURE COMPENSATION ALGORITHM USING ARPS ON 2D STRUCTURE

6.1 INTRODUCTION

As in the previous chapter, it is observed temperature had significant influence in the signature of the piezo sensor. For the damage detection or the monitoring of the structure temperature gives the false indication. Thus, compensation of the signature is required and in previous chapter technique was also developed. Here in this chapter algorithm has been developed to validate the compensation formulation using ARPS on the 2D structure.

6.2 PROPOSED DAMAGE DETECTION ALGORITHM

The proposed algorithm is the damage detection on the structure with compensation of the signatures due to temperature effect.

1. Acquire the signature of the structure in undamaged condition at room temperature *i.e.* 25±2ºC.
2. Again, read the signatures for undamaged case at higher temperature *i.e.* above 30 ºC.
3. Calibrate the horizontal and vertical shift per ºC temperature in the signature for the undamaged case.
4. Obtain the signature at temperature above 40 ºC for the damaged case.
5. Compute the compensation of the shift due to temperature on both the higher temperature for damaged and undamaged case.
6. Calculate the RMSD for the damaged case after compensation, which indicates the actual damage in the structure.

6.3 FABRICATION DETAILS OF EXPERIMENTAL PROTOTYPE STRUCTURE

The experimental specimen used earlier in chapter 4 was used in this study also. The steel plate of size 1200 × 970 mm^2, supported on box type pipe of cross section 38×38 mm^2 and 3mm thickness was used. The pipeline was welded along the steel plate and supported by wheel on four corners. The steel plate composes of carbon (0.23 %), manganese (1.5 %), sulphur (0.045%), phosphorus (0.045%) and silicon (0.40%) as per IS-2062, 2006.

In the test specimen ARPS developed in the same study was used as a specimen. Near to damage location 2 ARPS was attached in the steel plate and signatures were acquired for different temperature. Temperature of the sensor and the area around the sensor were increased by halogen lamp. Damage location was chosen as shown in Figure 6.1. In the pristine condition the hole was covered by plate of 150×150 mm in size. This plate is attached in the main plate by the four bolts of 10mm with 35Nm torque.

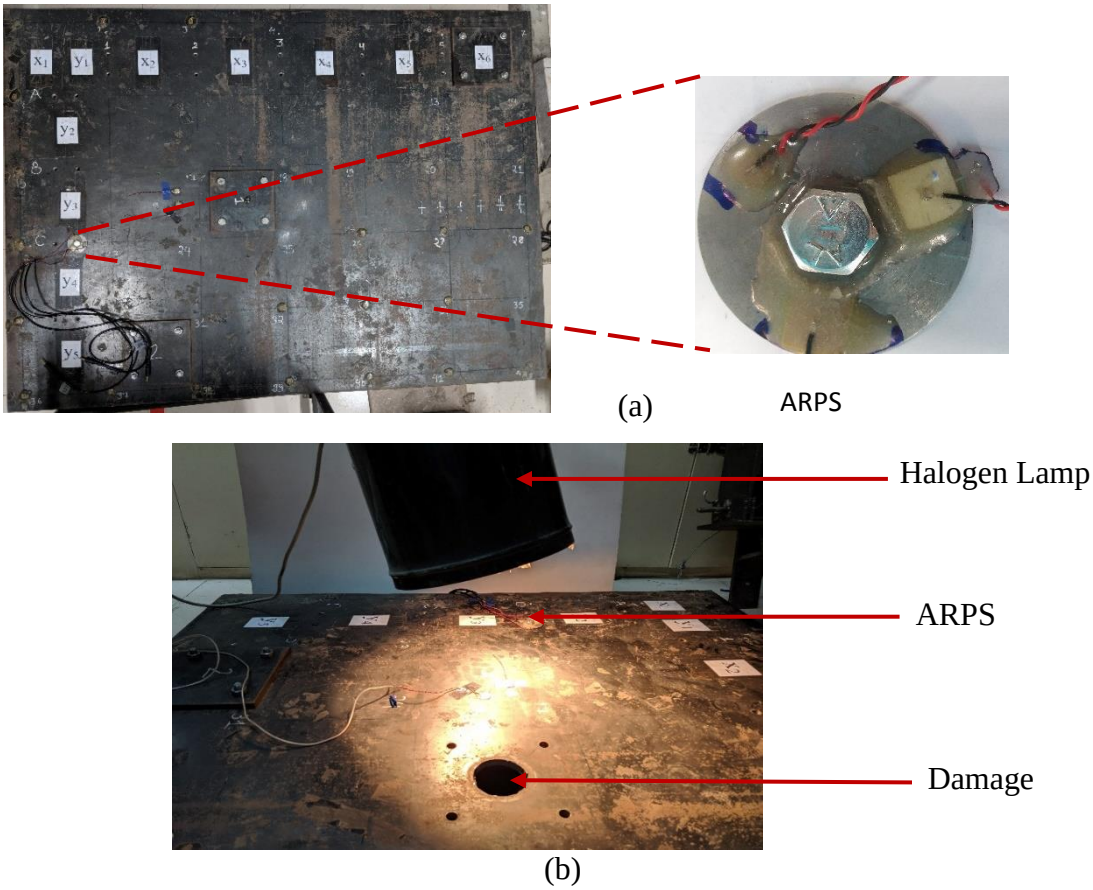

Figure 6.1: Experimental prototype structure (a) steel plate with ARPS (b) prototype structure with halogen lamp and damage

6.4 EXPERIMENTAL DETAILS

The ARPS attached to the steel plate, electrically excited at the frequency range of 30-400kHz with an impedance analyser (Agilent E4980A) to acquire admittance signature. At room temperature *i.e.* 25±2ºC signatures were acquired for undamaged case. With the halogen lamp temperature of the sensor and the area around the senor was increased to 30ºC. Signatures were obtained at same temperature for undamaged case. The cover plate of 150×150 mm was removed from the main plate to create damage on the structure. Temperature of the plate was increased to 45ºC with the same halogen lamp for the damaged case. Figure 6.2 shows the complete setup of the experiment.

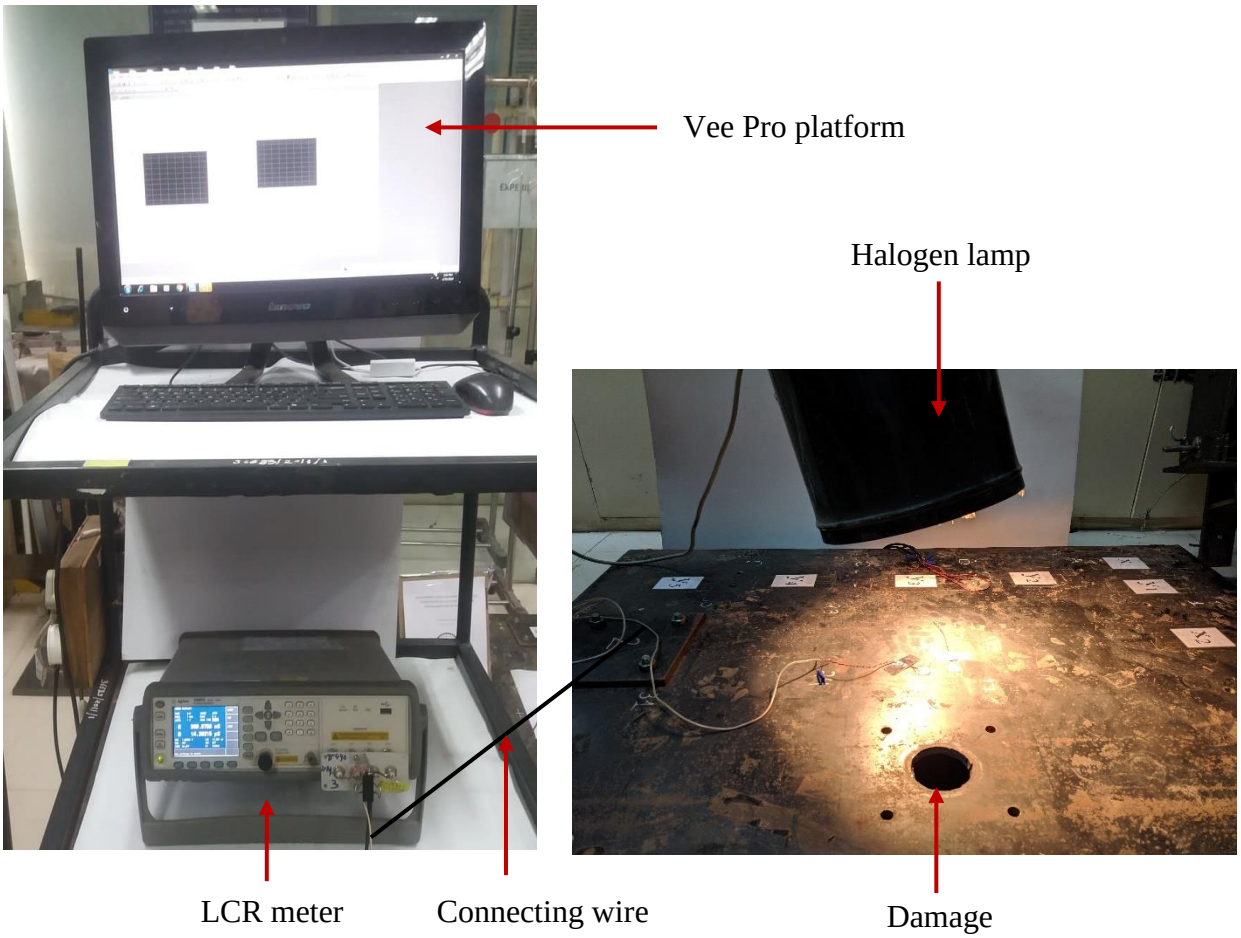

Figure 6.2: Complete experimental setup

6.5 OBSERVATIONS

As previously observed with the increase in temperature conductance signature shifts towards left and upward as validated in the present scenario. In Figure 6.3, 25 ºC and 30ºC reading are of undamaged case whereas 45ºC is the damaged condition. RMSD index of the 30 ºC (without damage) was 18.33% and for 45 ºC (with damage) was 35.01%.

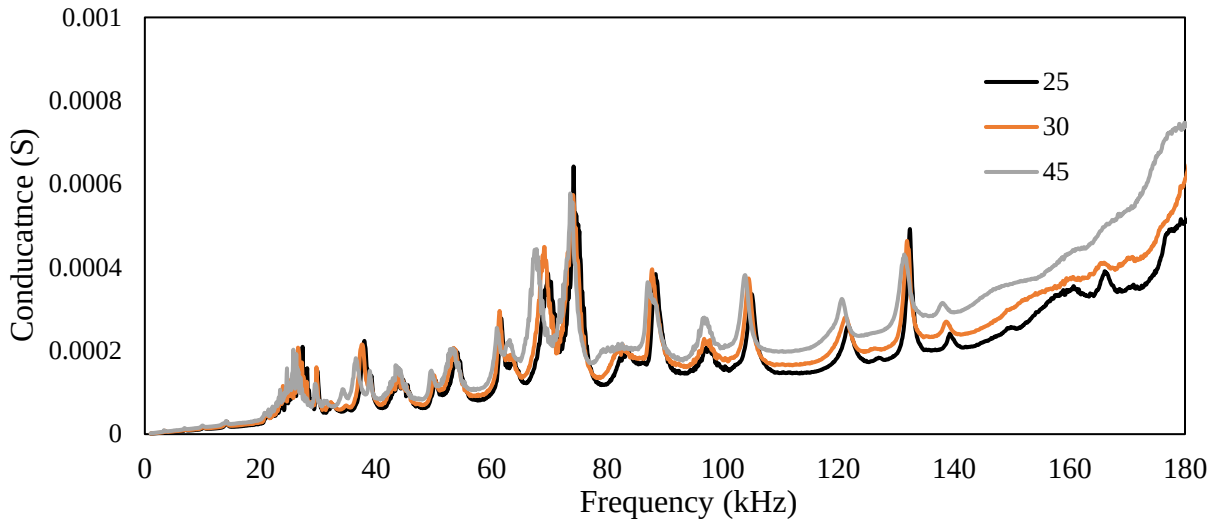

Figure 6.3: Conductance signature for damaged and undamaged condition with temperature effect

6.6 COMPENSATION OF THE SIGNATURE

Using the compensation formulation developed in the previous chapter compensation of the signature was computed. Figure 6.4 shows the compensated signature.

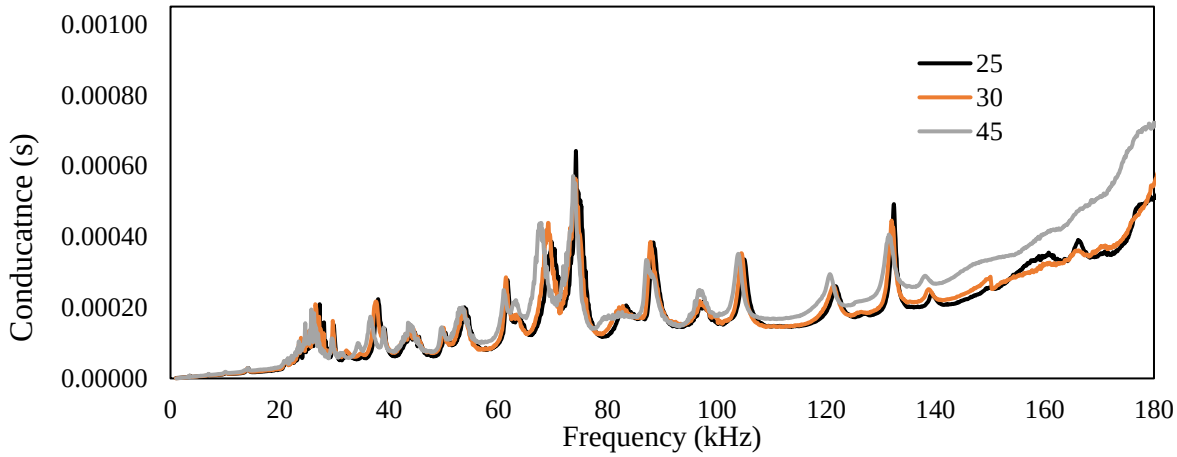

Figure 6.4: Conductance signature for damaged and undamaged condition with temperature effect after compensation

In Figure 6.4, 25ºC plot is the actual signature, 30ºC plot is compensated signature for undamaged condition. RMSD index calculated for compensated signature was found to be 11.93% for 35 ºC where as for 45 ºC 28.93%.

6.7 CONCLUDING REMARKS

This chapter validates the thermally compensated advanced reusable piezo sensor. Compensation formulation valid on the ARPS with damage detection. Algorithm developed in this study can be implemented on the real life structure where temperature variations are common.

CHAPTER 7

CONCLUSION AND FUTURE RECOMMENDATIONS

7.1 INTRODUCTION

This chapter summarizes the research conclusions and recommendations for future work. It also covers limitations of the research.

7.2 CONCLUSIONS AND CONTRIBUTIONS

Major conclusion drawn from this thesis are as follows:

1. For the first time, ARPS unit has been successfully developed using single bolt configuration and experimentally validated with satisfactory repeatability.
2. For the repeatability CC index is more suitable than RMSD. A value of CC greater than 99.5% indicates excellent repeatability.
3. The earlier algorithm of Naskar and Bhalla (2016) and Supriya (2018) has been successfully adapted to carryout damage detection and localization for 2D plate type structures. It has been successfully validated with ARPS on a large 2D steel prototype structure.
4. A new and simple temperature compensation algorithm has been developed suitable for practical application. It only needs signatures of piezo patch at two different temperature. The algorithm has been successfully verified on a large steel prototype structure.

7.3 RECOMMENDATIONS

1. Effect of temperature below 20ºC on the signatures piezo sensors can in studied.
2. ARPS approach may be extended for multiple damage scenario.
3. Effect of modulus of elasticity and density of PZT patch on different temperature can be studied.

7.4 LIMITATIONS

1. A little change in orientation of the reusable sensor challenges to gain repeatability of the sensor. Hence, ARPS should be aligned on the same position as aligned earlier to obtain better repeatability.
2. Frequency range greater than 150 kHz is not feasible for damage detection as temperature effect above this range is higher which signifies false damage.

PUBLICATIONS

1. **Baral, S**., Negi, P. and Bhalla, S. (2019), "*Effect of temperature on signatures of piezo sensors for EMI technique and its compensation*." UKIERI Concrete Congress, 5th -8th March, NIT Jalandar.

REFERENCES

1. Adhikari, S. and Bhalla, S. (2018), "*Modified Dual Piezo Configuration for Improved Structural Health Monitoring Using Electro Mechanical Impedance (EMI) Technique*", Journal of Experimental Techniques, Vol. 43, No. 1, pp. 25-40.
2. Aktan, A. E., Catbas, F. N., Grimmelsman, K. A. and Tsiko, C. J. (2000)"*Issues in Infrastructure Health Monitoring For Management.*"Journalof EngineeringMechanics, Vol. 126, No.7, pp. 711-724.
3. Baptista, F. G., Budoya, D. E., Dealmeida, V. A., and Ulson, J. A. C., (2014), "*An Experimental Study on the Effect of Temperature on Piezoelectric Sensors for Impedance-Based Structural Health Monitoring*." Journal of Sensors, Vol. 14, pp.1208-1227.
4. Bhalla, S. (2001), "*Smart System Based Automated Health Monitoring of Structures*" M. Eng. Thesis, Nanyang Technological University, Singapore.
5. Bhalla, S. (2004) "*A Mechanical Impedance Approach for Structural Identification, Health Monitoring and Non-Destructive Evaluation Using Piezo-Impedance Transducers*." PhD Thesis, School of Civil and Environmental Engineering, Nanyang Technological University, Singapore.
6. Bhalla, S. and Soh, C. K. (2004a) "*Structural Health Monitoring by Piezo-Impedance Transducers I: Modelling.*" Journal of Aerospace Engineering (ASCE), Vol. 17, No. 4, pp. 154–165.
7. Bhalla, S. and Soh, C. K. (2004b) "*Structural Health Monitoring by Piezo-Impedance Transducers II: Applications.*" Journal of Aerospace Engineering (ASCE), Vol. 17, No. 4, pp. 166–175.
8. Giurgiutiu, V., Reynolds, A. and Rogers, C. A. (1999), "*Experimental Investigation of E/M Impedance Health Monitoring for Spot-Welded Structural Joints*", Journal of Intelligent Material Systems and Structures, Vol. 10, No. 10, pp. 802-812.
9. Harper, D. (1883), "*Piezoelectric*", Online Etymology Dictionary.
10. Krishnamurthy, K., Lalande, F., and Rogers, C.A., (1996), "*Temperature Effects on Piezoelectric Elements Used as Collocated Actuator/Sensors*," Proceedings of SPIE North American Conference on Smart Structures and Materials, Vol. 2717, pp. 302-310.

11. Liang, C., Sun, F. P. and Rogers, C. A. (1994) "*Electro-Mechanical Impedance Modelling of Active Material System.*" Smart Material and Structures, Vol. 5, pp.171-186.

12. Lipski, A., Mrozinski, S. (2012), "*The Effects of Temperature on the Strength Properties of Aluminum Alloy 2024-T3*", Acta Mechanica et Automatica, Vol. 6, No. 3, pp. 62-66.

13. Na, S., Tawie, R. and Lee, H. K. (2012) "*Electromechanical Impedance Method of Fiber-Reinforced Plastic Adhesive Joints in Corrosive Environment Using A Reusable Piezoelectric Device."* Journal of Intelligent Material Systems and Structures, Vol. 23, No.7, pp. 737–747.

14. Na, S. and Lee, H. K. (2013) "*Steel Wire Electromechanical Impedance Method Using A Piezoelectric Material for Composite Structures with Complex Surfaces*." Composite Structures, Vol.98, pp. 79–84.

15. Narender, K., Rao, A. S. M., Rao, K. G. K. and Krishna, N. G. (2013), "*Temperature Dependence of Density and Thermal Expansion of Wrought Aluminum Alloys 7041, 7075 and 7095 by Gamma Ray Attenuation Method"*, Journal of Modern Physics, Vol. 4, No. 3, pp. 331-336.

16. Naskar, S. (2014) "*Experimental and Numerical Investigations on Metal Wire Based Variant of EMI Technique For SHM*." MTech Thesis, Department of Civil Engineering, Indian Institute of Technology (IIT) Delhi, India.

17. Naskar, S. and Bhalla, S. (2016) "*Metal-Wire-Based Twin One-Dimensional Orthogonal Array Configuration of PZT Patches for Damage Assessment of Two-Dimensional Structures"* Journal of Intelligent Material Systems and Structures, Vol. 27, No. 11, pp. 1440–1460.

18. Park, G.,Kabeya, K., Cudney, H. H. and Inman, D. J. (1999), "*Impedance-based structural health monitoring for temperature varying applications.*" JSME International Journal, Vol.42, No.2, pp.249-258.

19. Piceramic, (2018), "*Properties of PIC151*", Date of access 2018/10/15.

20. Shanker, R., Bhalla, S. and Gupta, A. (2010), "*Integration of electro-mechanical impedance and global dynamic technique for improved structural health monitoring*." Journal of Intelligent Material Systems and Structures, Vol. 21, No. 2, pp.285-295.

21. Srivastava, S., Bhalla, S. and Madan, A. (2017) "*Assessment of Human Bones Encompassing Physiological Decay and Damage Using Piezo Sensors In Non-Bonded Configuration*" Journal of Intelligent Material Systems and Structures, Vol. 28, No. 14, pp. 1977–1992.
22. Supriya, (2018) "*Development and evaluation of reusable bolted piezo sensor (RBPS) for structural health monitoring using EMI technique*." MTech Thesis, Department of Civil Engineering, Indian Institute of Technology (IIT) Delhi, India.
23. Tawie, R. and Lee, H. K. (2011) "*Characterization of Cement-Based Materials Using a Reusable Piezoelectric.*" Smart Materials and Structures. Vol. 20, No. 9, pp. 964-1726.
24. Thakuri, S. B. (2017) "*Evaluation of Reusable Piezo Sensors for Hydration And Corrosion Damage Assessment Of Reinforced Concrete Structures*." MTech Thesis, Department of Civil Engineering, Indian Institute of Technology (IIT) Delhi, India.
25. Yang, Y, Lim, Y. Y. and Soh, C. K. (2008) "*Practical Issues Related to The Application of Electromechanical Impedance Technique in the Structural Health Monitoring of Civil Structures: I. Experiment*". Smart Materials and Structures, Vol. 17, No. 3, pp. 14.
26. Yang, Y., Divsholi, B. S., Soh, C. K. (2010) "*A Reusable PZT Transducer for Monitoring Initial Hydration and Structural Health of Concrete.*" Sensors, Vol. 10, pp. 5193-5208.

APPENDIX -A

CONDUCTANCE SIGNATURE FOR DAMAGE LOCATION-1

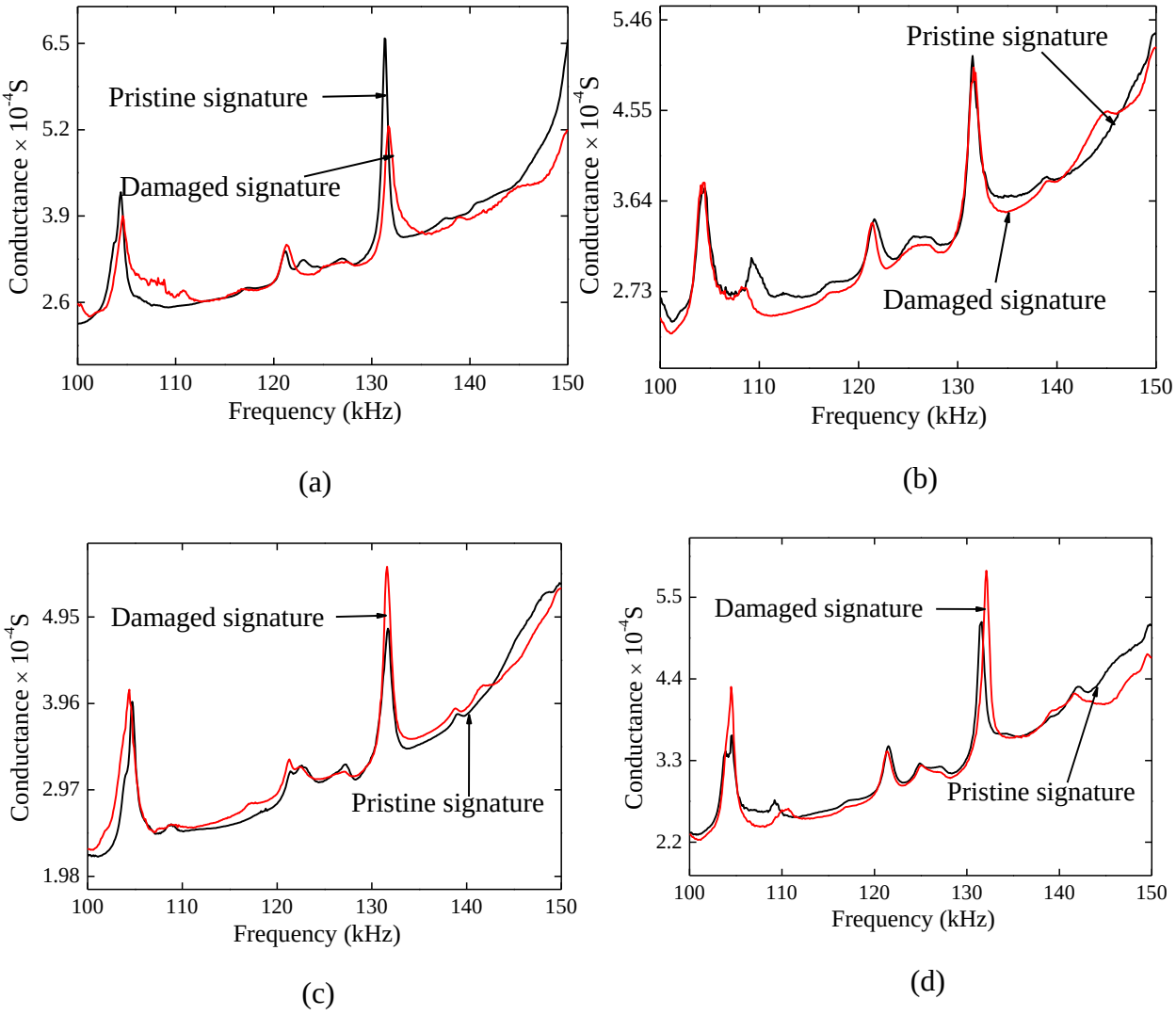

Figure A.1: Conductance signature for undamaged and damaged condition with CEL ARPS sensor at (a) location-1 (b) location-2 (c) location-3 and (d) location-4

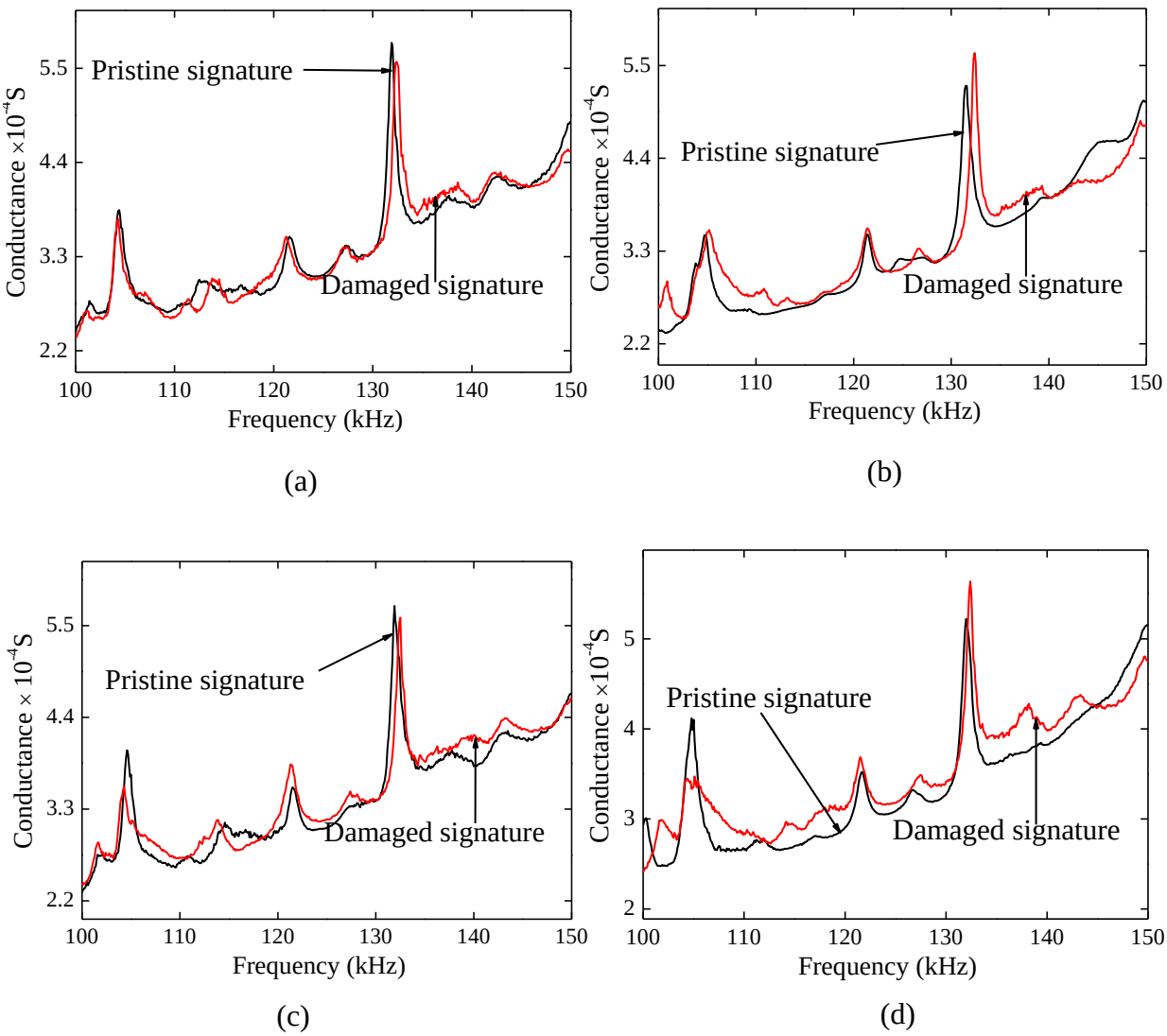

Figure A.2: Conductance signature for undamaged and damaged condition with CEL ARPS sensor at (a) location-A (b) location-B (c) location-C and (d) location-D

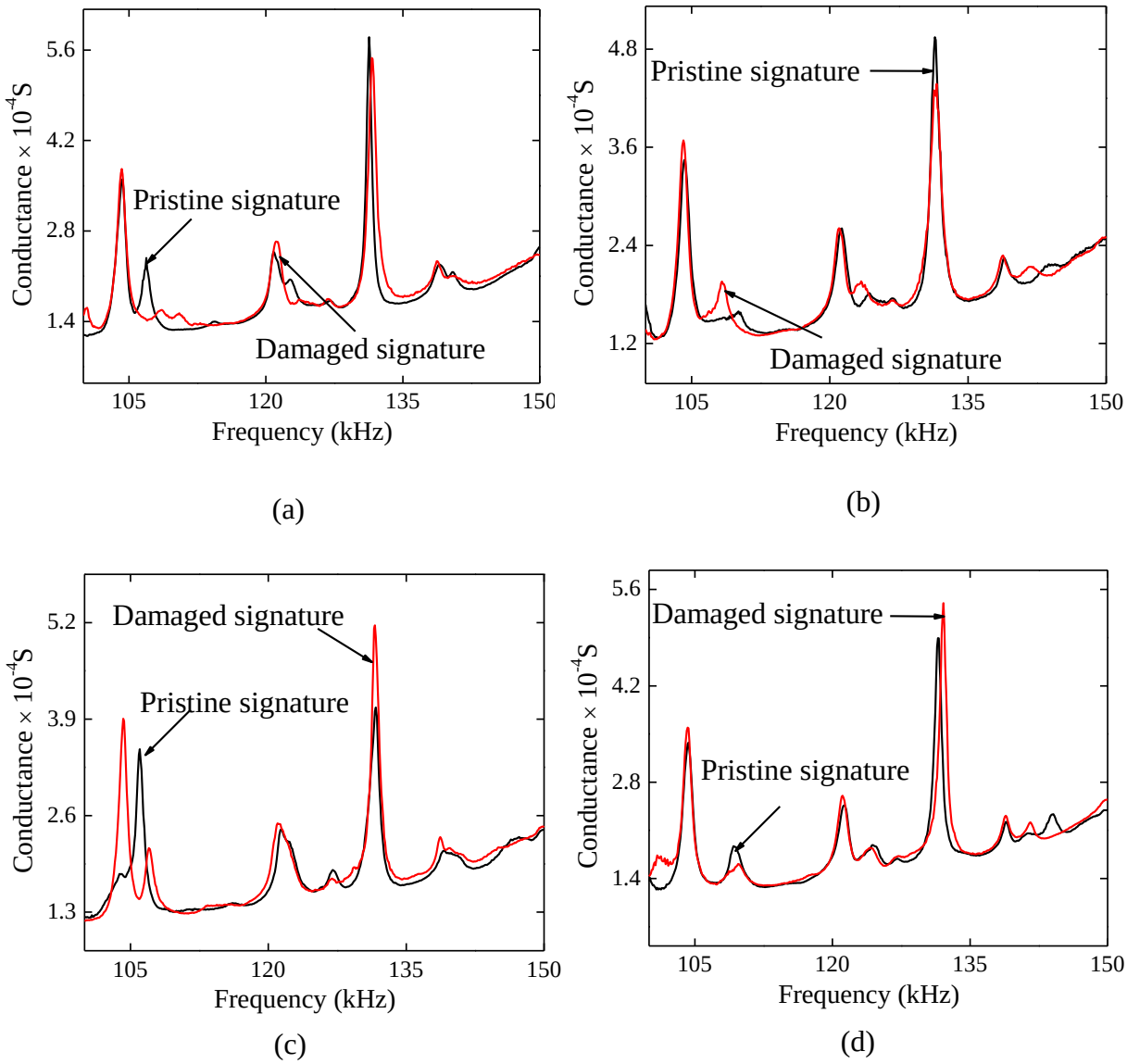

Figure A.3: Conductance signature for undamaged and damaged condition with PI-10 ARPS sensor at (a) location-1 (b) location-2 (c) location-3 and (d) location-4

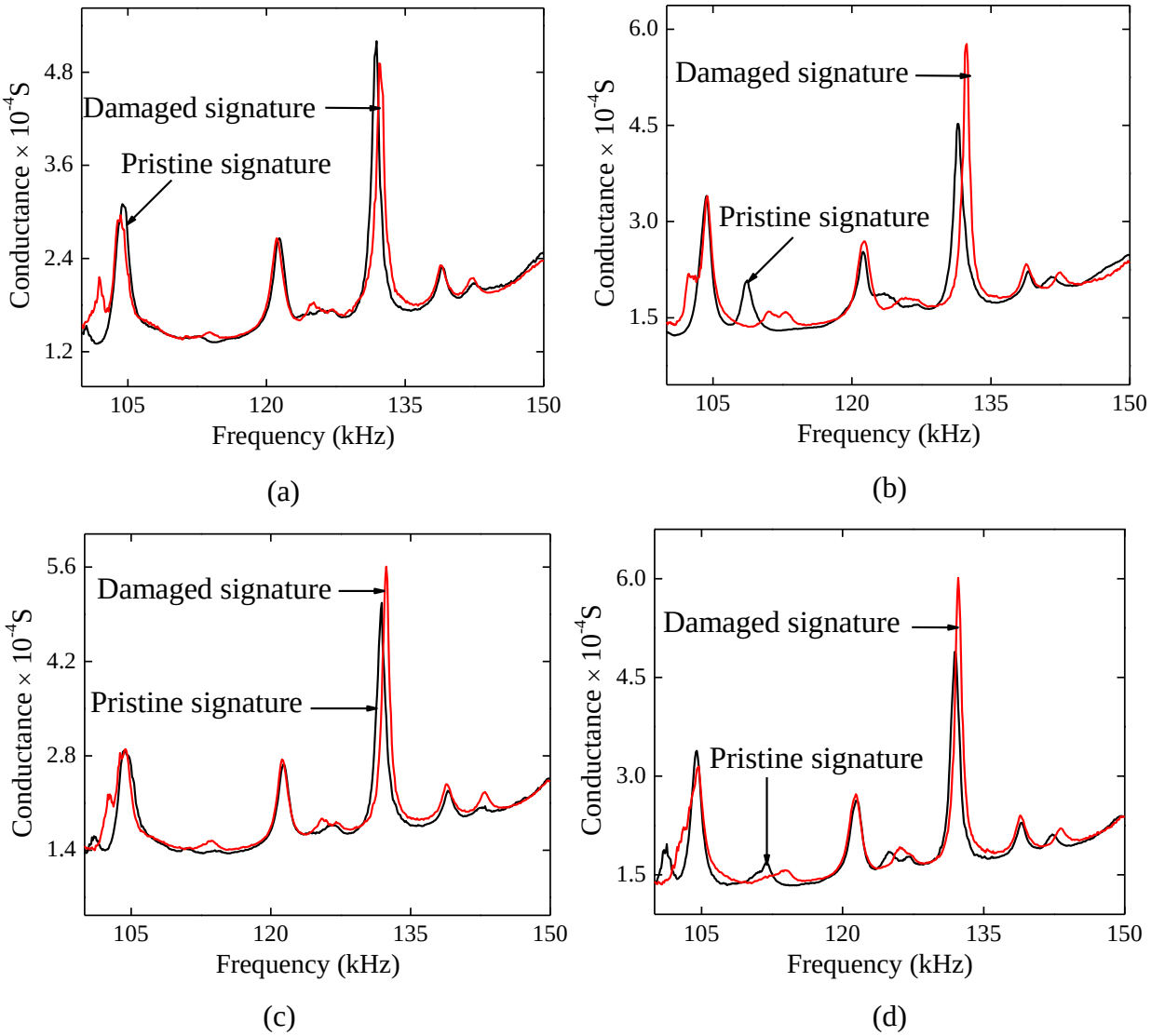

Figure A.4: Conductance signature for undamaged and damaged condition with PI-10 ARPS sensor at (a) location-A (b) location-B (c) location-C and (d) location-D

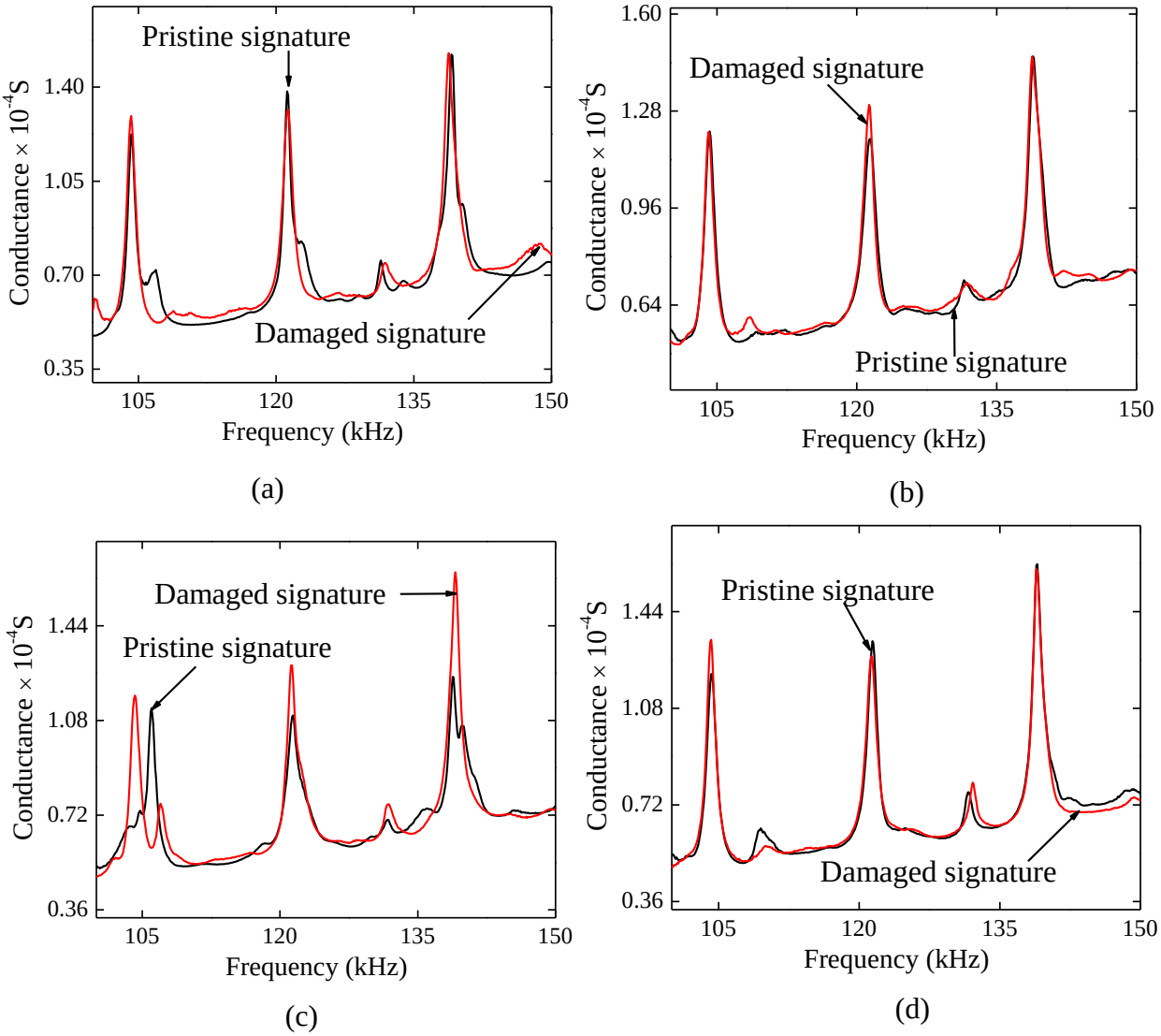

Figure A.5: Conductance signature for undamaged and damaged condition with PI-5 ARPS sensor at (a) location-1 (b) location-2 (c) location-3 and (d) location-4

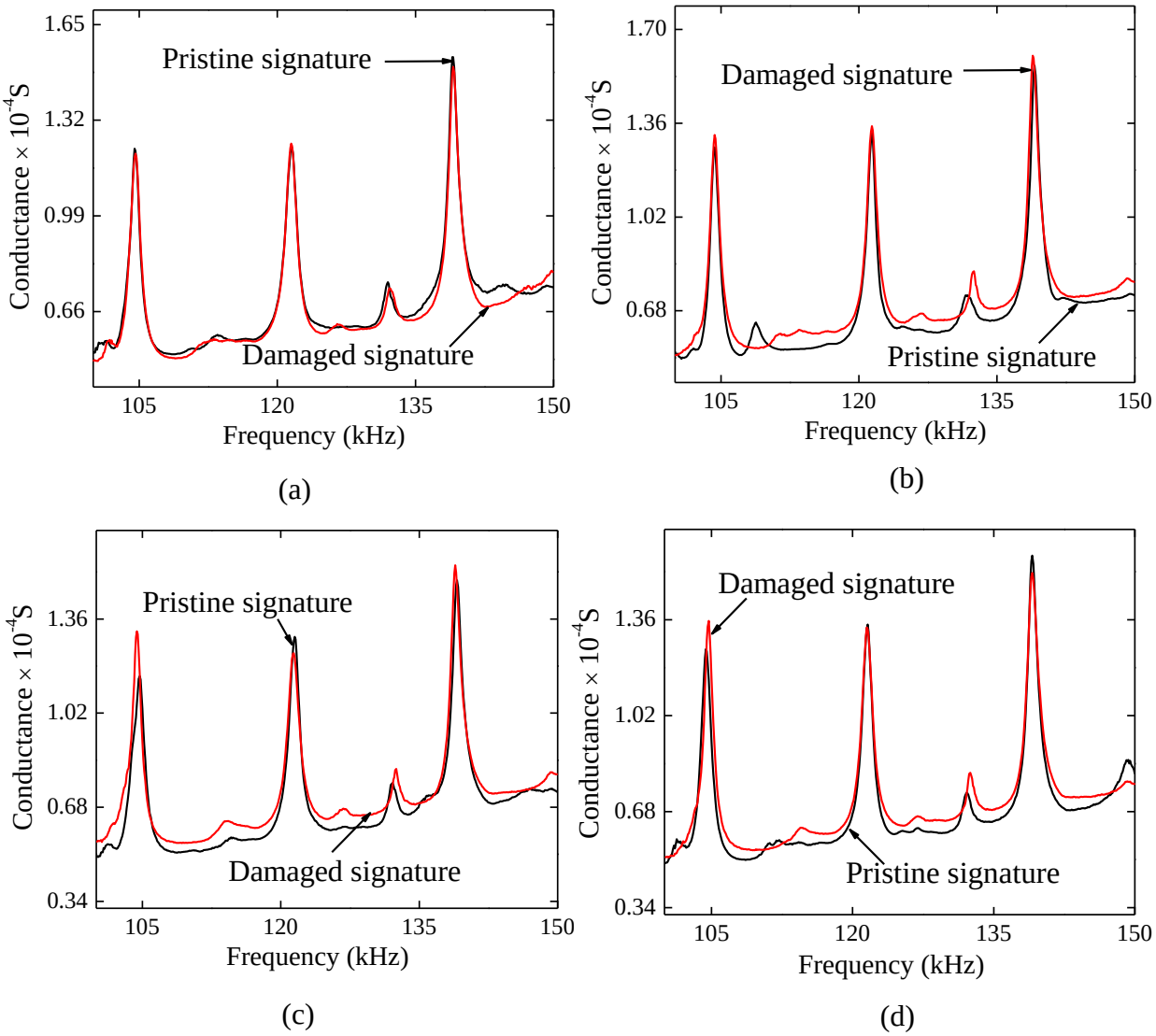

Figure A.6: Conductance signature for undamaged and damaged condition with PI-5 ARPS sensor at (a) location-A (b) location-B (c) location-C and (d) location-D

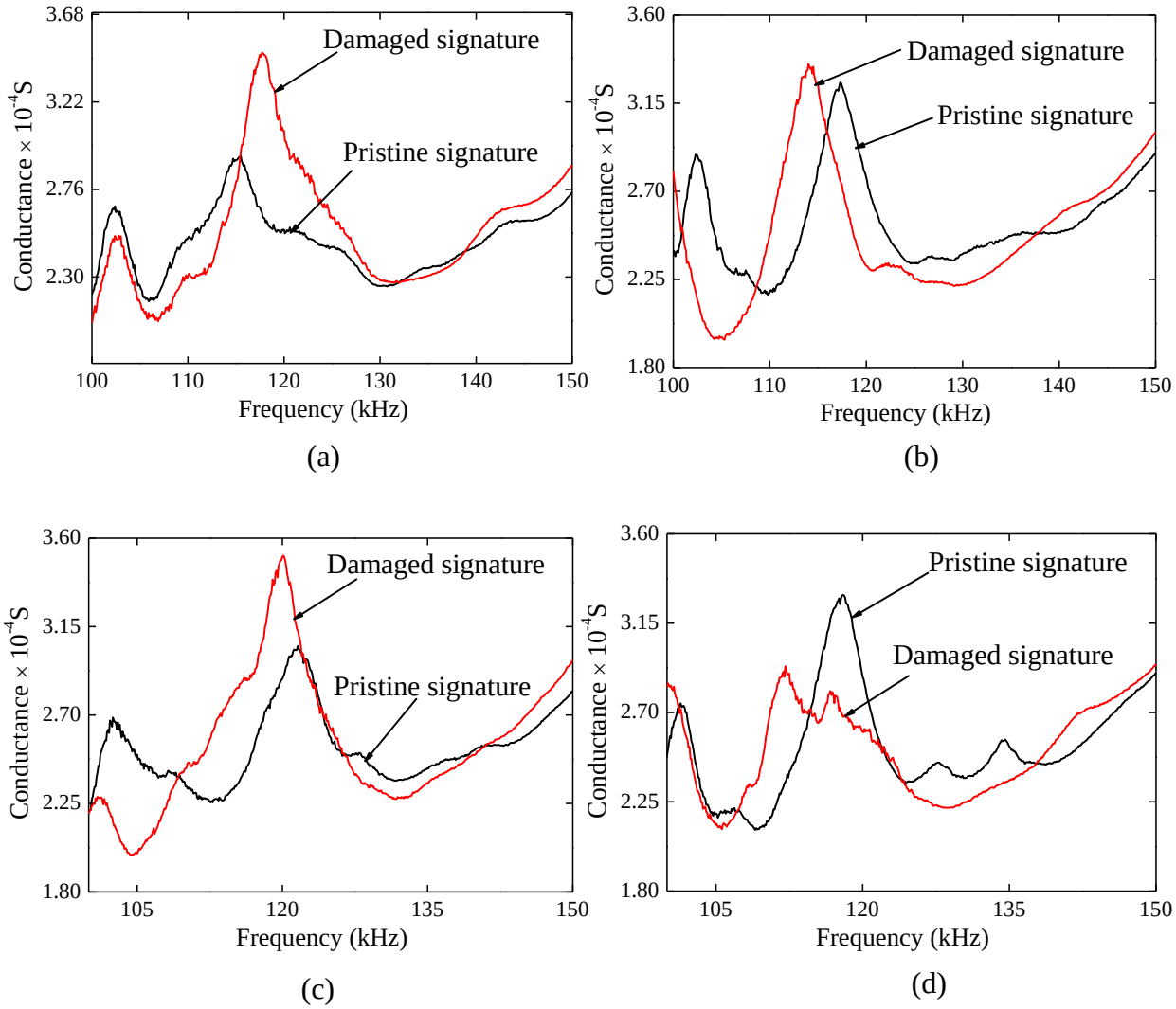

Figure A.7: Conductance signature for undamaged and damaged condition with RBPS sensor at (a) location-1 (b) location-2 (c) location-3 and (d) location-4

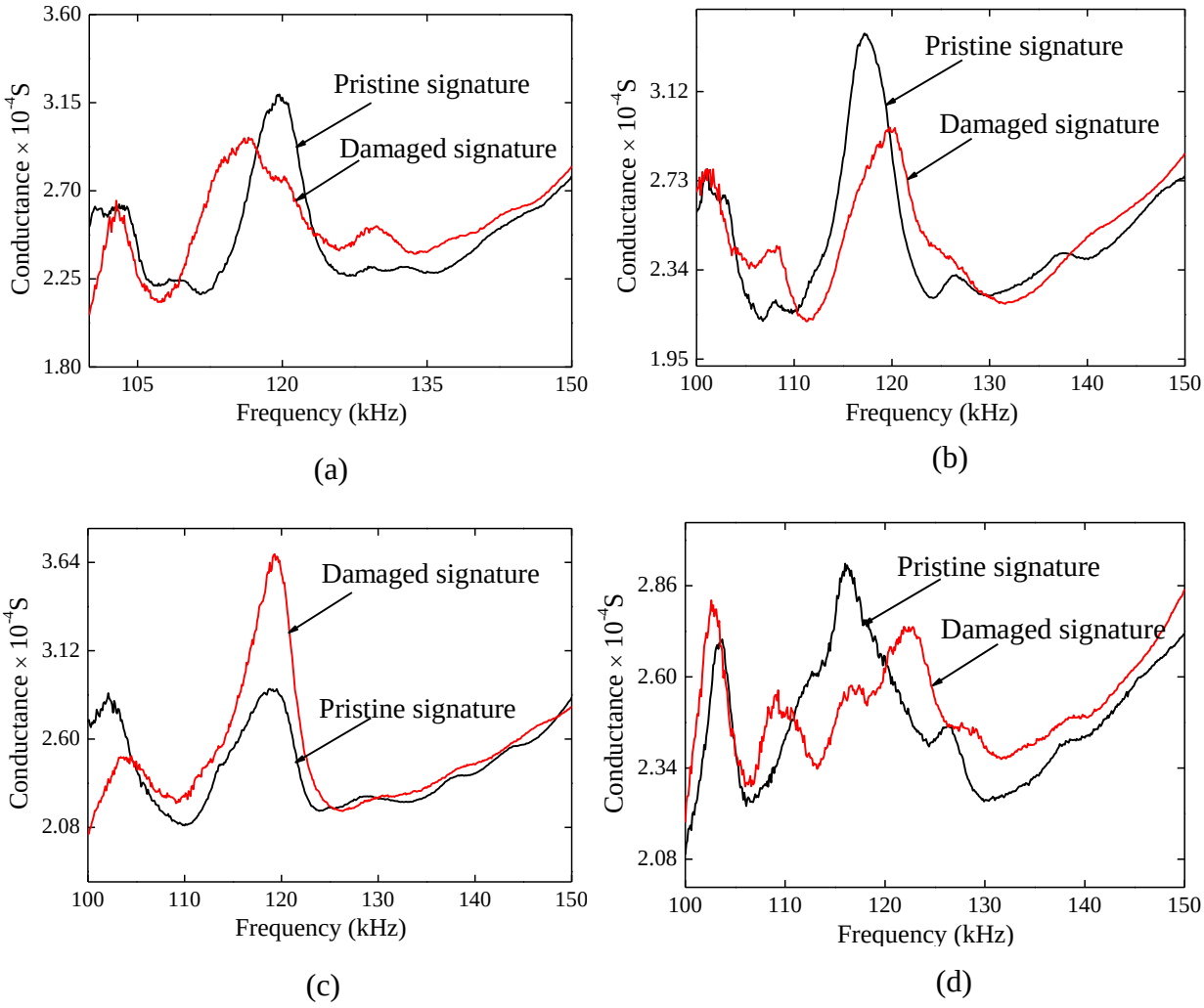

Figure A.8: Conductance signature for undamaged and damaged condition with RBPS sensor at (a) location-A (b) location-B (c) location-C and (d) location-D

APPENDIX -B

CONDUCTANCE SIGNATURE FOR DAMAGE LOCATION-2

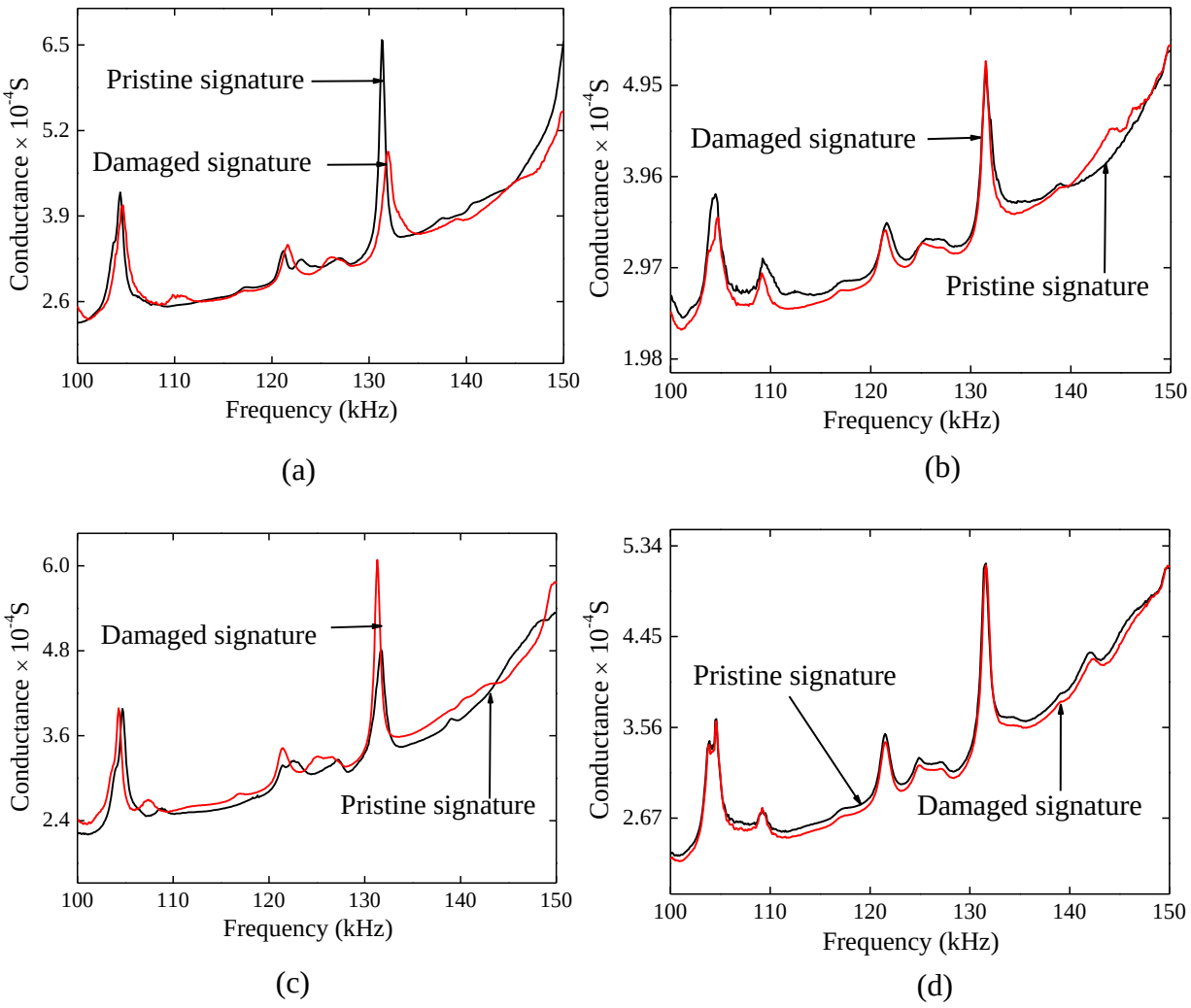

Figure B.1: Conductance signature for undamaged and damaged condition with CEL ARPS sensor at (a) location-1 (b) location-2 (c) location-3 and (d) location-4

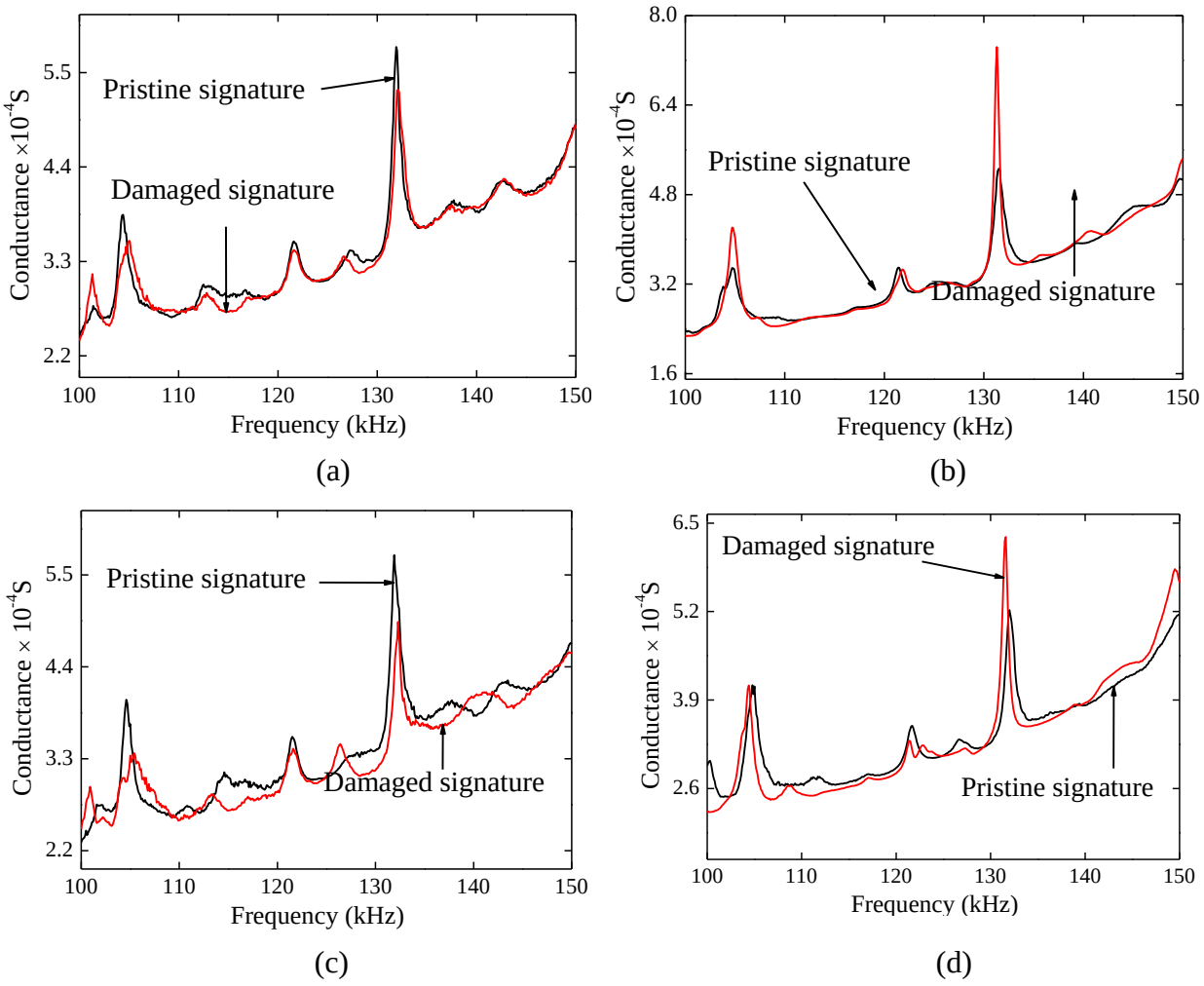

Figure B.2: Conductance signature for undamaged and damaged condition with CEL ARPS sensor at (a) location-A (b) location-B (c) location-C and (d) location-D

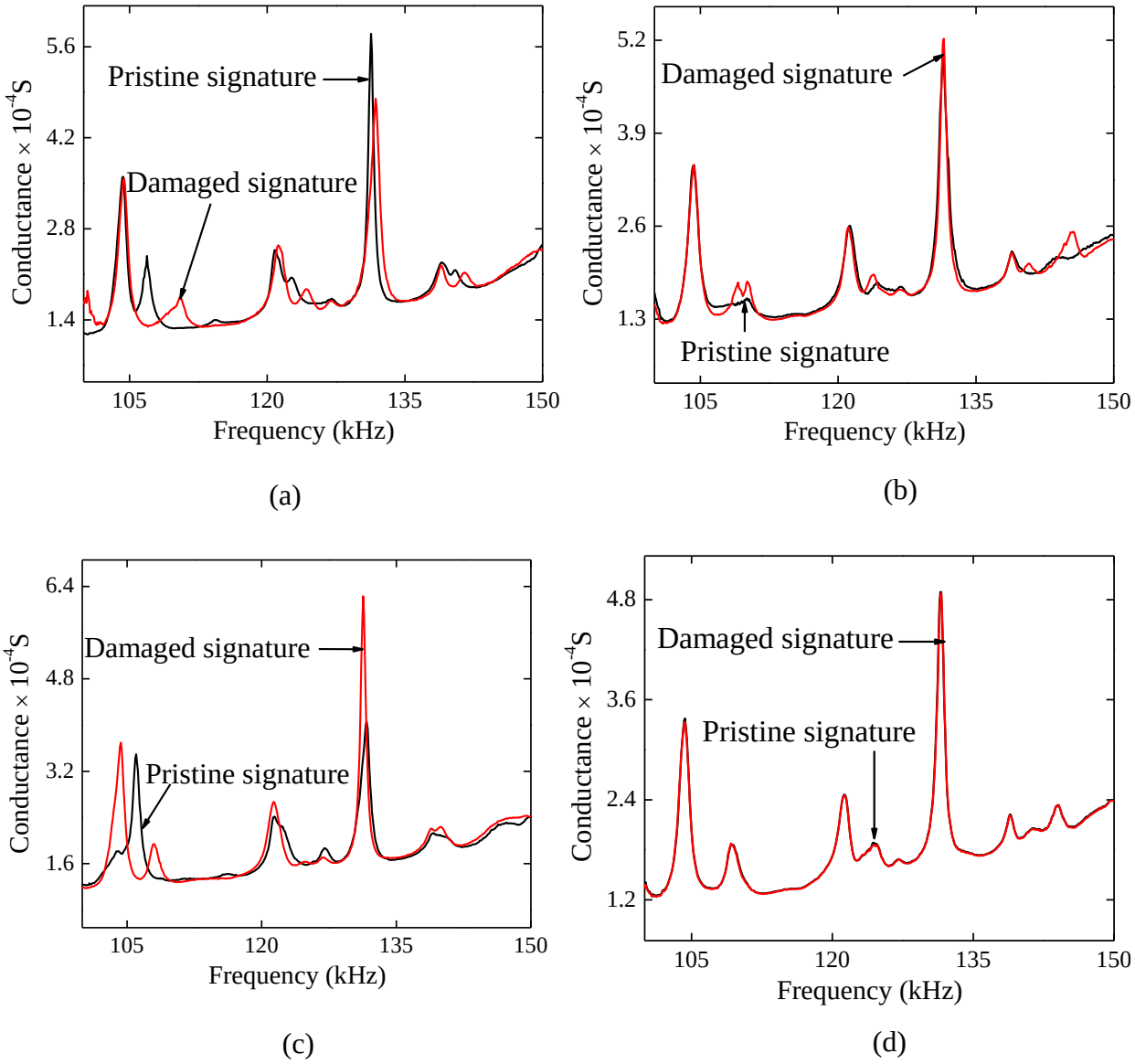

Figure B.3: Conductance signature for undamaged and damaged condition with PI-10 ARPS sensor at (a) location-1 (b) location-2 (c) location-3 and (d) location-4

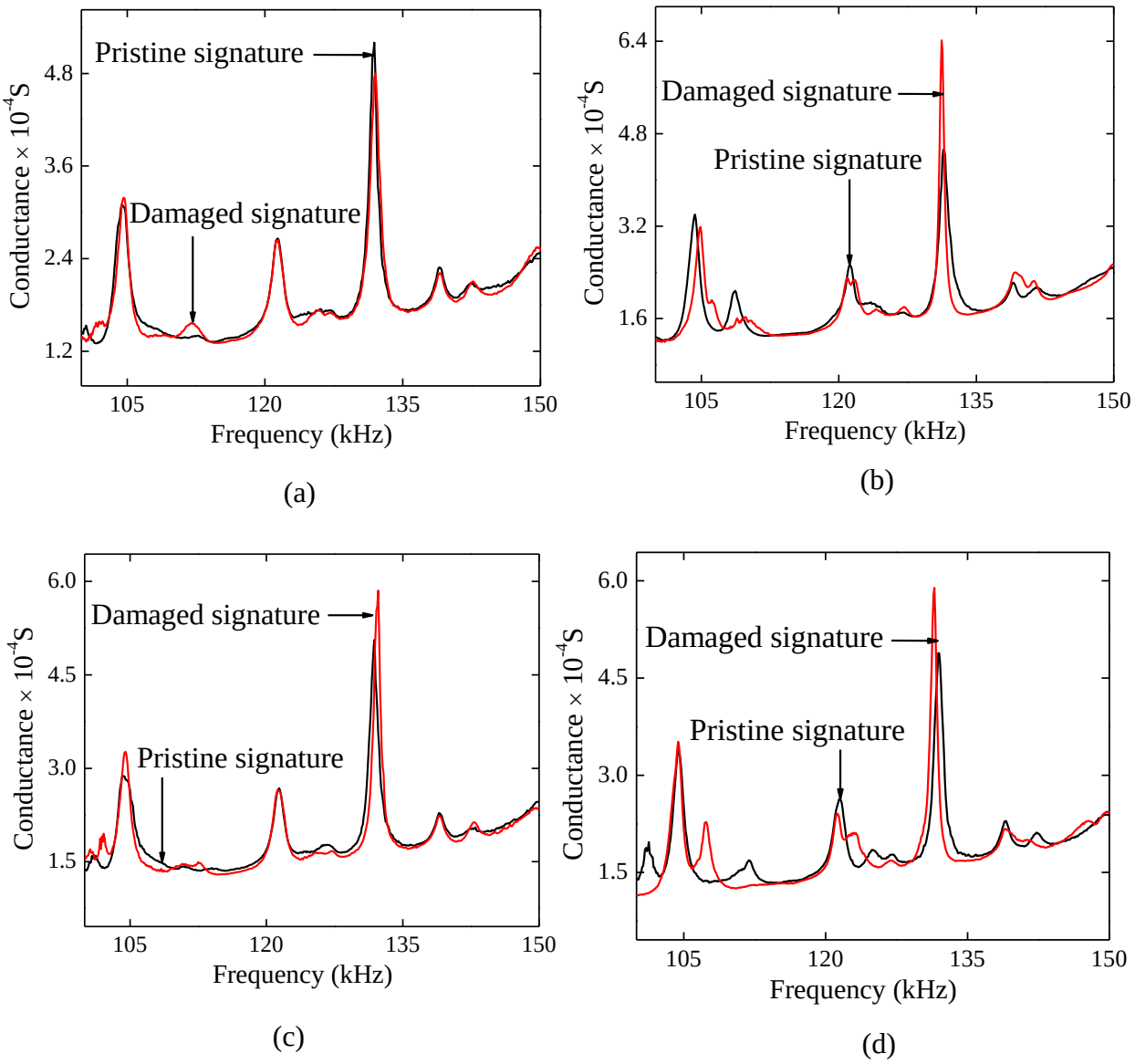

Figure B.4: Conductance signature for undamaged and damaged condition with PI-10 ARPS sensor at (a) location-A (b) location-B (c) location-C and (d) location-D

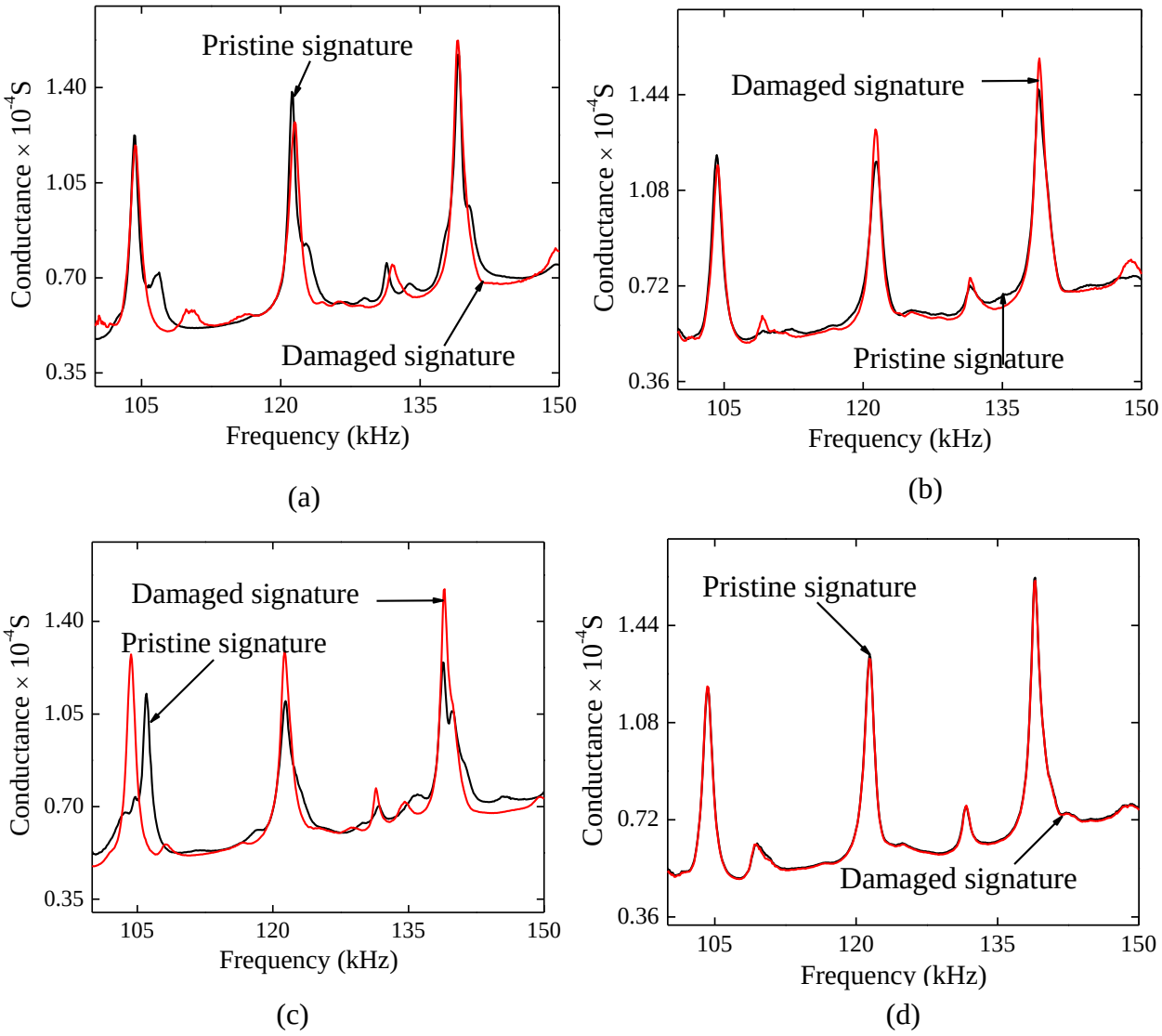

Figure B.5: Conductance signature for undamaged and damaged condition with PI-5 ARPS sensor at (a) location-1 (b) location-2 (c) location-3 and (d) location-4

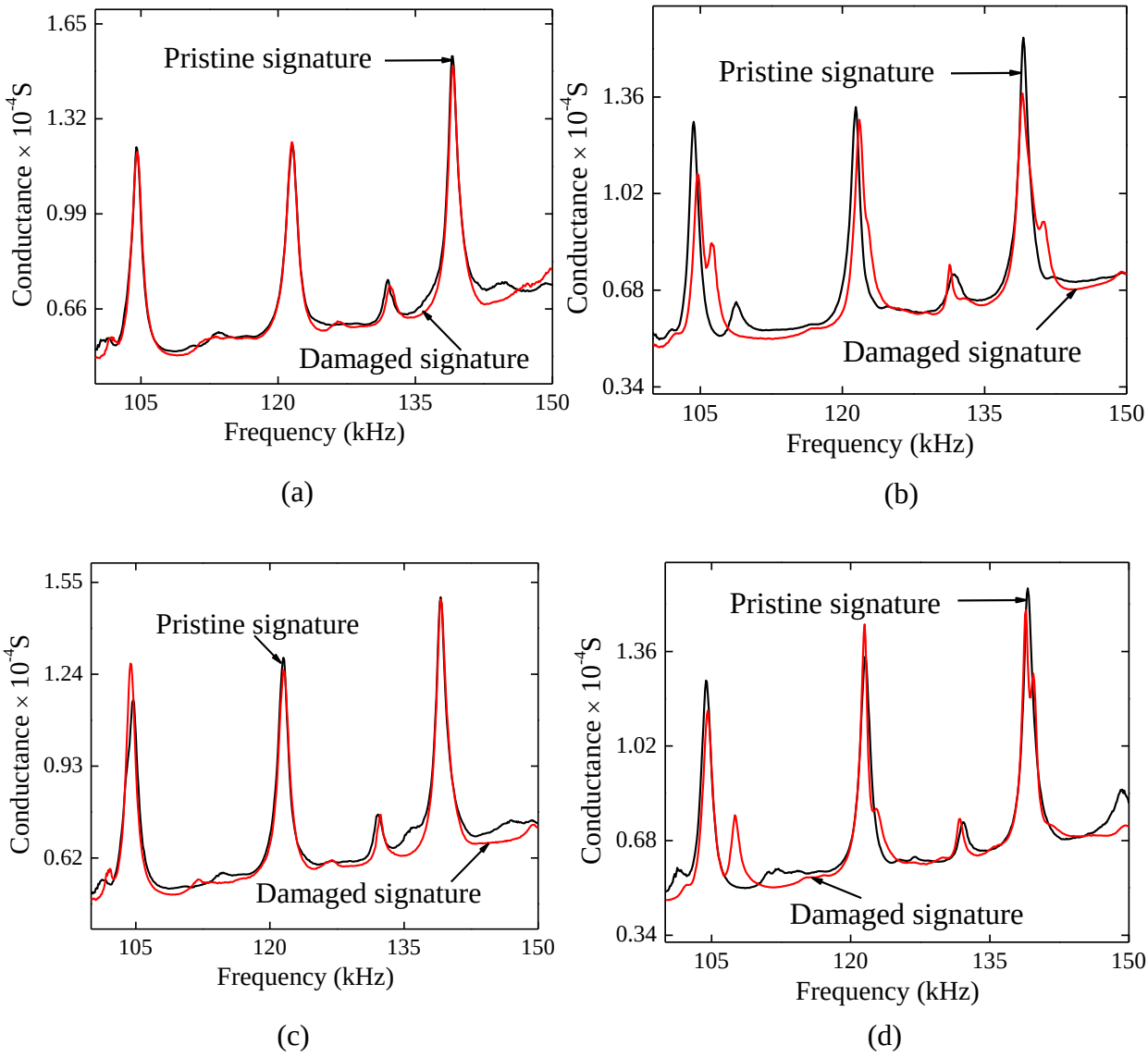

Figure B.6: Conductance signature for undamaged and damaged condition with PI-5 ARPS sensor at (a) location-A (b) location-B (c) location-C and (d) location-D

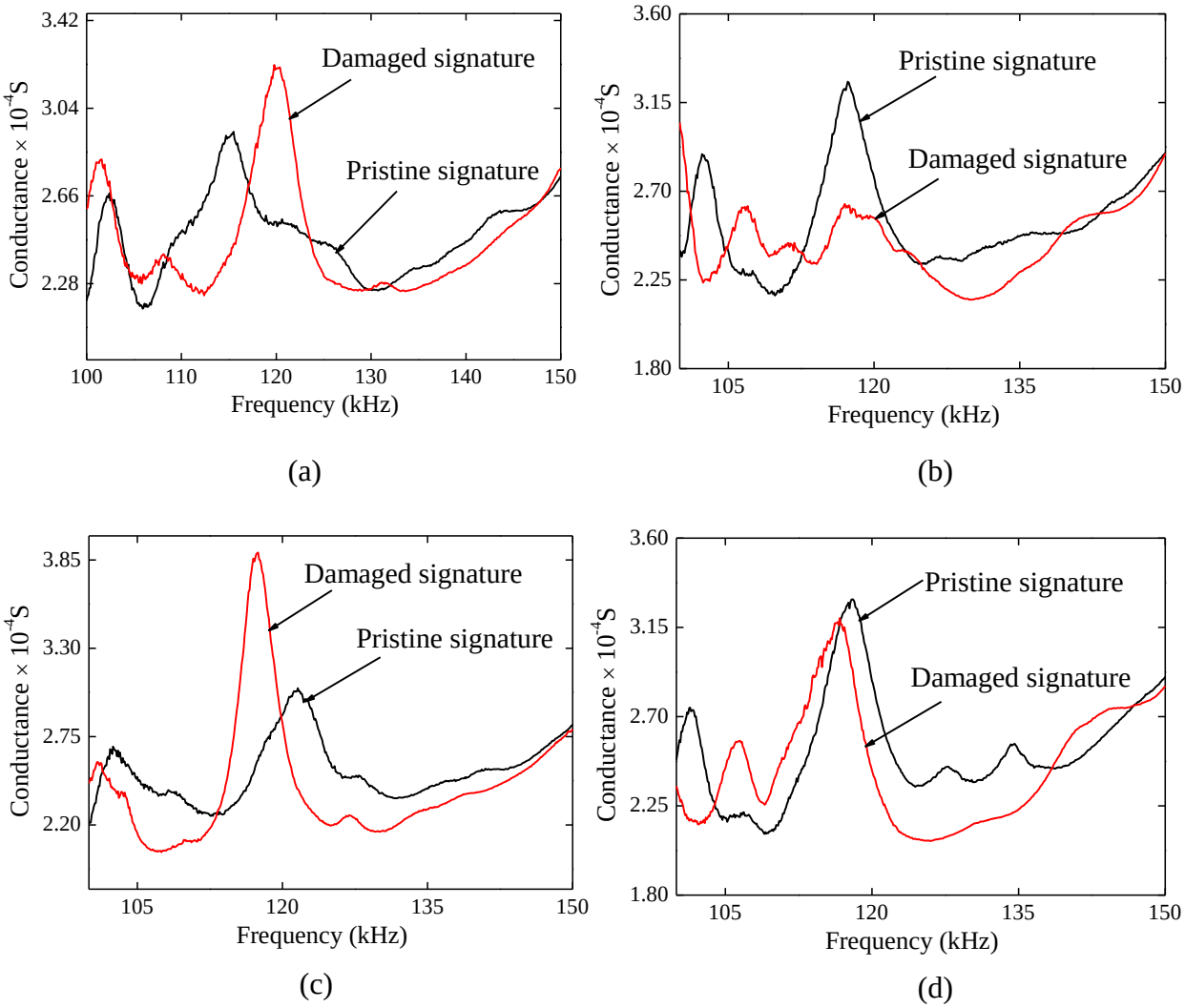

Figure B.7: Conductance signature for undamaged and damaged condition with RBPS sensor at (a) location-1 (b) location-2 (c) location-3 and (d) location-4

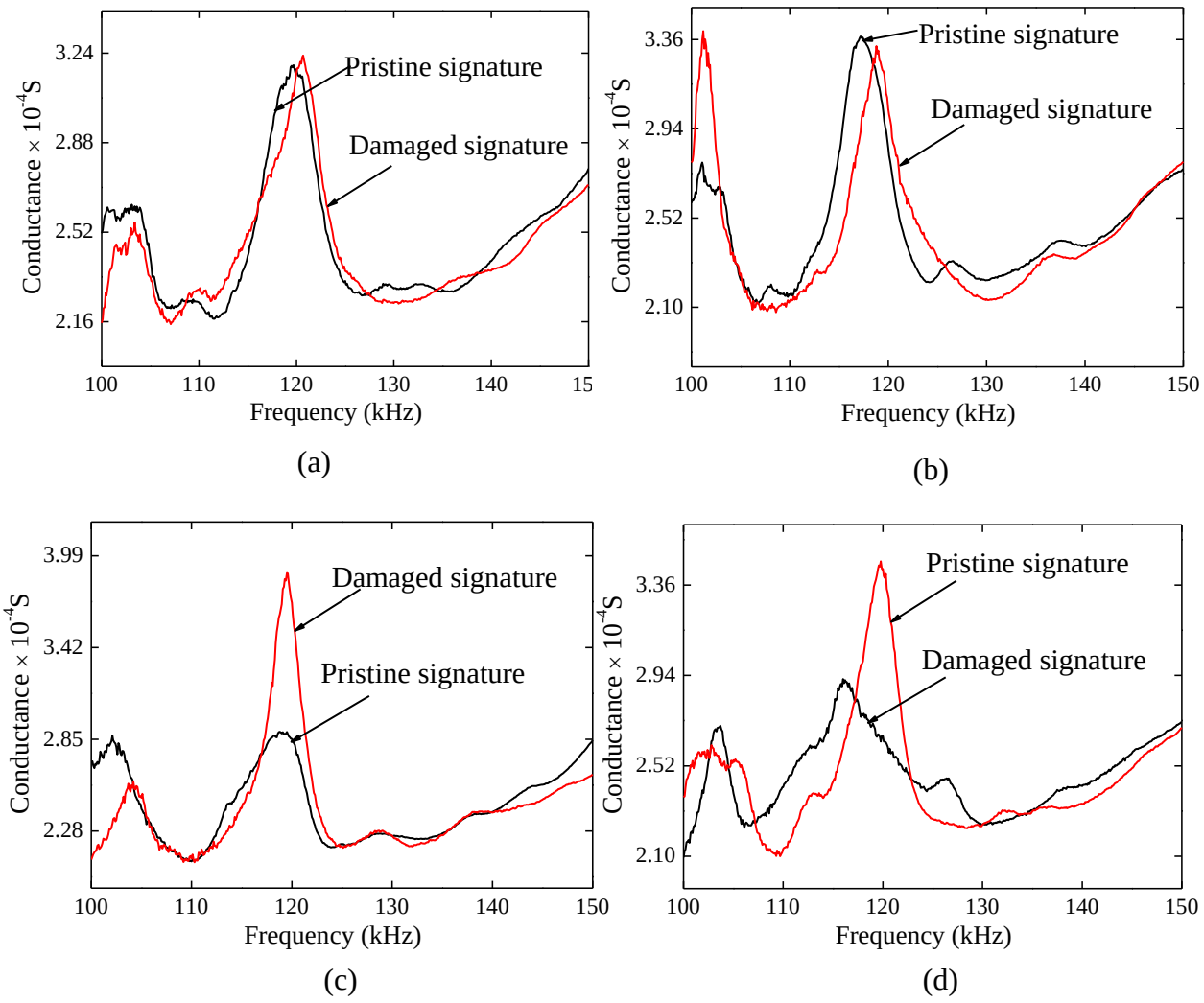

Figure B.8: Conductance signature for undamaged and damaged condition with RBPS sensor at (a) location-A (b) location-B (c) location-C and (d) location-D

APPENDIX -C

CONFERENCE PAPER

EFFECT OF TEMPERATURE ON SIGNATURES OF PIEZO SENSORS FOR EMI TECHNIQUE AND ITS COMPENSATION

Sushmita Baral[1], Prateek Negi[1], Suresh Bhalla[1]

[1] Department of Civil Engineering, Indian Institute of Technology (IIT) Delhi

Conference: Smart Materials

Theme: Smart Sensors

ABSTRACT

The electro-mechanical impedance (EMI) technique is a signature-based technique for structural health monitoring (SHM). It is a well-known fact that the signature of the piezo sensors is very sensitive to the temperature fluctuation. This can, however, trigger a false alarm. Experimental investigations conducted in controlled environments do not require temperature compensation to be carried out. However, in real life situations, temperature effects cannot be ignored. This paper investigates the effect of the temperature on the signature of the piezo sensors and its compensation. The present study involves accounting temperature effects on piezoelectric transducers exposed to a controlled increase in environmental temperature. The amount of horizontal and vertical shifts in the signatures is quantified by using experimental data. Both horizontal and vertical shifts are found to be frequency dependent, the amount of shift increasing with frequency. Further studies shall formulate a simple algorithm for compensation based on the horizontal and vertical shifts aided by piezo sensors.

Keywords: Piezo sensors, Electromechanical Impedance (EMI) technique, Structural Health Monitoring (SHM), temperature, compensation.

SUSHMITA BARAL is an M.Tech (Structural Engineering) student in Civil Engineering Department, Indian Institute of Technology (IIT) Delhi, Hauz Khas, New Delhi – 110016, India.

Telephone with Country Code: +919560636940 Email Id: sushmita.brl@gmail.com

PRATEEK NEGI is a project staff of Civil Engineering at Indian Institute of Technology (IIT) Delhi, Hauz Khas, New Delhi – 110016, India.

Telephone with Country Code: +919953919464 Email Id: negidynamic@gmail.com

SURESH BHALLA is a professor of Civil Engineering at Indian Institute of Technology (IIT) Delhi, Hauz Khas, New Delhi – 110016, India.

Telephone with Country Code: +91-011-2658-1117 Email Id: sbhalla@civil.iitd.ac.in

INTRODUCTION

All real-life structures are susceptible to damage due to various external and internal agents during their life spans. Thus, periodic maintenance is required to increase the functional life of the structures. Structural health monitoring (SHM) is a periodic monitoring of the structures for a safety point of view with the aim of identifying, locating and determining the severity of the damages in the structures. Also, it includes the determination of the remaining life of the monitored structure. Generally, any damage begins from an incipient stage but may finally result in a catastrophic damage over a period, if not treated on time. Thus, it is necessary to determine the damage in its early state to avoid its further propagation. The electro-mechanical impedance (EMI) technique uses smart materials i.e. lead zirconate titanate (PZT) patches to capture such type of damage.

Smart materials are those materials which are able to change the physical properties in a specific manner due to a certain specific type of stimulus input. Some common types of smart materials are piezoelectric materials, shape memory alloys, optical fibre, electro-rheological fluids etc. Piezoelectricity is derived from the Greek word *Piezo* which means to squeeze, thus the electricity generated by squeezing is piezoelectricity (Harper 1883). The piezoelectric behaviour was first studied by the Curie brothers extensively in the late 19^{th} century. Until now the researchers have invented several artificial crystals showing piezoelectric behavior other than the naturally occurring crystals. Commercially, two most common forms are PZT and Polyvinylidene fluoride (PVDF) flexible composites. PZT patches have higher strength and stiffness than PVDF. PVDF is ductile and has shape conformability whereas, PZT is brittle and not acquiescent with curved surfaces.

ELECTRO-MECHANICAL IMPEDANCE (EMI) TECHNIQUE

The EMI was first invented by Liang et al. (1994). It is a non-destructive technique which uses piezo sensors for condition monitoring of the host structures. A PZT patch acts both as an actuator and a sensor. When it acts as the sensor, it functions in direct mode in which it generates electric potential on the application of stress. In converse effect, it produces stress when an electrical signal is applied across its surface. In EMI technique the PZT patches bonded on the structures are electrically excited at a higher frequency in the range of 30-400 kHz by an impedance analyzer or an LCR meter. At this frequency range, the PZT patches actuate the structure and then senses the response reflected back from the structure in the form of an admittance signature. These signatures consist of a real part which is known as conductance (G) and an imaginary part known as susceptance (B). Any damage to the structure reflects a deviation in the admittance signature which is recorded in the frequency domain. Since the EMI technique uses a very high-frequency range, is capable of detecting damages in insipient stage and also immune to other low-frequency structural vibrations. However, these signatures are sensitive towards the change in the surrounding temperature. Several researchers have proposed methods to compensate for these changes from the obtained signatures. Next section covers past work on a study of the temperature effect.

TEMPERATURE EFFECT ON PIEZO SENSORS

Krishnamurthy et al. (1996) found a decrease in the magnitude of the impedance peaks of a free PZT patch due to the increase in temperature. They choose a range of 25 to 75 °C in which the dielectric and piezoelectric properties of piezo ceramic PSI-5A shows a linear trend. Though it is nonlinear at a border temperature range. Normalization of the variation of impedance with temperature eradicates the effect of a change in magnitude of impedance which makes the variation independent of frequency. Changes in temperature, boundary condition, loading effects etc. lead to a variation on the susceptance signature whereas little change in the conductance signature. Insignificant change in the resistive portion of electrical impedance suggests utilization of real part of electrical admittance for the damage response which minimizes the effect of temperature

Park et.al 1999 found significant horizontal and vertical shift in signatures due to a temperature in contrast to damage where the shifts are irregular. Empirical temperature compensation technique

was developed which can be applied in a complex structure. Compensation technique was validated on a bolted pipe joint, a gear, and a composite reinforced aluminum plate along with the experiments.

The experiments conducted in lab controlled environment gives the stable results but in actual field condition, it is not possible due to the fluctuation of temperature (Bhalla 2001). He performed the simulation study of each parameter controlling another parameter in which he found the horizontal shift in the signature is due to change in Young's modulus of the structure and vertical shift is due to the change in ε_{33} and d_{31}.

Structural peaks are more affected rather than the PZT peaks on various temperatures (Yang et. al. 2008). The shift of PZT resonance towards left is mainly due to the softening if the bonding layer, structural properties and piezoelectric properties PZT patch. Through simulation on FE software ANSYS, he validated the shift of the signatures is caused by a reduction of stiffness of the bonding layer against increasing temperature.

The variations in the amplitude of the impedance signatures were related to the temperature-dependence of the capacitance of the piezoelectric sensor (Baptista et al. 2014). As a result of temperature variation, the shift in the resonance peak is not constant but increases with the increase in the frequency. The frequency band used to calculate the damage indices played an important role in compensating for temperature effects by maximizing the correlation coefficient. Next section describes temperature related lab study aiming at the development of a raw simple compensation algorithm.

EXPERIMENTAL PROCEDURE

For the experiment, a piezo sensor of 10 × 10 × 0.3 mm was surface bonded on an aluminum plate of 200 × 25 × 2 mm using a two-part epoxy adhesive. Signatures were acquired through Agilent E4980A LCR meter using VEEPRO platform at the lab temperature. For the temperature range of 30-60 °C, the structure was placed on the oven and signature was acquired at an interval of 5 °C increase in the temperature. Figure 1 shows the complete setup of the experiment.

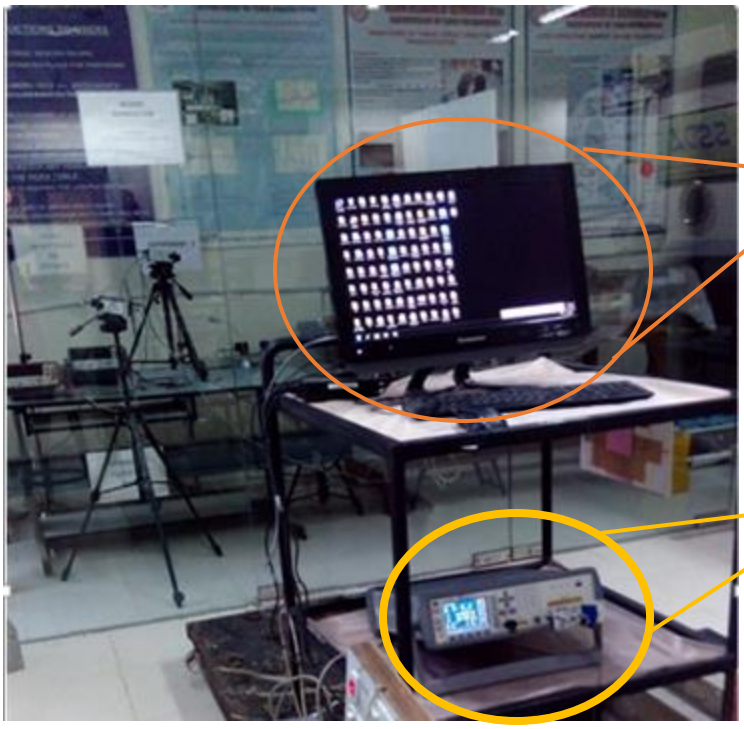

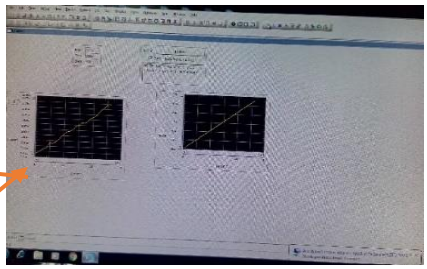

Veepro software

LCR meter

(a)

(b)

(c)

Fig 1: Complete set up of the experiment

(a) LCR meter and controlling PC

(b) Specimen inside oven

(c) Oven

OBSERVATIONS

Figure 2 shows a plot of the conductance and susceptance signatures in 50-150 kHz range.

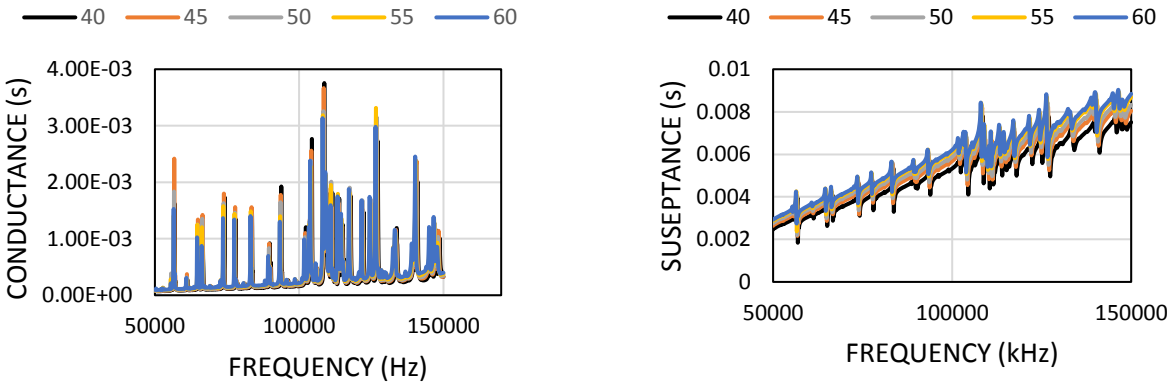

(a) (b)

Fig 2: Signature plot for various temperature

(a) Conductance (b) Susceptance

It is observed that both the conductance and susceptance signatures shift towards the left with the increasing temperature. The shift of the signature was computed horizontally by the iteration and vertically the average shift at each frequency point. Figure 3 and 4 shows the nature of shift horizontally and vertically.

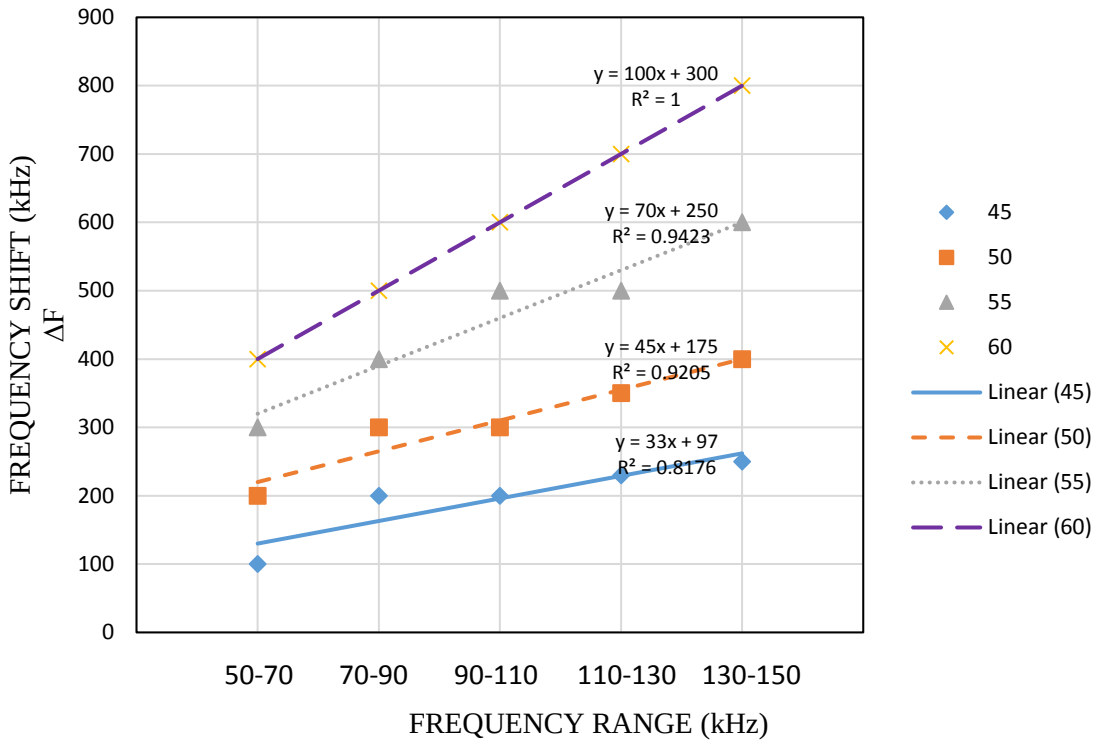

Fig 3: Horizontal shift as a function of frequency

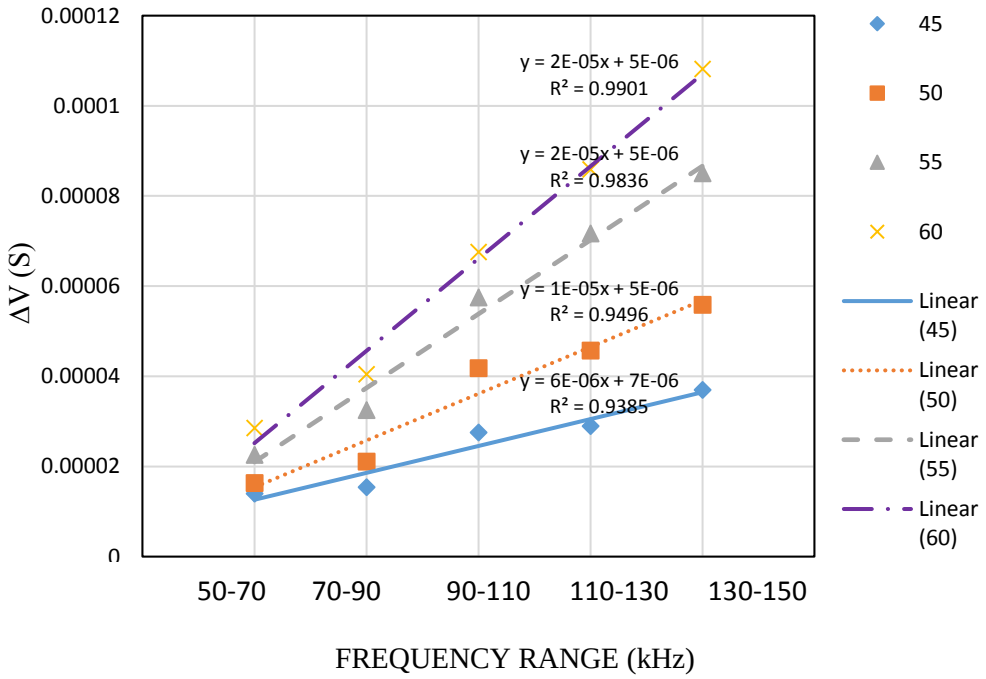

Fig 4: Vertical shift

Figure 5 represents vertical shift as function of temperature for various frequency intervals. The shift shows a linear variation with increase in the temperature for all the frequency changes. However, the slope of the curves increases for the higher temperatures.

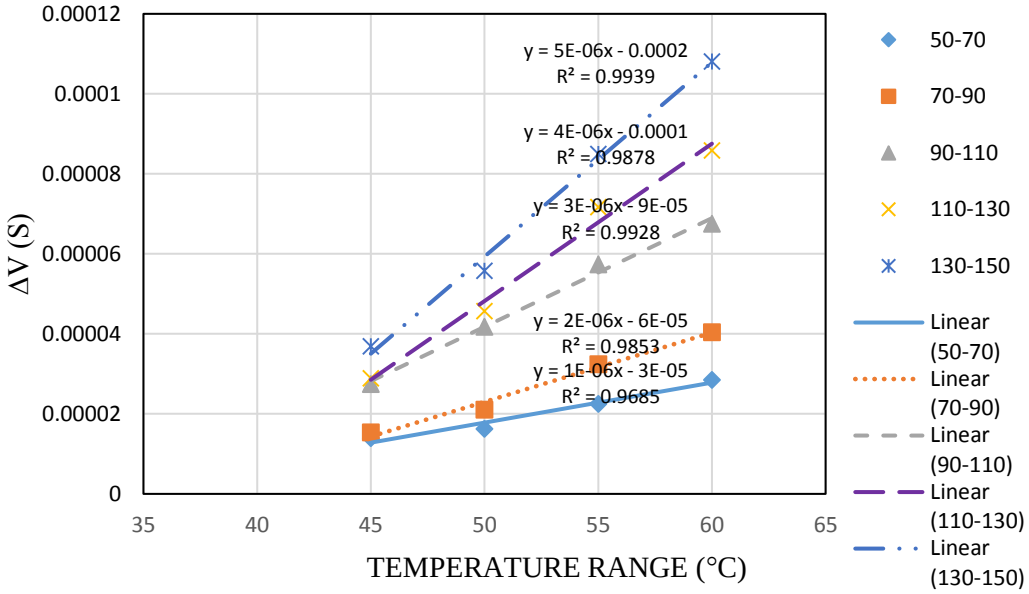

Fig 5: Vertical shift vs temperature for different frequency ranges.

From fig 3 to 5, it is clearly observed that both horizontal and vertical shifts are frequency dependent, the amount increasing with frequency. This fact shall be incorporated into the raw compensation technique to be formulated by the authors.

CONCLUSIONS

This paper has presented initial experiments conducted to study the effect of temperature on conductance signatures. The study finds a strong dependence of shifts on temperature and frequency. Based on these observations, a new compensation technique shall be formulated which will also utilize the signature of free PZT patches. Results shall be published in the next paper.

REFERENCES

1. Harper, D. (1883), "*Piezoelectric*", Online Etymology Dictionary
2. Liang, C., Sun, F. P. and Rogers, C. A. (1994), "*Electro-Mechanical Impedance Modelling Of Active Material System.*" Smart Material and Structures, Vol. 5, No.2, pp. 171-186
3. Krishnamurthy, K., Lalande, F., and Rogers, C.A., (1996), "*Temperature Effects on Piezoelectric Elements Used as Collocated Actuator/Sensors*," Proceedings of SPIE North American Conference on Smart Structures and Materials, Vol. 2717, pp. 302-310.
4. Park, G.,Kabeya, K., Cudney, H. H. and Inman, D. J. (1999), "*Impedance-based structural health monitoring for temperature varying applications.*" JSME International Journal, Vol.42, No.2, pp.249-258.
5. Bhalla, S. (2001), "*Smart System Based Automated Health Monitoring of Structures*" M. Eng. Thesis, Nanyang Technological University, Singapore.
6. Yang Y., Lim Y. Y., and Soh C. K. (2008), "*Practical issues related to the application of the electromechanical impedance technique in the structural health monitoring of civil structures*." Smart Material and Structure. 17,035008.
7. Baptista, F. G., Budoya, D. E., Dealmeida, V. A., and Ulson, J. A. C., (2014), "*An Experimental Study on the Effect of Temperature on Piezoelectric Sensors for Impedance-Based Structural Health Monitoring*." Journal of Sensors 14, 1208-1227.

APPENDIX-D

MATLAB program for the plot of admittance signature in free boundary condition

```
%signature_free.m
%MATLAB program to obtain free PZT electro-mechanical signatures
%based on 2D.
%This program does correction for twin peak case (for single peak situation, use Cf1=Cf2)
%The program is based on the new 2D model based on effective impedance.
%PZT parameters are based on measurement. Since the model considers only
% one-fourth of the PZT, a factor of 4 used in final answer


%PZT parameters for PIC 151
LA=0.005; HA= 0.0003; RHO=7800; D31=-2.10E-10;mu=0.3;
Y11E= 6.67e10; E33T=2.25337E-08; ETA= 0.01; DELTA= 0.01;

cf1 = 1;    %Peak correction factors, to be chosen by trial (for single peak situation, use Cf1=Cf2)
cf2 = 1;
% Default value is 1, user need to input suitable value

K=2*D31^2*Y11E/(1-mu);
N=1000

for I = 1:N,
f(I) = 1000*I;
x(I)= 0; %Zero value assigned to structual impedance
y(I)=0;
%Calculation of structural impedance

omega(I) = 2* pi * f(I);                    %Angular frequency in rad/s

%Calculation of wave number
cons = (RHO *(1-mu*mu)/ (Y11E * (1 + ETA * ETA)))^0.5;
k_real(I) =  cons * omega(I);
k_imag(I) =  cons * omega(I) * (-0.5 * ETA);

%Calculation of tan(kl)/kl
rl(I) = k_real(I) * LA * cf1;
im(I) = k_imag(I) * LA * cf1;

a(I) = (exp(-im(I)) + exp(im(I))) * sin(rl(I));
b(I) = (exp(-im(I)) - exp(im(I))) * cos(rl(I));
c(I) = (exp(-im(I)) + exp(im(I))) * cos(rl(I));
d(I) = (exp(-im(I)) - exp(im(I))) * sin(rl(I));
```

```
u(I) = c(I) * rl(I) - d(I) * im(I);
v(I) = d(I) * rl(I) + c(I) * im(I);
h(I) = u(I)^2 + v(I)^2;
r1(I) = (a(I) * u(I) - b(I) * v(I)) / h(I);
t1(I) = (-1.0) * (a(I) * v(I) + b(I) * u(I)) / h(I);
rl(I) = k_real(I) * LA * cf2;
im(I) = k_imag(I) * LA * cf2;

a(I) = (exp(-im(I)) + exp(im(I))) * sin(rl(I));
b(I) = (exp(-im(I)) - exp(im(I))) * cos(rl(I));
c(I) = (exp(-im(I)) + exp(im(I))) * cos(rl(I));
d(I) = (exp(-im(I)) - exp(im(I))) * sin(rl(I));
u(I) = c(I) * rl(I) - d(I) * im(I);
v(I) = d(I) * rl(I) + c(I) * im(I);
h(I) = u(I)^2 + v(I)^2;
r2(I) = (a(I) * u(I) - b(I) * v(I)) / h(I);
t2(I) = (-1.0) * (a(I) * v(I) + b(I) * u(I)) / h(I);
r(I) = 0.5 * (r1(I)+r2(I));
t(I) = 0.5 * (t1(I)+t2(I));

%Calculation of  impedance of PZT patch
multia(I) = (HA * Y11E) / (pi * (1-mu)* f(I));
Big_rt(I) = r(I) * r(I) + t(I) * t(I);
xa(I) = multia(I) * (ETA * r(I) - t(I)) / Big_rt(I);
ya(I) = multia(I) * (-1.0) * (r(I) + ETA * t(I)) / Big_rt(I);

%Calculation of conductance and susceptance
p(I) = x(I) + xa(I);
q(I) = y(I) + ya(I);
Big_p(I) = xa(I) * p(I) + ya(I) * q(I);
Big_q(I) = ya(I) * p(I) - xa(I) * q(I);
Big_R(I) = r(I) - ETA * t(I);
Big_T(I) = ETA * r(I) + t(I);
Big_pq(I) = p(I) * p(I) + q(I) * q(I);
temp_r(I) = (Big_p(I) * Big_T(I) + Big_q(I) * Big_R(I)) / Big_pq(I);
temp_i(I) = (Big_p(I) * Big_R(I) - Big_q(I) * Big_T(I)) / Big_pq(I);
t_r(I) = ETA - temp_r(I);
t_i(I) = temp_i(I) - 1;
multi1(I) = (LA * LA * omega(I)) / HA;
Gf(I) = 4*multi1(I) * (DELTA * E33T + K *t_r(I));
Bf(I) = 4*multi1(I) * (E33T + K *t_i(I));
end
subplot(2,1,1);
plot(f,Gf);
subplot(2,1,2);
plot(f,Bf);
```